General Motors Corporation
Legal Staff

Facsimile
(313) 974-0612

Telephone
(313) 974-1572

September 29, 1997

The Honorable Philip R. Recht
Deputy Administrator
NATIONAL HIGHWAY TRAFFIC
SAFETY ADMINISTRATION
400 Seventh Street, S.W., Room 5220
Washington, DC 20590

Dear Mr. Recht:

Re: **Settlement Agreement**
Section B. Fire Safety Research

Enclosed is the Failure Analysis Associates, Inc. report entitled "Development of Inspection Technology for NGV Fuel Tanks." This is the final report for Project B.7 "Development of Criteria and Methodologies for In-Service Inspections of Gaseous Fuel Pressure Vessels."

Sincerely,

David A. Collins
Attorney

Enclosure

c: James A. Durkin, Esq. (w/o enclosure)

Development of Inspection Technology for NGV Fuel Tanks

Failure Analysis Associates®

Failure Analysis Associates

Failure Analysis Associates, Inc.
Engineering and Scientific Services
149 Commonwealth Drive, P.O. Box 3015
Menlo Park, California 94025
(415) 326-9400 Fax (415) 326-8072
Internet Site: www.fail.com

FaAA-SF-R-97-05-04
Revision 1

Development of Inspection Technology for NGV Fuel Tanks

Prepared by:

Failure Analysis Associates, Inc.
Menlo Park, California

Prepared for:

General Motors Corporation
Research & Development Center
Warren, Michigan

May 1997
(Revised August 1997)

TABLE OF CONTENTS

Subject	Page
List of Tables	iv
List of Figures	v
EXECUTIVE SUMMARY	xi
1.0 INTRODUCTION	1
1.1 NGV Fuel Tank Designs	1
1.2 NGV Fuel Tank Inspection	2
1.3 Project Overview	2
1.4 Report Overview	3
2.0 DAMAGE TOLERANCE OF COMPOSITE STRUCTURES	4
2.1 Damage	4
2.2 Material Influences	5
2.3 Design Influences	6
2.4 Analytical Methods	7
2.5 Test Methods	8
2.6 Damage Tolerance of Composite Overwrapped Pressure Vessels	8
3.0 PHASE 1 -- IN-SERVICE INSPECTION OF NGV FUEL TANKS	12
3.1 NGV Service Environment	12
3.2 NGV Fuel Tank Inspection Environment	12
3.3 NGV Fuel Tank Inspection Methods	13
4.0 ACOUSTIC EMISSION INSPECTION	14
4.1 Wave Propagation in Thin Plates	15
4.2 Conventional Acoustic Emission Inspection of Pressure Vessels	16
4.3 Modal Acoustic Emission Testing	18
4.4 Acoustic Emission Testing	19
5.0 FIBER TOW TESTS	21
5.1 Wave Propagation in Rods	21
5.2 Test Setup	22
5.3 Results and Discussion	22
5.4 Conclusions	24

TABLE OF CONTENTS
(continued)

Subject	Page
6.0 PHASE 2 -- NGV FUEL TANK TESTING	**26**
6.1 Stage 1 - Initial Evaluation of Acoustic Emission Inspection	26
6.2 Stage 2 - Acoustic Emission Inspection of Damaged Tanks	28
6.3 Acoustic Emission from Tanks During Stage 2 Testing	35
7.0 DISCUSSION	**39**
7.1 Damage Tolerance of the NGV Fuel Tanks	39
7.2 Acoustic Emission Inspection of NGV Fuel Tanks	41
REFERENCES	**44**
TABLES	
FIGURES	

LIST OF TABLES

Table 1. Comparison of Candidate NGV Fuel Tank Inspection Methods

Table 2. Test Matrix for Tow Testing

Table 3. Theoretical Arrival Times

Table 4. NGV Fuel Tank Test Specimens

Table 5. Tank Damage

Table 6. Fatigue Testing

Table 7. Acoustic Emission Inspection

Table 8. Results for Tank 013

Table 9. Results for Tank 014

Table 10. Results for Tank 018

Table 11. Results for Tank 003

LIST OF FIGURES

Figure 1. Variation of Residual Tensile Strength with Impact Energy

Figure 2. Effect of Indenter on Visibility of Impact Damage

Figure 3. Effect of Fiber Elongation on Post-Impact Residual Strength

Figure 4. Effect of Resin Fracture Energy on Composite Interlaminar Fracture Energy

Figure 5. Effect of Fiber Treatment on Post-Impact Residual Strength

Figure 6. Impact Damage in a Rigid and Flexible Target

Figure 7. COPV Impact Test Facility at White Sands Test Facility

Figure 8. Burst COPV Following Impact

Figure 9. COPV Failed Upon Impact

Figure 10. Post-Failure COPV Test Facility

Figure 11. Plate Wave: Extensional Mode on the Top, Flexural Mode on the Bottom

Figure 12. Knee of the Curve [13]

Figure 13. Correlation of Long Duration Events with Residual Strength [15]

Figure 14. Total Events vs. Burst Pressure for Control (Undamaged) and Damaged Pressure Vessels [16]

Figure 15. Source Orientation Effects [24]

Figure 16. Waveforms due to Transverse Matrix Cracking [23]

Figure 17. Burst Pressure Correlation for Modal Based AE Analysis [31]

Figure 18. Mounting Tabs on a Tow Test Specimen

Figure 19. Completed Tow Test Specimen

Figure 20. Tow Specimen in Grips of Hydraulic Test Machine

Figure 21. Typical Transducer Mounting Locations on the Tow Test Specimens

Figure 22. Waveforms from One Event During Tow Test # 1 – Flexural Propagation

Figure 23. FFT of Waveforms in Figure 20

LIST OF FIGURES
(continued)

Figure 24. Waveforms from One Event During Tow Test # 1 – Extensional Propagation

Figure 25. FFTs from Waveforms in Figure 22

Figure 26. Typical Single Channel Event Recorded During Testing

Figure 27. Typical High Frequency, Short Duration Event

Figure 28. Fiber Break Signal with Flexural Component

Figure 29. Schematic of Possible Fiber Break Locations in the Tow Test Specimen

Figure 30. Typical Waveform Used for Source Location

Figure 31. Calculated Source Locations for Tow Test Specimen 4

Figure 32. Configuration of Tank 012 Sensors

Figure 33. Configuration of Tank 004 Sensors and Damage

Figure 34. Fiber Break Signal and FFT of Signal – Tank 004

Figure 35. Matrix Cracking Signal and FFT of Signal – Tank 004

Figure 36. Matrix Splitting Signal and FFT of Signal – Tank 004 with Slits

Figure 37. Type 2 Tanks on Pallet

Figure 38. Configuration of Tank 013 Sensors and Damage

Figure 39. Configuration of Tank 014 Sensors and Damage

Figure 40. Configuration of Tank 018 Sensors and Damage

Figure 41. Configuration of Tank 003 Sensors and Damage

Figure 42. Response from Leadbreak to Check Sensor Coverage of Entire Tank

Figure 43. As-Received Tank 013 in the Burst Test Chamber

Figure 44. Burst Test Chamber Just Prior to Testing

Figure 45. Acoustic Emission Acquisition Equipment

Figure 46. 2-inch Slit in the Overwrap of Tank 013

LIST OF FIGURES
(continued)

Figure 47. Circumferential Cracks Propagating from the Ends of the 2-inch Slit

Figure 48. Pendulum Impact Fixture in the Burst Test Chamber

Figure 49. Pyramid-Shaped Impactor

Figure 50. Impact Site Following 22.1 ft-lbs Impact

Figure 51. Extent of Damage from 22.1 ft-lbs Impact

Figure 52. Pendulum Impact Fixture for 221 ft-lbs Impact

Figure 53. Impact Site Following 221 ft-lbs Impact

Figure 54. Tank 013 in the Fatigue Test Chamber, 0° View

Figure 55. Tank 013 in the Fatigue Test Chamber, 180° View

Figure 56. As-Received Tank 014 in the Burst Test Chamber

Figure 57. Acoustic Emission Sensors on Tank 014

Figure 58. As-Received Tank 018 in the Burst Test Chamber, Left Side View

Figure 59. As-Received Tank 018 in the Burst Test Chamber, Right Side View

Figure 60. Large Impact Fixture Set-Up for Tank 018, Side View

Figure 61. Large Impact Fixture Set-Up for Tank 018, End View

Figure 62. Impact Test Facility Just Prior to Impact of Tank 018

Figure 63. Post-Impact Damage on Tank 018, Overall View

Figure 64. Post-Impact Damage on Tank 018, Close-Up

Figure 65. 8-inch Slit Cut in Tank 018

Figure 66. Ends of Slit Separated Following Pressurization

Figure 67. Circumferential Cracks at the Ends of the 8-inch Slit in Tank 018

Figure 68. Oblique View of Slit Following Pressurization

Figure 69. Ends of Slit Separated Following Fatigue Cycling, Overall View

Figure 70. Ends of Slit Separated Following Fatigue Cycling, Close-Up

LIST OF FIGURES
(continued)

Figure 71. Tank 018 Following 15000 Pressure Cycles

Figure 72. Tank 018 Following 15000 Pressure Cycles, Close-Up of Slits

Figure 73. Overall View of Tank 003

Figure 74. Tank 003 with Rubber Bumper Removed; White Material is Styrofoam

Figure 75. Rubber Bumper Following Removal

Figure 76. Tank 003 Following Removal of Styrofoam

Figure 77. As-Received Tank 003 in the Burst Test Chamber

Figure 78. Drop Test Set-Up for Tank 003

Figure 79. Tank 003 Orientation for Drop Test

Figure 80. Impact Site on Tank 003

Figure 81. Impact Site on Tank 003, Close-Up

Figure 82. Secondary Damage on Tank 003

Figure 83. Tank 003 in the Burst Test Chamber, Following the Drop Test

Figure 84. Failed Area on Tank 003

Figure 85. Failed Area on Tank 003, Close-Up

Figure 86. Failed Area on Tank 003, Oblique View

Figure 87a. Waveform from a Typical Noise Event Recorded During the Initial Pressurization of the As-Received Tanks

Figure 87b. FFT from a Typical Noise Event Recorded During Pressurization of the As-Received Type 2 Tanks

Figure 88a. Waveform from a Typical Structural Event Recorded During Pressurization of the As-Received Type 2 Tanks

Figure 88b. FFT from a Typical Structural Event Recorded During Pressurization of the As-Received Type 2 Tanks

LIST OF FIGURES
(continued)

Figure 89a. Waveform from a Typical Event Recorded During Pressurization of the As-Received Type 2 Tanks

Figure 89b. FFT from a Typical Event Recorded During Pressurization of the As-Received Type 2 Tanks

Figure 90a. Waveform from a Typical Event Recorded During Pressurization of the As-Received EDO Type 4 Tank

Figure 90b. FFT from a Typical Event Recorded During Pressurization of the As-Received EDO Tank

Figure 91a. Waveform from a Typical Event Recorded During Pressurization of a Type 2 Tank with a Saw Cut

Figure 91b. FFT from a Typical Event Recorded During Pressurization of a Type 2 Tank with a Saw Cut

Figure 92a. Waveform from a Typical Event Recorded During Pressurization of a Type 2 Tank with Impact Damage

Figure 92b. FFT from a Typical Event Recorded During Pressurization of a Type 2 Tank with Impact Damage

Figure 93a. Waveform from a Typical Event Recorded During Pressurization of the Type 4 Tank with Impact Damage

Figure 93b. FFT from a Typical Event Recorded During Pressurization of the Type 4 Tank with Impact Damage

Figure 94. Waveform from a Typical Fretting Event Recorded During Fatigue Cycling of a Type 2 Tank

Figure 95. Waveform from a Typical Noise Event Recorded During Type 2 Tank Fatigue Cycling

Figure 96. Waveform from a Typical Small Amplitude Event Recorded During Fatigue Cycling of the Type 4 Tank

Figure 97. Waveform from a Typical Event from the Impact Area Recorded During Fatigue Cycling of the Type 4 Tank

LIST OF FIGURES
(continued)

Figure 98a. Waveform from a Typical Small Amplitude, High Frequency Event Just Prior to Failure of the Type 4 Tank

Figure 98b. FFT from a Typical Small Amplitude, High Frequency Event Just Prior to Failure of the Type 4 Tank

Figure 99. Waveform Recorded during Pressurization Hold after Fatigue Cycling of a Type 2 Tank

Figure 100. Typical Events Versus Time Plot During Pressure Hold After 6,000 Fatigue Cycles of Tank 013

Figure 101. Number of Events During Each Pressure Hold After Fatigue Cycling of Tank 013

Figure 102. Number of Events During Each Pressure Hold After Fatigue Cycling of Tank 018

Figure 103. Number of Events During Each Pressure Hold After Fatigue Cycling of Tank 003

EXECUTIVE SUMMARY

On March 7, 1995 General Motors Corporation (GM) and the US Department of Transportation entered into an agreement (hereafter referred to as the Agreement or Settlement Agreement) to settle a dispute regarding the safety of 1970-1991 full-sized GM pickup trucks equipped with fuel tanks mounted outboard of the frame rails. Part of this Agreement involves establishment of a 5 year, $10 million motor vehicle fire safety research program to be funded by GM. The overall objectives of this research program are to better understand how vehicle fires start and spread, and to determine what can be done to prevent, contain, and extinguish such fires. To this end, GM and the National Highway Traffic Safety Administration have jointly developed 14 separate vehicle fire safety research projects. One of these projects (B.7), entitled "Development of Inspection Technology for NGV Fuel Tanks," is the subject of this technical report.

Compressed natural gas (CNG) powered vehicles have been the subject of much interest because of their low emissions. To address concerns regarding potential risks associated with CNG vehicles, GM, in conjunction with CNG component suppliers, undertook an innovative broad-based analysis of the CNG fuel system design that addressed a comprehensive range of issues including design, manufacturing, usage, servicing, and consumer considerations.

GM contracted with Failure Analysis Associates, Inc. (FaAA), to evaluate techniques for in-service inspection of composite overwrapped natural gas vehicle (NGV) fuel tanks. To achieve this objective, FaAA first performed a study of candidate inspection methods. This study considered 1) the types of damage that could be expected and would need to be detected, 2) the various inspection techniques that are suitable for composite overwrapped pressure vessels, and 3) the practical implementation of the fuel tank inspection method, including the required equipment and skill of the inspector. Acoustic emission inspection was identified as the most promising inspection technique, in large part because it is the one technique that can potentially be implemented without removing the fuel tank from the vehicle.

Tests were conducted on NGV fuel tanks at FaAA's Phoenix Test and Engineering Center to evaluate the damage tolerance of overwrapped NGV fuel tanks and the applicability of acoustic emission for detecting damage in NGV tanks. Tests were conducted on six NGV fuel tanks, both Type 2 (hoop-wrapped, metal lined) tanks and Type 4 (fully-wrapped, plastic lined) tanks. The tanks were subjected to different types of damage to the composite overwrap, including impact damage and saw cuts, followed by 15,000 pressure cycles in accordance with NGV2 service. The tanks were instrumented with acoustic emission sensors. The ability of the sensors to detect the presence of the damage initially and during the simulated lifetime was evaluated. This project did not address detection of defects in the liner of an overwrapped NGV fuel tank.

Testing demonstrated that acoustic emission inspection was able to detect the damage in the composite overwrap and changes in the damage during pressure cycling. This capability is a requirement for an NGV fuel tank in-service inspection method. The characterizations of acoustic emission signals, such as matrix cracking events, were verified by visual examination of the tank. Furthermore, acoustic emission inspection was demonstrated to be a practical method

for in-service NGV fuel tank inspection. The most difficult part of acoustic emission inspection is the interpretation of the data. However, once the methodology for a specific tank design is established, acoustic emission inspection lends itself to automated, computerized implementation, with little human intervention. Because testing was limited to six tanks, additional testing on a wider variety of tank designs and on a greater number of test specimens is required. The results of this project support the potential application of acoustic emission inspection to in-service inspection of NGV fuel tanks. However, many questions remain and additional work is required before a viable inspection method can be developed.

1.0 INTRODUCTION

Many automotive manufacturers are producing or considering production of compressed natural gas (CNG) powered vehicles. The use of natural gas offers a number of significant advantages over gasoline, including low emissions, improved fuel efficiency, and lower cost fuel. To address concerns regarding potential risks associated with CNG vehicles, General Motors (GM) in conjunction with CNG component suppliers, undertook an innovative broad-based analysis of the CNG fuel system design that addressed a comprehensive range of issues including design, manufacture, usage, maintenance, and consumer considerations.

This project, which is part of GM's overall effort, is motivated by the need to ensure safe operation of CNG powered vehicles. The focus of the project is on developing inspection technology to evaluate the integrity of the natural gas vehicle (NGV) fuel tank, which stores the pressurized natural gas fuel. During automotive service, a fuel tank is subjected to a wide variety of loads and environments, which may be detrimental to the tank during its lifetime. The primary operational loading is caused by the internal gas pressure, which cycles as the tank is filled and the vehicle is driven. The service environment includes ambient conditions of temperature and humidity, as well as potential exposure to a variety of chemicals. The tank may also be subjected to impact loads during its lifetime due to impact by road hazards, contact with cargo, and being dropped inadvertently. In this project, FaAA evaluated techniques for in-service inspection and assessment of NGV fuel tanks.

1.1 NGV Fuel Tank Designs

To minimize weight, NGV fuel tanks typically consist of a liner, which contains the gas, overwrapped with fibers to provide the strength needed to resist the internal pressure. The liner is typically metal or plastic and the overwrap is typically a composite material consisting of carbon or glass fibers in a resin matrix. The overwrap can cover just the cylindrical portion of the tank (hoop-wrapped tank) or it can cover the entire surface of the tank (fully-wrapped tank). These various combinations of NGV fuel tank designs are categorized in the ANSI/NGV2 specification [1]:

Type 1 - All metal tank
Type 2 - Metal liner with hoop wrapped fiber reinforcement
Type 3 - Metal liner with fully wrapped fiber reinforcement
Type 4 - Non-metallic liner with fully wrapped fiber reinforcement

In all of the overwrapped tank designs (Types 2, 3, and 4), the load is shared between the liner and the fiber overwrap. Therefore, the structural integrity of these tanks depends in large part upon maintaining the integrity of the overwrap for the life of the tank. Fuel tanks meeting ANSI/NGV2 are designed for a 15 year service life.

1.2 NGV Fuel Tank Inspection

One of the objectives of inspecting in-service NGV fuel tanks is to detect changes in the fiber overwrap, such as impact damage, that can reduce the life of the tank. The current NGV fuel tank specification, ANSI/NGV2, requires a visual inspection of the tank at least every three years for external damage and deterioration. The inspection is to be performed by a qualified person in accordance with the manufacturer's established reinspection criteria and the applicable Compressed Gas Association Guidelines. For fiber overwrapped tanks (Types 2, 3, and 4), the applicable CGA specification is C-6.2, Guidelines for Visual Inspection and Requalification of Fiber Reinforced High Pressure Cylinders [68]. A new, comprehensive CGA guide for visual inspection of all NGV cylinders, CGA C-6.4 is expected to be published in 1997.

Although visual inspection is the only method currently specified for NGV fuel tanks, the American Society for Testing and Materials (ASTM) is currently developing a specification for acoustic emission examination of gas-filled filament-wound composite pressure vessels [12]. One of the objectives of the new specification is to define an inspection technique that provides a more objective and thorough evaluation of the structural condition than does visual inspection, particularly if the visual inspection does not include the areas under the mounting straps and other inaccessible areas.

1.3 Project Overview

This project addressed two questions applicable to inspecting in-service NGV tanks to assess the structural integrity of the tank:

1. Will the NGV fuel tank perform satisfactorily if the composite overwrap is damaged?

2. Can the presence of damage in an NGV fuel tank be detected by inspecting the tank?

Work was performed in two phases. In Phase 1, a study was conducted to evaluate various inspection techniques for their potential applicability to in-service inspection of NGV fuel tanks. Both technical and practical aspects of the inspection techniques were considered in the evaluation. Phase 1 identified acoustic emission inspection as the most promising method. In Phase 2, tests were conducted to evaluate the capability of acoustic emission to detect damage in overwrapped NGV tanks. Type 2 and Type 4 tanks were damaged and then subjected to cyclic pressure loading. Acoustic emission was monitored on as-received tanks and on impacted tanks, while the tanks were undergoing monotonic and cyclic loading. Laboratory tests were also performed to characterize the acoustic emission response of the fiber overwrap used in the Type 2 tanks.

In the Phase 2 fatigue testing, the load cycle was defined as from approximately 0 psig (empty) to 3,600 psig (operating pressure). Tanks were subjected to 15,000 cycles, which corresponds to the NGV2 design lifetime of a tank (1,000 cycles per year for 15 years). Periodic inspection of NGV tanks was simulated by stopping the cyclic loading every 3,000 cycles, corresponding to 3

years of service, and performing an acoustic emission inspection of the tank. The internal pressure was increased until significant acoustic emission was detected. The acoustic emission response of the tank during pressurization and hold was used to evaluate the level of damage in the tank.

1.4 Report Overview

This report presents work performed in this project, along with background information to familiarize the reader with relevant topics, including acoustic emission inspection and damage tolerance of composite structures. Damage tolerance of composite structures, including composite overwrapped pressure vessels, such as NGV fuel tanks, is summarized in Section 2. The Phase 1 evaluation of in-service NGV fuel tank inspection methods is described in Section 3. Section 4 discusses acoustic emission inspection and Section 5 describes the fiber tow testing. The testing of NGV fuel tanks in Phase 2 is presented in Section 6. Section 7 provides a discussion of the project results in the context of the project objectives.

2.0 DAMAGE TOLERANCE OF COMPOSITE STRUCTURES

Evaluating the effect of damage on overwrapped NGV fuel tanks was one of the objectives of this project. This section discusses damage tolerance of composite structures, in general, and damage tolerance of composite overwrapped pressure vessels (COPVs), in particular. An overwrapped NGV fuel tank is an example of a COPV.

Damage tolerance of composite structures, in general, and composite overwrapped pressure vessels, in particular, has been addressed through research and practical experience [e.g., 33-37]. The response of composite materials to impact loading is fundamentally different than the response of metals. Metals absorb the incident kinetic energy of the impactor through elastic and plastic deformation. Because a composite has a severely limited ability to deform plastically, the incident impact energy produces a complex damage zone, in which the extent and nature of damage depends on details of the impact event and the material and geometry of the composite structure. Damage created by the impact event may include delamination, matrix cracking, and fiber breakage. The impact produces a composite structure with degraded properties, which depend on the nature and extent of the damage. Experimental and analytical methods are employed to define the damage and the residual properties of the composite. Generalizations are difficult when discussing impact of composites, because few standards are available for testing or analyzing the damage tolerance of composite structures.

Damage produced in a composite laminate and the subsequent residual properties of the laminate will vary, depending upon the specific impact conditions. Impact events range from low velocity impact by a large mass, such as a dropped tool, to moderate velocity impact by a smaller mass, such as a stone on the highway, to hypervelocity impact by a small mass, such as a micro-meteoroid in space. This discussion focuses on low to moderate velocity impact, which includes many of the impact events that occur during fabrication, handling, and operation of composite structures, including NGV fuel tanks.

2.1 Damage

Impact damage in a composite laminate can include matrix cracking, delamination, and fiber breakage. Matrix cracking is attributed to transverse tensile stresses caused by membrane response of the structure to the impact. Delaminations tend to occur at interfaces between laminate plies with different fiber orientations. Fiber breakage is caused by contact stresses in a local region at the impact point. Fibers also break at higher impact energies, which may cause complete perforation of the composite structure.

The type and extent of damage depends on a number of impactor and composite structure parameters. As shown in Figure 1, impact energy can be used to define three regions of different impact damage and associated residual strength of the composite structure [34]. In Region I, no damage and no strength reduction occurs because the impact energy is below a damage threshold. In Region II, above the damage threshold energy, a small surface indentation may be observed at the contact point. In addition, significant internal delamination and matrix cracking

occurs. Damage and strength reduction increases with impact energy until a maximum damage size and strength reduction is reached. Fiber breakage occurs at higher energy levels in Region II. In Region III, complete perforation of the structure occurs and the damage and residual strength remain constant with increasing impact energy. The specific impact energies associated with each regime depend on the specific characteristics of the impactor and the composite structure.

Damage size can been defined in terms of the projected delamination area observed on an ultrasonic C-scan or radiograph of the post-impacted specimen. Using this definition, the damage size for a specific composite material varies linearly with the kinetic energy of the impactor. Different linear relationships will hold for different laminates, especially for laminates with different numbers of plies. The ability to visually detect impact damage in a composite structure depends on the indenter size and contact pressure, as shown in Figure 2 [36]. In many cases, significant internal damage is caused by impact with no apparent indication on the surface of the structure. This is particularly true in carbon/graphite fiber reinforced composite structures.

2.2 Material Influences

The response of a composite material to impact loading depends upon the properties of the individual constituents, fiber, matrix, and fiber-matrix interface. Generally speaking, damage due to low impact energies is associated with failure of the matrix (matrix cracking) and interface (delamination) whereas damage due to high impact energies includes fiber failure.

2.2.1 Fiber

Fibers are the primary load carrying constituent in a composite structure. For low velocity impact, the ability of the fiber to store energy elastically has a significant effect on the damage tolerance of the composite. Therefore, fiber strain energy is one parameter that can be increased to improve the impact properties of the composite. For a specific fiber material, higher fiber elongation results in higher energy absorption. For example, the advantage of Kevlar fibers for impact resistance can be characterized by the large area under the stress-strain curve for Kevlar reinforced composites. Fibers are also important in the post-impact residual strength of the composite structure. Fibers with high elongation tend to exhibit good post-impact residual tensile strength, as shown in Figure 3 [37]. Fibers with high compressive stability, due to their modulus and/or diameter, tend to exhibit good residual compressive strength.

2.2.2 Matrix

In a composite material, the matrix serves to transfer load between fibers and to stabilize and support the fibers. An increase in elongation and toughness of the matrix results in improved impact resistance of the composite. Much work has been done to improve damage tolerance by developing a tougher matrix material using techniques such as adding plasticizers, adding rubber particles, adding polymer interleaf plies, and employing thermoplastic materials. The addition of polymer or adhesive interleaf plies suppresses delamination by increasing interlaminar toughness and reduces damage at the impact site by effectively increasing the contact area. The effect of

resin toughness on composite interlaminar fracture energy is illustrated in Figure 4 [33]. Use of a toughened matrix also produces a composite with improved post-impact compressive strength, due to the reduced level of damage and improved resistance to fiber buckling. The matrix properties do not appear to significantly affect the tensile residual strength in the fiber direction, which is primarily a fiber dominated property.

2.2.3 Fiber-Matrix Interface

The strength of the fiber-matrix interface, which is often dependent upon the specific fiber surface treatment, also has a significant effect on both the impact damage and the residual strength of the composite. A lower strength interface tends to produce large areas of fiber splitting and delamination with poor residual compressive properties. This may be desirable where impact resistance is more important than residual compressive strength. A higher strength interface produces a more local damage zone, which will improve the subsequent residual properties. However, the fiber treatment associated with a stronger interface may be more notch sensitive resulting in a lower residual tensile strength. The effect of surface treatment on residual tensile and compressive strength is illustrated in Figure 5 [33].

2.2.4 Strain Rate Dependence

Because some composite materials exhibit a strain rate dependence, caution is advised when using data from static tests to characterize the dynamic impact response of a composite. When tested in the fiber direction, carbon fiber composites tend to be rate insensitive, whereas graphite fiber and Kevlar fiber composites exhibit an increasing modulus and strength with increasing strain rate. For matrix-dominated properties, such as interlaminar fracture toughness, the effect of strain rate also depends upon the specific materials and the range of strain rate. Generally speaking, brittle matrix materials, such as thermosets, do not exhibit a significant strain rate dependence, whereas tougher matrix materials, such as thermoplastics, do.

2.3 Design Influences

In addition to the materials used in a composite structure, the design of the structure also affects its damage tolerance. Significant design features include the laminate stacking sequence (lay-up) and the geometry of the structure.

2.3.1 Stacking Sequence

Damage tolerance of a laminate depends upon the stacking sequence. Unidirectional laminates tend to split and fail at low impact energies. The addition of 45° plies increases the flexibility of the laminate and its ability to absorb energy. Placing 45° plies on the external surfaces of a laminate helps to protect the load-carrying 0° plies from damage. The mismatch in bending stiffness between adjacent plies has a significant effect on the level of delamination damage that occurs at the interface. Therefore, adjacent plies with abrupt changes in fiber orientation will have a lower damage tolerance. Other ways to improve damage tolerance in a laminate include

using woven fabrics and three-dimensional reinforcement to resist delamination, and employing more than one fiber in a hybrid composite to take advantage of the superior impact resistance of a particular fiber. Post-impact residual strength can also be improved in these ways, but not always. For example, using external 45° plies may improve impact damage protection but may decrease post-impact compression strength due to damage in these external plies.

2.3.2 Geometry

For low velocity impact loading, the size and geometry of the component is significant in determining the resulting damage, because they influence the component's ability to store energy elastically. Geometry plays a role in determining the response of a composite structure to impact loading, as shown in Figure 6. In a thin, flexible composite structure, initial failure occurs in the plies opposite the impact site due to tensile stresses applied as the part flexes in response to the impact load (bottom illustration in Figure 6). The matrix cracks are deflected at the lowest ply interface to form a delamination. This process of matrix cracking and delamination can then be repeated and progress throughout the structure.

In a thicker, stiffer composite structure, the initial failure occurs at the surface where the impact load is applied, due to the local contact stress field (top illustration in Figure 6). Structures with less constraint, such as a beam, tend to be capable of absorbing more energy than a more constrained structure, such as a plate. For low velocity impact, the size of the composite structure is linearly related to the amount of impact energy required to initiate damage (damage initiation threshold energy). However, once damage initiates, large structures are not necessarily better at absorbing energy than small ones. Therefore, care must be exercised when using one specimen size or geometry to represent the impact response of a structure of a different size or geometry. These differences are less important in high velocity, low mass impact, because the damage tends to be more localized to the vicinity of the impact.

2.4 Analytical Methods

Low velocity impact is modeled using analytical methods of varying sophistication, from simple spring mass models to finite element models. The spring mass models give good predictions when the mass of the impactor is large with respect to the composite structure and when the impactor contact times are relatively long. A number of springs can be used to represent the various responses of the composite structure, including the flexural, shear, and membrane responses. Energy-balance models have been used to predict the maximum contact force and the contact duration, as compared to the entire time-history of the impact event. Stress waves produced by an impact event have also been modeled and used to predict the response of a laminate. The dynamic impact event has also been approximated by a static indentation, in which the elastic response of the indenter and the structure are modeled. The contact between a spherical indenter and a composite structure can be modeled with a modified Hertzian contact law. In composites, permanent indentations generally occur even for small loads, and the loading response is different from the unloading and reloading response. Accurate modeling of the contact force history requires experimental development of the contact law for a specific

impactor-structure combination. Although beam and plate models can be used to predict overall structure response and contact force history, more detailed models are required to accurately predict the local response near the impact site and the complex failure of the composite structure due to the impact event. For example, delamination caused by impact depends upon transverse shear and normal stresses, which may not be accounted for in simple models.

Impact damage in a composite laminate is a complex condition, which may include failure of the matrix, fiber, and fiber-matrix interface. Therefore, impact damage is sometimes modeled as an equivalent crack or hole, which is an approximation for predicting residual tensile strength. The diameter of the equivalent hole and the length of the equivalent crack are equal to the width of the damage as measured on an ultrasonic C-scan. The laminate tensile strength decreases from its undamaged value to that of a laminate with a hole of diameter equal to the size of the impactor.

In compression, post-impacted laminates exhibit strength reduction due to local instabilities caused by the matrix cracking and fiber-matrix interface damage. The residual compression strength tends to reach a minimum value, where little additional reduction results from further damage. Delaminations caused by impact can buckle under compressive loading parallel to the delamination. In some cases, the delamination can grow, causing further decrease in compressive strength.

2.5 Test Methods

Low velocity impact is usually simulated using a falling weight fixture or a swinging pendulum, such as a Charpy or Izod pendulum test. The drop weight tests offer the advantages of evaluating different test conditions, including specimen and impactor geometry, and generating quantitative data, such as impactor velocity and force, which facilitates understanding of the energy absorption process in the material. Indentation tests have also been used as a simple, static test to characterize damage tolerance and correlate with data from other impact test techniques. The high velocity low mass impact is typically simulated with a ballistic device, such as a gas gun.

2.6 Damage Tolerance of Composite Overwrapped Pressure Vessels

A composite overwrapped pressure vessel (COPV) is a pressure vessel fabricated by filament winding a composite material over a liner. The resulting structure provides pressure containment capability at a lower weight than an all metallic pressure vessel. The liner, which can be a metal or polymer, provides the fluid containment, while the overwrap, which is typically wet-wound glass, carbon, or Kevlar fibers, provides the structural strength. The proportion of load shared between the liner and the overwrap depends on the design of the COPV. In a COPV with a plastic liner, the overwrap effectively carries all the load.

2.6.1 Applications of COPVs

COPVs have commonly been used in a variety of applications. Commercial products include self-contained breathing apparatus (SCBA) and NGV fuel tanks [1-3]. These lightweight tanks

are particularly advantageous for aerospace applications, such as spacecraft propellant storage tanks [4-10]. Because aerospace COPVs are optimized for minimum weight, they are typically thinner than commercial tanks. The service environments for COPVs are as varied as their applications. At one extreme are the spacecraft propellant tanks, which are handled with the care afforded an aerospace component and used just once. At the other extreme are the NGV fuel tanks, which are mass produced and then used for many years in an extremely varied and uncontrolled service environment.

In recent years, COPVs have replaced metallic tanks for use as spacecraft pressure vessels. The high specific strength and stiffness of a graphite-epoxy composite overwrap enable up to 50 percent weight savings to be achieved by using COPVs instead of metal tanks. Typical liner materials for space applications include aluminum alloys, stainless steel, and titanium. COPVs have been used as gaseous helium bottles and propellant tanks in the Space Shuttle, launch vehicles, upper stage boosters, and spacecraft. In these applications, the stored energy released during burst of a COPV can cause significant damage due to the resulting blast wave and broken fragments. A leaking COPV can also pose a hazard to ground personnel, due to the toxicity and flammability of stored gases, such as nitrogen tetroxide and hydrazine.

Current COPVs for military applications are designed, analyzed, and qualified per MIL-STD-1522A, "Standard General Requirements for Safe Design and Operation of Pressurized Missile and Space Systems" [26]. However, MIL-STD-1522A does not address COPVs, in general, or the composite overwrap, in particular. Results of a survey of COPV manufacturers indicated no consistency in the design, analysis, fabrication, and inspection of COPVs for space applications [21]. In addition, much of the information concerning COPVs is considered proprietary by the manufacturers. No procedures and specifications exist for inspecting and evaluating COPVs that are subjected to impact events during fabrication, handling, or service. Therefore, the USAF and NASA initiated a project entitled Enhanced Technology for Composite Overwrapped Pressure Vessels to evaluate COPVs and COPV technology and to recommend specifications applicable to COPVs used in space applications.

As composite structures, COPVs are susceptible to impact loads that can cause damage, which may not be visible, especially in carbon reinforced overwraps. Although graphite-epoxy is less susceptible to environmental and chemical degradation than fiberglass, concern exists for significant loss of strength due to impact, which may not be visibly apparent. In an Army study, the burst strength of a graphite epoxy COPV was reduced by a factor of four by dropping a nine pound hammer on it from a height of six inches [21]. Factors that affect the post-impact burst strength of a COPV include the pressure vessel size, the overwrap thickness, and the impact conditions.

COPVs are also subject to environmental and chemical degradation, especially in glass reinforced overwraps. Reported service failures of fiberglass NGV tanks and SCBAs have been attributed to chemical exposure and stress corrosion cracking. The Gas Research Institute investigated the cause of NGV tank failures and evaluated the use of COPVs for NGV tanks [11-19]. FaAA investigated the failure of a fiberglass, overwrapped SCBA cylinder, that was

attributed to stress corrosion cracking of the fiberglass composite following exposure to a highly acidic liquid [69].

2.6.2 Enhanced Technology for Composite Overwrapped Pressure Vessels Project

An ongoing USAF and NASA sponsored project, entitled Enhanced Technology for Composite Overwrapped Pressure Vessels, is assessing COPVs for spacecraft applications and developing realistic requirements for these structures [20-30]. One focus of the Enhanced Technology for Composite Overwrapped Pressure Vessels project is impact damage tolerance of COPVs. The project is addressing the prevention of impact damage during manufacturing and service, the effect of impact loading on COPV material, and the residual properties of impacted COPVs. Tests are being conducted to evaluate designs for handling and shipping containers that mitigate COPV damage when an impact event occurs. Techniques for visibly indicating that an impact event has occurred are being evaluated.

Impact testing includes evaluation of variables, such as impact location on the COPV, the internal pressure and fluid in the COPV, and the geometry of the impactor. The post-impact residual strength of the COPV is being evaluated. Other tests are intended to measure the impact threshold for visible damage and for damage that reduces the burst strength by 20%. The impact test facility at White Sands Test Facility, illustrated schematically in Figure 7, accommodates impact testing of empty tanks and tanks pressurized with liquid or gas. The hazards associated with potential burst of a pneumatically pressurized tank makes this a unique capability of White Sands. The test facility includes an instrumented impact drop tower and a high speed video camera to record the contact of the impact tup on the tank.

Test specimens used in the USAF project are primarily flight-qualified graphite-epoxy COPVs built by major US COPV manufacturers. The COPV designs include spherical and cylindrical tanks with steel and aluminum liners overwrapped with graphite/epoxy. The operating pressures are either 4,500 psig or 6,000 psig. The spherical COPVs are 10.15 and 19 inches in diameter and have 0.18 inch thick overwraps. The cylindrical COPVs are 20 to 25 inches long × 6.6 to 15 inches diameter and have 0.035 to 0.041 inch thick overwraps.

One noteworthy result of the Enhanced Technology for Composite Overwrapped Pressure Vessels project concerns impact testing of empty and pressurized tanks. As expected, the presence of internal pressure during impact has a significant effect on the resulting overwrap damage. Impact of an empty tank produces a local indentation at the impact site, with broken fibers and cracking away from the site. Damage from impact of a pressurized tank is more localized to the impact site, typically consisting of an indentation containing cracks associated with broken fibers. The difference in damage is consistent with the difference in support provided by the internal pressure and the corresponding response of the overwrap to the impact load.

Results of impact testing showed that internal pressure at the time of impact also effects the residual burst strength of a COPV. In particular, the effect is design dependent. For spherical

tanks, a higher residual strength was measured in tanks that were impacted while pressurized. For cylindrical tanks, internal pressure reduced residual burst strength. Evidence was obtained that the effect of pressure on residual burst strength may depend upon the pressure level and may not be monotonic. Therefore, residual strength measured by testing empty tanks may not be conservative with respect to the strength of pressurized tanks. This finding provides an important caution for impact testing empty tanks to characterize the residual burst strength of impacted pressurized tanks.

No difference was reported between the response of tanks that were pressurized with liquid or gas during impact. Naturally, pneumatic burst testing does produce greater damage and fragmentation than hydraulic testing.

The burst failure of virgin tanks was also found to be different than that of impacted tanks for both spherical and cylindrical designs. Virgin spherical tanks fail at the boss and virgin cylindrical tanks fail in the cylindrical region. However, in both cases, post-impacted tanks fail at the impact site.

Two supposedly identical COPVs were subjected to the same impact loading while pneumatically pressurized in the White Sands impact test facility [27]. The COPVs were pressurized to 6,300 psig when impacted at 15 ft-lbs with a 0.5-inch diameter impactor in the cylindrical region just below the transition to the dome. One COPV survived the impact load and was subsequently pressurized to failure at 7,500 psig, as shown in Figure 8. The second COPV failed 0.7 seconds after being impacted, as shown in Figure 9. Significant damage was done to the test facility, including the thick steel containment structure surrounding the tank, as shown in Figure 10. The destructive force of the energy stored in the COPV is seen in the bent steel fixtures in the figure. The difference in damage tolerance of these two COPVs was attributed to variability in the tanks.

3.0 PHASE 1 -- IN-SERVICE INSPECTION OF NGV FUEL TANKS

In Phase 1 of this project, a study was conducted to evaluate potential techniques for in-service inspection of composite overwrapped NGV fuel tanks. Applicable literature was reviewed and relevant information obtained to compare the practical and technical features of candidate techniques. The study addressed the NGV service environment, inspection environment, and inspection methods.

3.1 NGV Service Environment

This portion of the Phase 1 study addressed the following questions:

- What is the NGV service environment and how can it affect an NGV tank?
- What types of damage and degradation need to be detected by the inspection technique?

The NGV service environment study considered a number of potentially detrimental conditions, including corrosion, material aging, ultraviolet exposure, vibration and wear, impact, chemical exposure, temperature, and moisture, and any combination of these conditions. Impact damage, chemical exposure, and ambient conditions were identified as the service conditions of greatest concern. The relative importance of these factors depends, in part, on the particular design of the fuel tank. Impact damage will be a primary concern for a carbon fiber overwrapped tank but of less concern for a glass fiber overwrapped tank because the more brittle carbon fiber is more easily damaged due to impact loading. For example, the 1996 Los Angeles failure of a Type 4, carbon fiber overwrapped tank has been tentatively attributed to impact damage to the overwrap. Just the opposite is true for chemical exposure, which is more important for a glass fiber overwrapped tank than for a carbon fiber overwrapped tank because glass fibers are more chemically sensitive than carbon fibers. In 1994, two glass-fiber overwrapped, Type 3 tanks failed, one in northern California and one in Minnesota. These failures were attributed to stress corrosion cracking of the fiberglass overwrap due to exposure to acid.

3.2 NGV Fuel Tank Inspection Environment

The following questions were addressed in this portion of Phase 1:

- What is the expected inspection environment?
- Who will perform the inspection and what skills can this person be expected to have?

The Phase 1 study defined the inspection environment as an automotive garage environment manned by auto mechanics with specialized training in NGV fuel tank inspection. Auto mechanics are familiar with computer-controlled diagnostic equipment commonly found in a modern automotive repair shop. Systems are in-place for training and certifying mechanics to perform a variety of different specialized tests, such as a smog test or safety inspection. The

ability to perform the inspection with the tank in place was considered advantageous, in order to prevent damage by removing and reinstalling the tank.

3.3 NGV Fuel Tank Inspection Methods

The available methods for inspecting composite overwrapped NGV fuel tanks were evaluated in order to address the following questions:

- What are the candidate techniques that could be used to inspect NGV tanks?
- What are their practical and technical capabilities and limitations for this application?

The Phase 1 study evaluated a wide variety of inspection techniques, including visual, optical, dye penetrant, magnetic particle, radiography (X-ray), ultrasonics, thermography, shearography, eddy current, microwave, and acoustic emission. In the evaluation, emphasis was placed on inspection techniques that had been successfully used to inspect composite structures, in general, and composite pressure vessels, in particular. The various techniques were compared according to their technical capabilities and practical features relevant to in-service inspection of NGV fuel tanks. The results of this comparison are summarized in Table 1.

Phase 1 considered information from the scientific literature, including data from the on-going USAF/NASA Enhanced Technology for Composite Overwrapped Pressure Vessels project. FaAA's experience with inspecting composite structures, including NGV fuel tanks, was also considered in Phase 1. FaAA has inspected composite structures employing a variety of techniques, including visual, ultrasonics, X-ray, thermography, and eddy-current methods. FaAA previously inspected overwrapped NGV fuel tanks using ultrasonic and X-ray computed tomography (CT) techniques. Although ultrasound is a standard inspection technique for composite laminates, its ability to detect defects in the filament wound overwrap was inhibited by the many fiber tows oriented in different directions. CT inspection did provide a three-dimensional image of damage in the composite overwrap, but the associated cost and hazard make CT impractical for in-service NGV fuel tank inspections.

The evaluation of candidate inspection techniques identified acoustic emission inspection as the most promising approach for NGV fuel tanks for both practical and technical reasons. Acoustic emission inspection has the practical advantage of being the only inspection technique that can inspect the entire fuel tank without removing the tank from the vehicle. In this way, acoustic emission augments visual inspection, which also provides useful information about the condition of the tank. The acoustic emission inspection methodology and equipment are consistent with the postulated inspection environment. A review of work performed on composite materials and COPVs used for NASA and the Department of Defense indicated that acoustic emission inspection shows promise as a viable inspection technique for fiber overwrapped NGV fuel tanks. Therefore, in Phase 2, acoustic emission inspection was evaluated for detecting the presence of impact damage in overwrapped NGV fuel tanks during 15 years of simulated service.

4.0 ACOUSTIC EMISSION INSPECTION

Acoustic emission refers to the "sound" made by a structure when it fails. Some familiar examples of acoustic emission are sounds made by breaking a dry twig or a piece of glass. In these familiar cases, the sound is audible by the human ear. In other structures, the amplitude and/or frequency of the sound produced is outside the range that can be heard by the human ear. However, acoustic emission sensors with the ability to "hear" these sounds can be attached to a structure in order to detect changes which can lead to failure. The objective is to detect localized failure in a material before it causes catastrophic failure of the structure. Because structural failure is typically a progressive process that occurs over time, acoustic emission inspection can serve as an early warning system to prevent catastrophic failure.

In industrial applications, acoustic emission inspection is intended to detect the transient elastic waves that are created by a material as it strains under load. In an acoustic emission inspection, acoustic emission sensors are attached to the structure and "listen" for emissions while a load is applied to the structure. Acoustic emission sensors are made of piezoelectric material, which converts the elastic waves into electrical impulses. Specialized acoustic emission electronic equipment and computer software are used to acquire, analyze, and store information about the elastic waves. This information can include the entire wave, features of the wave, such as its amplitude and frequency, or the number of waves (acoustic emission events), including their magnitude and duration.

For inspecting NGV fuel tanks, acoustic emission has several advantages over other inspection techniques. Foremost amongst these are the ability to remotely detect damage and to monitor damage growth in real-time. However, the challenge encountered in using acoustic emission is the interpretation of the data. The typical approach is to attach resonant acoustic emission sensors to the structure to be monitored, detect all events, and then plot these as a function of time or pressure. Features in the plots are then correlated to possible damage mechanisms to infer information about the state of the tank. The problem with these methods is that they do not differentiate the different damage mechanisms that occur in the fuel tank, some of which may or may not contribute to the ultimate failure.

Recent work in acoustic emission has shown that these qualitative techniques can be replaced by wave mode analysis (modal acoustic emission), much as is done in seismology. If the true surface displacements of an emission source are analyzed, much more information about the source can be obtained. Features of the emission, such as wave mode shapes, relative mode amplitudes, and frequency content contain information about the source. Thus, modal acoustic emission analysis provides capabilities to sort the events according to source and to analyze only the data that is pertinent to the potential failure of the structure. Modal acoustic emission was the approach used in this project.

Once the damage mechanisms have been identified, two approaches are available to analyze the strength of a damaged composite structure, such as a pressure vessel. One approach is a strength of material analysis. This method requires the ability to locate the damage and then determine

defect size. While the strength analysis approach is straightforward, determining defect size in a composite is very difficult.

A second method of evaluating a damaged composite structure is a statistical strength analysis based on the failure mechanism. For many composites, the mechanism responsible for ultimate failure is fiber rupture. Thus, by using acoustic emission inspection to monitor the number of fiber break signals, one could determine if fibers are failing at a rate greater than that predicted by the statistical strength distribution for a 'standard' vessel. If they are, then the vessel is no longer fit for service. From an acoustic emission standpoint, this method is much more tractable, since rate and distribution analysis of fiber breaks is easier than defect size determination. Thus, modal acoustic emission provides the physical link to the statistical strength theory for the composite structure, in this case, the overwrapped NGV fuel tank.

4.1 Wave Propagation in Thin Plates

Many structures are geometrically plate-like, that is, the thickness is much less than the other two dimensions. Acoustically, a thin plate is one in which the wavelength of the propagating disturbance is much greater than the thickness of the plate. If this is true, then classical plate theory can be used to predict the propagating wave characteristics. From this theory, two types of waves can be predicted: extensional, or in-plane (tension/compression), and flexural, or out-of-plane (bending). The dispersion (velocity) equation for the extensional mode is

$$c_l = \sqrt{\frac{E}{\rho(1-\nu^2)}} \tag{1}$$

where: c_l is the extensional mode velocity
E is Young's modulus
ρ is density
ν is Poisson's ratio.

For the flexural mode the relationship is

$$c_f = \sqrt[4]{\frac{D}{\rho h}\omega^2} \tag{2}$$

where: c_f is the flexural mode velocity
$D = Eh^3/12(1-\nu^2)$
ω is the circular frequency (/s)
ρ is density
h is the plate thickness
ν is Poisson's ratio.

The important point to note about the dispersion relationships for the two modes is that the flexural mode is a function of frequency, while the extensional mode is not. Therefore, one can distinguish between the two modes based on their respective propagation characteristics.

Examples of plate waves in a 0.125 inch thick aluminum plate are shown in Figure 11. The waves were excited by breaking a Pentel 2H 0.3 mm diameter pencil lead on the surface of the plate to excite the flexural mode, and on the edge of the plate to excite the extensional mode. (Pencil lead breaks are typically used "standard" sources of acoustic emission.) In Figure 11, notice that the higher frequencies arrive earlier in the waveform, as predicted by Equation 2. Higher order plate theories can be used to account for the dispersion seen in the extensional mode and for the fact that the flexural mode equation has infinite velocities at infinite frequencies.

4.2 Conventional Acoustic Emission Inspection of Pressure Vessels

Acoustic emission inspection is a standardized technique for inspecting metal pressure vessels [2-4]. Acoustic emission inspection was subsequently adapted to inspection of low pressure, composite vessels, such as chemical storage tanks and railroad tank cars [5-8]. According to the standards, the acoustic emission inspection method is limited to fiberglass reinforced plastic vessels operating at pressures up to 65 psia. Acoustic emission equipment, including sensors, electronics, and software, are commercially available to perform the inspection according to the specification. Recent work addresses application of acoustic emission inspection to all steel (Type 1) NGV fuel tanks [9-11] and development of a specification for acoustic emission inspection of composite overwrapped (Types 2, 3, and 4) NGV fuel tanks [12].

The inspection of pressure vessels using acoustic emission has typically consisted of attaching resonant sensors to the vessel and then capturing events that are excited due to sources in the vessel. Various parameters, such as the number of acoustic emission events, event rate, amplitude, duration, and energy, are then used to describe the detected signals. This approach is sometimes referred to as parameter-based acoustic emission. The test configurations (material, damage type, loading) are then varied in known ways to produce dominant damage mechanisms. The correlation between damage type and acoustic emission is then made through these tests.

Researchers, such as Mitchell [13-14], have approached the problem of acoustic emission inspection of NGV fuel tanks from a purely empirical standpoint. In this work, two sensors were mounted on NGV tanks made with glass and carbon fibers wrapped over a plastic liner to monitor the number of acoustic emission events (counts) as a function of pressurization. One of the tanks was a control tank (no damage), the other had been damaged by impact loading. To determine the burst pressures of the tanks, the authors pressurized the tanks and noted the point at which the slope of the counts versus pressure curve began to increase significantly ("the knee of the curve"), as shown in Figure 12. They then determined the pressure where this "knee" occurred, and used this pressure to correlate to burst pressure, which varied by 47%. Although this study is limited because only two tanks were tested, differences in the two tanks were observed using this approach. While this method does show promise, it has some drawbacks. The

major one is that the authors in no way include any material analysis or failure modes in their study. Ignoring the material and its failure modes can lead to misinterpretation of data and ambiguous analyses and results.

Correlations between other acoustic emission parameters besides counts have been attempted. The work by Hamstad [15] covers many of these correlations. In this study, epoxy impregnated Kevlar-49 fiber was wound onto spherical aluminum shells (114 mm diameter × 2 mm wall thickness). Manufacturing variations, such as winding tension, fiber volume and winding angle, were incorporated into the specimens. Specimens were then damaged using varying impact energies. Hamstad found that damage growth could be separated into stable and unstable growth by monitoring acoustic emission during load holds. If acoustic emission activity was occurring and increasing during the load holds, it was identified with unstable growth. If no acoustic emission activity or decreasing activity occurred, it was identified with stable defect growth. For the specimens with unstable growth, the number of events and event durations were correlated with burst pressure, which varied by 40%. However, for the specimens with stable growth, the burst pressures did not correlate with any of the typical acoustic emission parameters. Results of the testing are shown in Figure 13. Some specimens, such as Data Point "D" in Figure 13, did not exhibit high event rates (which typically indicates significant damage), but still burst at low pressures. Hamstad found that if a substandard fiber lot is used, or the matrix does not redistribute the stresses of broken fibers correctly, burst pressures below average will result. The events produced by these failures may not fall into the acoustic emission event parameters predicted by correctly manufactured vessels, and thus the correlations fail to screen these vessels.

Gorman [16] approached the problem of acoustic emission inspection of composite pressure vessels from a statistical strength viewpoint in his 1990 work on burst pressure prediction. He hypothesized, based on work by Rosen [17] and Phoenix and Wu [18], that randomly located events during pressurization do not affect the strength of the vessel. To reduce these random events, he first pressurized, or proofed, the graphite/epoxy vessels (20 inch diameter × 42 inch long) to 80% of predicted burst pressure. After this the vessels were then impacted and cycled. Results for a control vessel (no damage) and an impacted vessel are presented in Figure 14. By monitoring only the load hold events (due to instrumentation limitations), Gorman was able to correlate the number of events with burst pressure, which varied by less than 20%. He further showed that the number of events at the most active sensor produced an even better correlation, thus confirming in a crude way the stress concentration concept in the statistical strength theory. Thus, by proofing the vessels prior to damage, Gorman was able to reduce the number of events which do not affect the strength of the vessel. This allowed him to only monitor events which corresponded to the damage caused by the impact, and ignore other events.

While the conventional, parameter-based acoustic emission methods have shown promise, acoustic emission has not gained the reputation of other inspection methods, such as ultrasonics and X-ray. This is mostly due to the qualitative nature of acoustic emission inspection as conventionally implemented. If the specimen geometry, material or loading is changed, the results of the acoustic emission tests are no longer valid, and the parameter based analysis must be re-evaluated for a new set of tests. The resonant sensors and narrowband filtering used in

conventional acoustic emission provide only a small window of data for the researcher to analyze. The connection between the acoustic emission parameters and a source mechanism is tenuous at best, due to attenuation, sensor response, wave propagation and instrumentation. Nevertheless, even with these limitations, acoustic emission has shown the capability to detect substandard vessels. For acoustic emission to become accepted as a quantitative inspection technique, the physics of the source and its relationship to the behavior of the structure must be correlated to the acoustic emission measurement.

4.3 Modal Acoustic Emission Testing

Existing standards for acoustic emission inspection of composite pressure vessels do not apply to composite vessels operating at high pressure, such as overwrapped NGV fuel tanks. Application of acoustic emission inspection to high pressure composite vessels has been the subject of much research [19-32]. Current research into acoustic emission inspection of high pressure composite pressure vessels focuses on applying a modal acoustic emission, waveform-based approach. In the modal acoustic emission approach, entire waveforms from the true surface displacements of the stress wave are captured and analyzed, rather than waveform features, as is done in the parameter-based approach. The development of high fidelity sensors and high fidelity, high speed digital data acquisition equipment has made the modal acoustic emission approach practical. Once the waveforms are captured, they can then be analyzed, characterized, and compared with theory to provide a measure of structural response. For example, with modal acoustic emission, acoustic emission caused by fiber breakage can be distinguished from emission caused by matrix cracking. Modal acoustic emission can also be used to determine the location of the emission source, so that a defect or damaged area can be located and not just detected. While a waveform-based acoustic emission inspection method results in a larger amount of data captured, the greater amount of data in the waveform provides the researcher with much more information about the source.

The waveform based acoustic emission approach also solves the problem that structurally insignificant flaws may produce emission. By studying the waveforms, defect sources can be identified and their severity determined. Another common problem with acoustic emission inspection is discriminating noise sources, such as electromagnetic interference (EMI), fill noise and mechanical noise, in the data. With modal acoustic emission, emission from noise sources and from damage growth mechanisms can be easily separated by acquiring and analyzing the broadband signal.

While the modal acoustic emission testing and analysis methods are in their infancy, the real-time monitoring capability coupled with the amount of data about the source available to the researcher makes this technique unique. By combining the damage identification capabilities of modal acoustic emission with the statistical strength analysis methods, pressure vessel strength and lifetime predictions should become more accurate.

Wave propagation measurements have been made by Gorman [26], and Prosser and Gorman [27]. These papers show that wave propagation in engineering structures can be detected and

analyzed, and compared closely with that predicted by theory. Effects of the source and source orientation on the resultant wave propagation have also been studied. Results by Gorman and Prosser [24] and Prosser [23] have shown that the source orientation has a large effect on the mode produced. Wave shape changes as the source is varied from an out-of-plane source (90°) to an in-plane source (0°) are shown in Figure 15. These results have been used in successful monitoring of fatigue crack growth in metallic structures. A waveform from the in-plane crack growth in a [0/90] composite is presented in Figure 16. The composite was loaded in tension along the 0° fibers until transverse matrix cracking occurred in the 90° plies. Notice the similarity of the waveform in Figure 16 to the 0° waveform shown in Figure 15. Thus, approaching the problem from the wave propagation viewpoint provides the basis for a physics based analysis in which acoustic emission sources are discriminated and identified.

The first application of modal acoustic emission to pressure vessels was the testing of aluminum lined Kevlar overwrapped pressure vessels [31]. The vessels had been in service for 10 years and were being burst tested to determine if any strength degradation had occurred over the lifetime of the vessel. In monitoring the vessels, two types of events were seen, short duration high frequency events, and high amplitude/high frequency events. The former events were thought to be due to single fiber breaks, the latter due to fiber bundle breaks. Since a fiber bundle break was felt to control the strength of the vessel much more than a single fiber break, the large amplitude events were used in the analysis. The data was normalized by dividing the high frequency/high amplitude events by the total number of events. Correlation with burst pressure which varied by less than 17%, as shown in Figure 17. The data is sorted based on whether the overwrap was bonded to the liner or not. The higher strain to failure of the aluminum liner may have influenced the failure of the fiber bundles.

4.4 Acoustic Emission Testing

All acoustic emission testing in this project was performed using the modal acoustic emission approach described in Section 4.3. Testing was conducted for FaAA by Digital Wave Corporation of Englewood, CO, using their F4000 Fracture Wave Detector AE system. The system consisted of B1025 broadband acoustic emission sensors, G/A 2040 preamplifiers, with -20, 0, 20, and 40 dB of gain, signal conditioning modules, and high speed analog-to-digital (A/D) acquisition capabilities.

The B1025 sensor is a high fidelity, piezoelectric transducer with a flat response from 50 kHz to over 1 MHz. Displacements on the surface of the transducer are converted to a voltage by the piezoelectric element. The G/A 2040 preamplifier amplifies this output voltage, 100 times for the tank testing. The amplified output from the preamplifier is input to a signal conditioning module that has both a high pass and low pass filter, along with a separate gain stage. The signal conditioning module also independently triggers the system to record an event. The independent trigger allows more selective capture of waveforms. For example, the system can be set to trigger only on signals containing a significant amount of high frequencies, but the low frequency portion of the signal will still be recorded when the system triggers. When triggered, the A/D boards digitize the signal from the conditioning module at a user selectable rate of 1, 5, or 10

MHz. A computer then stores the digitized waveforms. The system is also capable of independently recording parameter inputs such as load, strain, temperature, and pressure. For the tank tests, the pressure was recorded continuously during testing.

Once stored, waveforms were analyzed using Digital Wave's WaveDetector software. The software provides a variety of tools to analyze modal acoustic emission data, including the ability to look at individual event waveforms, calculate the frequency content of the waveforms through fast Fourier transforms (FFTs), perform digital bandpass filtering, and calculate events versus time curves for each test.

Four to eight sensors were attached to each tank using hot melt glue. The hot melt glue was used as both a couplant and adhesive between the sensors and the tanks being tested. The glue is easily applied, allows for simple removal of the sensors, and does not distort the waveform if applied in a thin layer. On one tank, a single sensor was applied with epoxy for comparison with the hot glue. No significant difference was noted in the performance of the sensors with the different adhesives.

All sensors were calibrated prior to their use in this project. A convenient technique for calibrating the frequency response of a piezoelectric sensor is a face-to-face calibration. A standard generating sensor is excited with a constant amplitude chirped sine wave whose frequency is swept from 1 kHz to 1.5 MHz. The receiving sensor undergoing calibration provides an output voltage as a function of frequency which is indicative of its receiving response.

A more accurate technique is the absolute sensor calibration. Digital Wave uses a laser interferometer calibration method to measure the absolute displacement response of the B1025. Such a calibration allows the sensitivity of the sensor to be positively calibrated in V/m as a function of frequency. This calibration technique is similar to the United States National Institute of Standards and Technology (NIST) Standard for acoustic emission sensors [70].

5.0 FIBER TOW TESTS

Modal acoustic emission was used to monitor carbon/epoxy fiber tow (bundle) specimens tested in uniaxial tension. The tow specimens were tested as a prelude to testing NGV tanks over-wrapped with the same carbon fiber/epoxy composite. The tow specimens are fiber dominated and the modal acoustic emission from the tow should contain a large number of events from fiber bundle breaks. The modal acoustic emission from the tows was recorded with a four channel Digital Wave Corporation F4000 Fracture Wave Detector (FWD) system.

5.1 Wave Propagation in Rods

Understanding the effect of boundary conditions on wave propagation in elastic solids is critical to understanding and interpreting the recorded modal acoustic emission. Common test specimen geometries include thin plates, thin rods, bars, and bulk media; all of which have different wave propagation characteristics. In Phase 2 of the project, tension tests were conducted on bundles of fibers (tows) impregnated with resin to characterize the acoustic emission response of the overwrap in the Type 2 tanks.

The tow test specimens closely resemble thin rods; they have a roughly circular cross-section and are much longer than the radius. In the frequency range used by modal acoustic emission, a large wavelength to radius ratio exists, and the rod (tow) can be modeled using a strength of materials approach. Using this approach, two possible modes of wave propagation in a rod are possible, a non-dispersive longitudinal mode and a dispersive flexural mode. The velocity equation for the longitudinal mode is given by:

$$c_l = \sqrt{\frac{E}{\rho}}, \tag{3}$$

where: c_l is the longitudinal wave velocity
E is the Young's modulus
ρ is the density.

For the flexural mode, the velocity is given by:

$$c_f = \left(\frac{EI}{\rho A}\right)^{1/4} \omega^{1/2}, \tag{4}$$

where: c_f is the flexural wave velocity
I is the moment of inertia of the rod
A is the cross-sectional area
ω is the circular frequency of the wave.

As in the case of the plate, Section 4.1, the important difference between these two modes is the flexural mode velocity is dependent on frequency and the longitudinal mode is not. Thus, one can distinguish between the two modes based on their propagation characteristics.

More complete and complex theories of wave propagation in rods exist that include the effects of lateral inertia, Poisson's ratio, rod diameter and rotational displacements. These theories account for the dispersive nature of the longitudinal mode at high frequency to rod diameter ratios, and the fact the flexural mode has an infinite velocity at infinite frequencies. Given the specimen size and frequencies of interest, Equations 3 and 4 are good approximations.

5.2 Test Setup

The tow specimens were fabricated from 61 cm strands of Grafil (34-700 carbon fiber) fiber impregnated with epoxy (Dow amine cure DER 383, Huntsman Chemical Jeffamine D-320, Dupont DCH-99). The epoxy/fiber strand was cut into manageable 30 cm lengths and aluminum tabs were glued to the ends. Figure 18 shows the epoxy/fiber strand in the fixturing used to mount the tabs to the strand. High shear strength epoxy (Loctite PN14600) was used to glue the tabs to the strand. The completed tow samples, such as the one shown in Figure 19, contained approximately 12,000 fibers and had a gage length of 22.4 cm. For testing, each tow specimen was placed in an MTS 880 hydraulic test machine and then instrumented with acoustic emission sensors.

For modal acoustic emission monitoring, four broadband, high fidelity sensors (Digital Wave Corp. B1025) were attached to the sample. The B1025 has a flat response from 50 kHz to over 1 MHz. The sensors were held in place with clothes pins, and coupled to the tow specimen with vacuum grease. The tow specimen in the hydraulic test machine with the sensors attached is shown in Figure 20. Typical sensor mounting locations are shown in Figure 21. The relative locations of the sensors are critical for accurate source location of the recorded waveforms. After placing the tow test specimen in the MTS grips and positioning the sensors on the tow, lead breaks were performed near both ends of the sample to insure the acoustic emission system was functioning properly and that good coupling of the sensors to the sample was obtained.

Four different tensile tests were then performed, as shown in the test matrix, Table 2. The samples were pulled at a constant rate, ranging from 0.0025 cm/min to 0.013 cm/min. The fourth tow test specimen was notched in the center using a razor to produce a small cut. This notch created a stress concentration during the test which should cause the nearby fibers to break first. The notched sample was pulled at 0.0025 cm/min. For all tests, the Fracture Wave Detector was configured the same. Each channel has independent signal and trigger filters and gain settings. All four channels were set to the values shown in Table 2.

5.3 Results and Discussion

A variety of sources for acoustic emission were identified during the tow tests, including matrix cracking and splitting, fiber and fiber bundle breaks, and mechanical noise from the grips.

Determination of which recorded signals are from damage occurring in the sample and which are random noise is an important part of the data analysis. Signal arrival times, amplitudes, frequency content, and duration can all be used to discriminate damage growth signals from noise. These methods are often applied simultaneously to discriminate signals.

To accurately use arrival times, theoretical velocity values must first be calculated. Using Equations 3 and 4 and typical modulus and density values ($E/\rho = 10^8$ m^2/s^2) for the tow test material, longitudinal and flexural mode velocities in the tow specimen were calculated. The flexural mode velocity for the fiber/epoxy tows is approximately 2000 m/s at 150 kHz. The extensional mode velocity is approximately 10,000 m/s. Using these velocity values and the distances between sensors, time of flight from one sensor to another was calculated. Table 3 shows the theoretical time for each mode to travel from one sensor to another. Waveforms with arrival time differences less than those shown in Table 3 originate between the sensors in question.

A waveform recorded during tow Test 1 is shown in Figure 22. The arrival time difference between Sensors 1 and 2 is approximately 30 μs (microseconds), indicating that the modal acoustic emission originated above the top sensor. The mode of propagation is flexural, indicating an out-of-plane source. The FFT of the waveform, Figure 23, indicates that the majority of the energy in the waveform is below 200 kHz. The arrival times, mode of propagation and frequency content all contribute to the analysis that the signal is the result of some mechanical source. This signal was identified as mechanical noise from the grips and was discarded.

The waveform and FFT from another signal recorded during tow Test 1 are shown in Figure 24. The mode of propagation is longitudinal, indicating an in-plane source. The arrival time difference between Sensors 3 and 4 is approximately 8 μs indicating that the signal originates below the bottom sensor. The FFT, Figure 25, shows that a significant portion of the signal energy is above 500 kHz, with a peak near 1 MHz. While the arrival times indicate the source is outside the sensor array, the in-plane source and high frequency content lead to the conclusion the signal is either the result of a fiber bundle break or matrix crack.

5.3.1 Typical Signals

Aside from noise, three typical acoustic emission event types were identified during the tow testing. The first type, shown in Figure 26, was an event that was recorded with significant amplitude on a single channel only. The waveform has a short duration and a significant percentage of the energy is in high frequency components. The single channel events are small amplitude events that occur near the individual sensors. The waveform is most likely attenuated before traveling to the other sensors. These small amplitude events may be due to sources, such as matrix cracking, single fiber breaks, and fiber debonds. Determination of the source mechanism for the small amplitude events would require visual verification using microscopic examination, which was beyond the scope of this study.

The second typical signal was a high frequency, short duration pulse recorded on all four channels, shown in Figure 27. These waveforms have a short duration, significant high frequency content, and are propagating in the longitudinal mode. The high amplitude of the signal indicates that the source released a significant amount of energy.

The third signal was similar to the second, except for a large trailing flexural mode in the waveform. An example of this type of signal is presented in Figure 28, which shows a fiber break signal with a flexural mode component. The large low frequency portion (near 70 μs) of the wave form in Channel 1 is a flexural mode. The flexural mode is still visible in Channel 2, near 100 μs, but it has been attenuated. Also, the difference in velocity between the longitudinal mode and flexural mode is clearly seen in the arrival time differences between Channels 1 and 2.

These different events have several possible source mechanisms. The second and third signal types can possibly be explained by single fiber breaks or fiber bundle breaks. A fiber/bundle break near the center of the tow is essentially an in-plane source and should produce only longitudinal mode vibrations. A fiber/bundle break near the surface of the tow will produce a longitudinal wave from the fiber separation, as well as a flexural mode from the moment generated by the off-axis stress redistribution. The different possible source locations are illustrated in Figure 29.

5.3.2 Source Locations

Waveform arrival times can be used to calculate the location of the acoustic emission source. The small notch cut into tow test Specimen 4 produced a stress concentration near the notch. The fibers in the tow should fail near the notched area first. Using sensor locations and large amplitude waveforms recorded before the crack splitting, source locations were calculated. The relative arrival times at each sensor were calculated from the first peak of the nondispersive longitudinal mode. A typical waveform used for source location is shown in Figure 30. Source locations are then calculated using the velocity of the longitudinal mode (10,000 m/s), the arrival times, and sensor locations. A plot of the calculated source locations for Specimen 4 is shown in Figure 31. Figure 31 also shows that the sources are in the vicinity of the notch. As predicted, the fibers failed in the area near the notch.

5.4 Conclusions

Several conclusions can be drawn from the acoustic emission data recorded during the tow tests:

- Fiber and/or fiber bundle breaks in the carbon/epoxy tow generate longitudinal waveforms with significant high frequency content. The events attributed to fiber breaks provided a basis for the analysis of waveforms from subsequent tank testing.

- Source location methods can generate the locations where acoustic emission occurred in the carbon/epoxy tow samples to within 1 mm.

- Flexural mode waves are strongly attenuated in the loaded samples.

Determination of whether the large amplitude signals are generated from single fiber breaks or from a large number of fibers (a fiber bundle) breaking is difficult without microscopic analysis. The relatively high energy of the events implies that the source releases a large amount of energy. A single fiber break, although locally very energetic, is unlikely to produce enough energy to generate such a large amplitude modal acoustic emission event. Therefore the large amplitude, four channel, longitudinal mode events are attributed to fiber bundle breaks. The waveforms attributed to fiber bundle breaks are consistent with an in-plane source of short duration. The signals attributed to fiber bundle breakage were also used for source location. The locations generated from these signals are from the expected location of fiber breakage, near the stress concentration caused by the notch.

6.0 PHASE 2 -- NGV FUEL TANK TESTING

In Phase 2, NGV fuel tank testing occurred in two stages. The purpose of the Stage 1 testing, which occurred in February 1996, was to obtain an initial evaluation of acoustic emission inspection of NGV fuel tanks. The success of Stage 1 led to further testing in Stage 2 in March 1997, in which acoustic emission was used to detect damage in NGV fuel tanks. All acoustic emission testing of NGV tanks was performed at FaAA's Phoenix Test and Engineering Center. Tanks were tested in both the burst test facility and the fatigue test facility. FaAA was supported by personnel and acoustic emission equipment from Digital Wave of Englewood, CO, a provider of acoustic emission technology, equipment, and inspection services. The modal acoustic emission approach described in Section 4.3 was used in all of the testing.

During Phase 2, acoustic emission was measured during pressurization of NGV fuel tanks. Pressure was monotonically increased to a prescribed level and then held. Pressure was also cycled between ambient and a maximum pressure level. Acoustic emission testing was performed on as-received tanks and on damaged tanks. Damage was introduced by impacting the overwrap with a pendulum impactor, by dropping the tank, or by cutting slits in the overwrap. Tests performed in Phase 2 are summarized in Tables 4 through 7, which describe the NGV fuel tank test specimens, the damage done to the tanks, the fatigue testing conditions, and the acoustic emission inspection. Specific results for each of the tanks are summarized in Tables 8 through 11.

6.1 Stage 1 - Initial Evaluation of Acoustic Emission Inspection

The purpose of Stage 1 testing was to obtain an initial evaluation of acoustic emission inspection of NGV fuel tanks. Acoustic emission sensors were mounted on Type 2 tanks and data collected to: i) characterize the sound transmission in the overwrap and liner, ii) evaluate the acoustic emissions during pressurization of an undamaged tank, and iii) evaluate the acoustic emissions during pressurization of a tank with cuts in the overwrap.

The tanks used in the Stage 1 testing were Type 2 tanks manufactured by Pressed Steel Tank of Milwaukee, WI (Table 4). The tanks consist of a steel liner with a carbon/epoxy overwrap in the cylindrical section of the tank. The tanks are designed so that the overwrap carries a majority of the internal pressure load. Tests were conducted on one tank, approximately 61 inches × 16.4 inches diameter (Tank 012 in Table 4), and on a smaller tank, approximately 50 inches × 11.3 inches diameter (Tank 004 in Table 4). Acoustic emission was measured while the tanks were pressurized, held at pressure, and depressurized.

Tests were first conducted to characterize the sound transmission in the composite overwrap while the tanks were unpressurized. These tests involved transmitting a signal from one location on the overwrap, from a pencil lead break or an ultrasonic pulser, and receiving signals with acoustic emission sensors placed at different locations on the tanks. By moving the transmission locations, the ability of the overwrap to transmit the acoustic emission either along the fibers in the circumferential direction or across the fibers in the longitudinal direction was determined.

The acoustic velocity in various directions relative to the fiber orientation in the overwrap was also measured in this way. Results of these tests were used to define the number and locations of acoustic emission sensors required to provide full coverage of each. For the large tank, Tank 012, eight sensors were used, as shown in Figure 32. Three sensors were located at 120° circumferential spacing at two longitudinal locations just inboard of the straps securing the tank. Two other sensors were located at approximately +/- 60° positions at the longitudinal center of the tank. Six acoustic emission sensors were sufficient for the smaller tank, Tank 004, as illustrated in Figure 33. These sensors were located at 120° circumferential spacing near either end of the overwrap.

Acoustic emission testing of Tank 012 occurred while the tank was pressurized with natural gas to its operating pressure. Acoustic emissions were attributed to gas flow and valve noise, which were identified using the modal acoustic emission method. The ability to discriminate emissions from gas flow and emissions from structural changes of interest is a required capability for accurate inspection of NGV fuel tanks.

Acoustic emission was measured during hydraulic, cyclic pressurization of Tank 004. During these tests, the waveforms observed were typically small amplitude with short durations. Example waveforms are shown in Figures 34 and 35. The waveform in Figure 34 is thought to have been caused by a fiber break, due to its wide frequency content. The basis for this hypothesis is that the source function for a fiber break should approximate a delta function, which has a wideband, flat frequency response. The waveform in Figure 35 was likely due to matrix cracking, again based on the frequency content.

Two longitudinal slits were then machined in the overwrap of Tank 004 as a means of introducing defects into the overwrap (Table 5). The locations of the slits are shown schematically in Figure 33. One slit, 2 inches long × 0.050 inches deep, was located near one end of the overwrap and the other slit, 2 inches long × 0.030 inches deep, was located near the opposite end of the overwrap. The two slits were offset by approximately 2 inches in the circumferential direction. These slits are twice as long as the 1 inch long longitudinal flaws specified in ANSI/NGV2. Acoustic emission of damaged Tank 004 was measured during hydraulic pressurization and pressure cycling. Five pressure cycles were applied to maximum pressures of 3,600 psig, 4,500 psig, and 4,800 psig.

After several cycles of pressurization, visual observation of the tank showed that circumferential cracks were propagating from the ends of the slits. These cracks occurred in the matrix between hoop fibers. The length of the cracks increased with successive pressure cycles. The slit was also delaminated from the underlying composite material. This delamination was also a form of matrix cracking, which was proceeding circumferentially around the tank along a longitudinal band defined by the length of the slit.

The observed cracking and delamination from the slits was reflected in the acoustic emission data, which was attributed primarily to matrix cracking rather than fiber breakage. Large amplitude flexural mode signals, Figure 36, were seen to be originating from the slits. As the

tank was cycled further, the number of the large flexural mode signals began to decrease, as the disbond damage growth slowed. Even though the number of signals increased dramatically after the slits were introduced, most of these signals were the large matrix crack growth signals. Only a few of the fiber breakage signals were recorded. This acoustic emission data interpretation is consistent with the observed response of the tank.

The results of the Task 1 testing were as follows:

- Acoustic emission in the overwrap of the two tanks was measured and characterized using the Digital Wave equipment. Acoustic emission signals were obtained from the overwrap on both tanks using a practical number of acoustic emission sensors.

- For Tank 012, which was pressurized with natural gas, acoustic emission signals were attributed to gas flow and valve noise and not to the composite overwrap. The modal acoustic emission method was able to identify the source of the emissions.

- The presence of the slits in the overwrap of Tank 004 was evident in the acoustic emission data.

- Under cyclic loading, circumferential cracks between hoop fibers grew from the ends of the slits in Tank 004. Visible crack growth was noted after the first pressurization cycle was applied. Crack growth from the slits was detected in the acoustic emission data. Acoustic emissions from each of the two slits were discriminated.

- Under cyclic loading, the slits delaminated from the underlying overwrap on Tank 004. These delaminations were also reflected in the acoustic emission data.

The results of the Stage 1 testing successfully demonstrated the potential of acoustic emission inspection for NGV tanks and led to further testing in Stage 2.

6.2 Stage 2 - Acoustic Emission Inspection of Damaged Tanks

The Stage 2 NGV fuel tank testing was designed to evaluate the ability of acoustic emission inspection to detect damage and to characterize the response of damaged NGV fuel tanks. The same acoustic emission techniques employed in Stage 1 were used to test Type 2 and Type 4 NGV fuel tanks in Stage 2. Damage was introduced into the overwrap by impacting with a pendulum impactor, by dropping the tank, and by cutting slits in the overwrap. Acoustic emission was measured while the tanks were hydraulically pressurized either monotonically or cyclically.

6.2.1 Test Specimens

In Stage 2, tests were conducted on three Type 2 tanks fabricated by Pressed Steel Tank of Milwaukee, WI, and one Type 4 tank fabricated by Edo Canada of Calgary, Alberta, Canada (see

Table 4). The Type 2 tanks (Tanks 013, 014, and 018 in Table 4), are steel lined, carbon fiber, hoop wrapped tanks approximately 34.4 inches long × 16.2 inches diameter. The tanks are autofrettaged at a pressure of 7,100 psig. Two of the Pressed Steel tanks are shown in Figure 37, along with an unwrapped steel liner that was used to define the impact test method. The Type 4 tank (Tank 003 in Table 4) has a thermoplastic liner fully wrapped with carbon fiber and is approximately 36.3 inches long × 17.7 inches diameter.

6.2.2 Test Conditions

In general, the Stage 2 testing involved the following sequence of events:

1. Attach acoustic emission sensors to the as-received tank. The number of sensors used on each tank is listed in Table 7.

2. Apply an increasing hydraulic pressure until significant acoustic emission is detected. This testing was performed in the burst test facility at a nominal pressurization rate of 25 psig/s. The pressure was relieved following acquisition of acoustic emission data.

3. Damage the empty tank by impact and/or slitting. Table 5 describes the damage done to each tank.

4. Apply an increasing hydraulic pressure until significant acoustic emission is detected. This testing was performed in the burst test facility at a nominal pressurization rate of 25 psig/sec. The pressure was relieved following acquisition of acoustic emission data.

5. Apply 3,000 cycles of hydraulic pressure varying from 0 to 3600 psig. Table 6 describes the cyclic pressure conditions for each tank. Fatigue testing was performed in the fatigue test facility. For the Type 2 tanks, each pressure cycle occurred in 20 seconds and consisted of a 1 second hold, a 9-11 second ramp up to maximum pressure, a 1 second hold, and a 7-9 second ramp down. A longer pressure cycle of 30 seconds was required to accommodate the greater expansion of the Type 4 tank. The fatigue cycle for the Type 4 tank consisted of a 1 second hold, a 16 second ramp up to maximum pressure, a 1 second hold, and a 12 second ramp down.

6. Apply an increasing hydraulic pressure to 4,500 psig or until significant acoustic emission is detected, whichever comes first. Hold the pressure for 100 seconds and then relieve the pressure. This testing was performed in the fatigue test facility.

7. Repeat Steps 5 and 6 until failure or 15,000 cycles, whichever comes first.

Variations from this general procedure are described in the discussion of testing performed on each tank.

As-received tanks and damaged tanks were internally pressurized until significant acoustic emission response was obtained. The difference in the acoustic emission response before and after impact damage provided an indication of the ability of acoustic emission to detect and characterize the damage. Tanks were then subjected to cyclic pressurization, as described in Table 6. These fatigue tests were performed to simulate the 15,000 filling cycles during the tank's lifetime. Every 3,000 cycles, the tank was subjected to a single pressurization cycle to a higher pressure in order to characterize the acoustic emission response of the tank at this point in its lifetime. These periodic tests were performed to simulate acoustic emission inspection of the tank every three years. In most cases, the fatigue cycles were performed to 3,600 psig and the periodic pressurization cycles were performed to 4,500 psig.

6.2.3 Acoustic Emission Instrumentation

Each tank was instrumented with acoustic emission sensors and internally pressurized hydraulically. Acoustic emission and pressure data were obtained continuously during all pressurization tests. Sensor locations for each tank are shown in Figures 38-41.

For most tests, six sensors were used during the pressurization tests to monitor the composite overwrap. The six sensors were located in two bands around the tank approximately 5 inches from each end of the overwrap. In each band, three sensors were spaced 120° apart circumferentially. To insure that the sensors provided complete coverage of the tank, pencil lead breaks were performed at various locations on the tank. During the lead breaks, the sensors were monitored to determine if the break was received by each sensor. The recorded waveforms from a lead break performed near Sensor 6 are shown in Figure 42. The wave generated by the lead break arrived at all sensors, even Sensors 1 and 2, which were located on the opposite side and end of the tank. Based on the results of the lead breaks, the configuration of six sensors was determined sufficient to detect events occurring anywhere in the overwrap.

From the acoustic emission events observed during testing of Tank 013, four equally spaced sensors were determined to be the minimum required to provide adequate sensor coverage of the overwrap. For practical reasons, only four sensors were used for tests on Tank 014 (Figure 39). The four sensors were placed 180° apart at the same two longitudinal locations as on Tank 013.

Seven sensors were used on Tank 003, four to monitor the overall response of the overwrap and three to monitor the response of the damaged area (Figure 41). The four sensors were located 180° apart at two longitudinal locations. The three sensors were positioned on either side of the damaged area and oriented along an external fiber, as shown in Figure 41.

One acoustic emission sensor, Sensor 7, was used on Tank 013 to evaluate the type of glue used to attach the sensors to the overwrap. Sensor 7 was used on the as-received and damaged tank and removed prior to fatigue testing of Tank 013. All of the sensors, with the exception of Sensor 7, were attached with hot glue. Sensor 7, which was located near Sensor 2, was attached with an epoxy adhesive (Figure 38). The results of Tank 013 testing indicated that the type of glue had no significant effect on the acoustic emission response. Consequently, Sensor 7 was not used on subsequent testing of Tanks 014, 018, and 003.

6.2.4 Damage

Tanks were damaged in three different ways:

1. Impact using a pendulum impact tester
2. Drop test
3. Machined slits in the overwrap

Damage done to each tank is summarized in Table 5. The location of the damage on each tank is shown schematically in Figures 38-41.

Impact loading was applied to Tank 013 with two different pendulum impact fixtures, a small fixture and a large fixture. With the small fixture, tanks were impacted while they were in the burst test chamber. A pyramidal shaped impactor was used with a 0.109-inch radius point. By varying the weight, impact energies of 22.1 ft-lbs and 221 ft-lbs were applied with the small fixture. The damage caused by the pyramid impactor included hoop cracks, fibers lifted from the surface, and dents in the overwrap. The 221 ft-lbs impact created a 0.125 inch deep dent in the overwrap. The large pendulum impact fixture was used to apply an impact energy of 2,050 ft-lbs. A flat impactor (17 inches long × 2 inches wide) was used to apply the impact load along the entire length of the overwrap. Damage caused by the flat impactor appeared as a series of white circumferential lines, similar to scuff marks, along the length of the overwrap.

Damage was imparted to Tank 003 by dropping it on its "shoulder" (cylinder to dome transition region) onto a concrete pad. The tank was positioned at a 45° angle with its center of gravity 5 feet above the concrete. The drop produced a circular damage zone containing a crack at the point of impact. The tank subsequently contacted the concrete at the opposite end, which produced small, light, scuff marks.

A hand saw was used to cut longitudinal slits in the overwrap of Tanks 013 and 018. Two slits were cut in Tank 013, one 2 inches long × 0.050 inches deep and one 3 inches long × 0.125 inches deep. The depth of the 0.125 inch deep slit was equal to the 0.125 inch depth of the 221 ft-lbs impact damage, which provided a comparison between damage of equal depth and different extent. One slit, 8 inches long × 0.180 inches deep, was cut completely through the overwrap in Tank 018.

6.2.5 Tank 013

Tests and results for Tank 013 are summarized in Table 8. Tank 013 is shown in the burst test facility in Figure 43. Four of the eight acoustic sensors can be seen in the figure along with the wires connecting each sensor to a preamplifier. An overall view of the burst test facility just prior to pressurization is shown in Figure 44. In Figure 44, the lid of the test chamber is on and the preamplifiers are placed on top of the lid. Wires connect the preamplifiers to the acoustic emission electronics in the adjoining room, shown in Figure 45. The as-received Tank 013 was

pressurized to 7,293 psig, which produced significant acoustic emission. This pressure is slightly above the autofrettage pressure of 7,100 psig.

The 2 inch slit in the overwrap (near Sensor 5) is shown in Figure 46. The slit was located 4.5 inches from the open end of the overwrap. The circumferential crack to the left of the slit in Figure 46 was present in the overwrap of the as-received tank and was attributed to the autofrettage pressurization. Tank 013 containing the 2 inch slit was pressurized to 5,533 psig, which produced audible noise and significant acoustic emission. Visual examination of the tank following pressurization revealed that the autofrettage cracks were more prominent. It also revealed two new circumferential cracks from the ends of the slit, indicated by the yellow lines in Figure 47. These cracks eventually go all the way around the circumference of the tank after fatigue cycling. Subsequent pressurization of the tank also caused the ends of the slit to separate circumferentially and to delaminate from the underlying overwrap.

The pendulum impact fixture was designed to impact the tank while it was in the burst test chamber, as shown in Figure 48. A close-up view of the pyramid-shaped impactor is shown in Figure 49. The impact site following the 22.1 ft-lbs impact is shown in Figure 50. Several hoop cracks and two shallow dents were created by the impact. The visual extent of the damage, indicated by the rectangular region in Figure 51, is approximately 1.5 inches circumferentially × 0.5 inches axially. Pressurization of the tank to 5504 psig produced audible noise and significant acoustic emission. Following pressurization, the fibers in the damaged area were lifted from the surface, but no apparent crack growth was observed.

Weight was added to the pendulum impact fixture in order to increase the impact energy to 221 ft-lbs, as shown in Figure 52. The tank was also rotated so that the impact occurred at approximately the same longitudinal location but at a circumferential location approximately the same distance from Sensor 2 as the 22.1 ft-lbs impact. The appearance of the 221 ft-lbs impact damage, which includes circumferential cracks, fibers lifted off the surface, a 0.125 inch deep dent, and a shallow dent, is shown in Figure 53. The size of the visibly damaged area is approximately 2.25 inches circumferentially × 0.5 inches axially. No change in the damage was observed following pressurization of the tank to 5529 psig.

A second slit, 3 inches long × 0.125 inches deep was cut into the overwrap of Tank 013 approximately 5 inches from the closed end of the overwrap. The depth of the slit was equal to the depth of the dent caused by the 221 ft-lbs impact. Pressurization of the tank to 4994 psig produced audible noise and significant acoustic emission.

Following post-damage characterization in the burst test facility, Tank 013 was moved to the fatigue test facility for cyclic pressure testing. Views of the tank in the fatigue test chamber are shown in Figures 54-55. Cyclic loading was stopped every 3,000 cycles to allow a visual examination and acoustic emission damage characterization. Under cyclic loading, circumferential cracks grew from the two areas of impact damage and from the ends of the two slits. These cracks were marked on the surface of the tank with yellow and red markers, so that they would be easier to track and photograph. These lines are seen in Figures 54-55, which

illustrate the circumferential crack growth. In Figure 54, the 2 inch long slit is visible in the upper right above Sensor 5, with yellow lines indicating the circumferential cracks emanating from each end of the slit. The pair of yellow lines in the center of the tank are associated with cracks from the 3 inch long slit, which is seen in the upper center of Figure 55 between Sensors 3 and 6. Due to fatigue cycling, the ends of the two slits separated and the slits delaminated from the underlying overwrap. The two impact damaged areas and their associated cracks are shown in the left of Figure 54 near Sensors 2 and 7. Notice that the crack propagates between the two damage areas and continues around the circumference of the tank.

6.2.6 Tank 014

Tests and results for Tank 014 are summarized in Table 9. The as-received Tank 014 is shown in the burst test chamber in Figure 56. In Figure 57, notice the circumferential cracks in Tank 014, which are presumed to be associated with the autofrettage pressurization. The white areas on the top of the tank are typical scuff-type damage observed on the as-received tanks. The four acoustic emission sensor locations are shown in Figure 57. For practical reasons of schedule and convenience, four sensors, rather than seven, were used on Tank 014. The sensors were located at the same axial locations as on the other Type 2 tanks, but the sensors were located 180° rather than 120° apart. Previous testing of Tank 013 indicated that four sensors was the minimum required to cover the overwrap.

The as-received Tank 014 was pressurized to 7,200 psig, which is just above the autofrettage pressure of 7,100 psig. For Tank 014, the acoustic emission sensors were removed during the subsequent fatigue testing. Following 3,000 pressure cycles, the tank exhibited a similar acoustic emission response when pressurized to 7,200 psig, indicating no affect of the fatigue cycling.

6.2.7 Tank 018

Table 10 summarizes the testing and results for Tank 018. The as-received Tank 018 is shown in the burst test chamber in Figures 58 and 59. The seven acoustic emission sensor locations are visible in these figures. These are the same locations used on Tank 013. Pressurization of the as-received Tank 018 produced significant acoustic emission at 7,200 psig, just above the autofrettage pressure of 7,100 psig.

The test set-up for impacting Tank 018 in the large impact test facility at an impact energy of 2,050 ft-lbs is shown in Figures 60 and 61. As shown in the figures, the impactor is a steel box section 2 inches wide × 17 inches long, so that the impactor contacted the tank along the entire length of the overwrap over a 2 inch circumferential length. The test facility just prior to release of the pendulum is shown in Figure 62. Views of the post-impact damage are shown in Figures 63 and 64. The damage appears as a series of light circumferential lines approximately equally spaced along the length of the overwrap. The circumferential extent of the damage is greater toward the closed end of the tank. The post-impact Tank 018 was pressurized to 7,200 psig and exhibited no significant difference in acoustic emission response from the as-received tank, indicating no significant effect of the impact on the overwrap.

The 8 inch long × 0.18 inch deep slit in the overwrap of Tank 018 is shown in Figure 65. The tank was pressurized to 4,530 psig, which produced significant acoustic emission. Following one pressure cycle, the ends of the slit separate, as shown in Figure 66, and circumferential cracks propagate from the ends of the slit, as shown by the yellow lines in Figure 67. Prior to fatigue testing, a few remaining fibers were cut so that the slit penetrated through the entire thickness of the overwrap, as shown in Figure 68. After 3,000 pressure cycles in the fatigue chamber, the ends of the slit separate further, as shown in Figures 69 and 70. Views of the tank after 15,000 cycles, shown in Figures 71 and 72, show that the ends of the slit are separated by approximately the same distance as after 3,000 cycles. Cracks emanating from the ends of the slit propagated all the way around the circumference of the tank, indicated by the yellow lines in Figure 71. Also, the entire band of the overwrap was observed to be delaminated from the liner.

6.2.8 Tank 003

Results and testing for Tank 003 are shown in Table 11. Tank 003, a Type 4 tank fabricated by Edo, is shown in Figure 73. The external rubber bumpers on the shoulders of the tank were removed for this test. The white area in Figure 74 corresponds to the prior location of the bumper, which is shown following removal in Figure 75. The white material is the Styrofoam underneath the bumper, which was removed prior to testing, as shown in Figure 76. Tank 003 is shown in the burst test chamber for characterization of the as-received tank in Figure 77. Six of the seven acoustic emission sensor locations are also visible in Figure 77. Four of the sensors (Sensors 1-4) were positioned 180° apart at two axial locations, 3 inches from the closed end of the overwrap and 11.5 inches from the open end of the overwrap. The other three sensors (Sensors 5, 6, and 8) were positioned on either side of the impact site along an external fiber direction. Pressurization of the as-received Tank 003 to 6,062 psig produced significant acoustic emission.

The set-up for the drop test of Tank 003 is shown in Figure 78. The tank was positioned at a 45° angle with its center of gravity 5 feet above the concrete pad, as shown in Figure 79. Following the drop, the primary area of damage occurred at the impact site on the shoulder of the tank, as shown in Figures 80 and 81. The visible damage appears as a circular area approximately 3 inches in diameter containing a 2.25 inch long crack. Two smaller areas of damage at the opposite end of the tank are shown in Figure 82.

Following the drop test, Tank 003 was pressurized in the burst test chamber to characterize the response of the damaged tank. The tank is shown in the chamber in Figure 83, which also shows the relative position of acoustic emission sensors near the damaged area. Pressurization of the tank to 3667 psig produced significant acoustic emission and no visible change in the tank.

The tank was first cycled to 3,600 psig in the burst test chamber. After 230 cycles, the tank was moved to the fatigue test chamber, where it failed following a total of 8,146 pressure cycles, 6,000 cycles to 3,600 psig and 2,146 cycles to 4,000 psig. Failure occurred at approximately 3,700 psig during the ramp up on Cycle 8147. Photographs of the failed tank are shown in

Figures 84 through 86. As shown in the figures, failure occurred at the site of primary impact damage.

6.3 Acoustic Emission from Tanks During Stage 2 Testing

This section summarizes the analysis of the acoustic emission data obtained during the Stage 2 testing of NGV fuel tanks. Acoustic emission was recorded during pressurization of as-received and damaged Type 2 and Type 4 tanks.

6.3.1 As-Received Tanks

Each as-received tank was pressurized to characterize the initial modal acoustic emission response of the tank. The pressure was increased until significant acoustic emission was measured. This initial characterization served two purposes. First, it exercised existing acoustic emission sources, so that subsequent recorded emissions would primarily be caused by the damage and pressurization performed in the Stage 2 testing. Second, the characterization of the as-received tanks provided an indication of the types of acoustic emission, including noise, that could be expected in subsequent Stage 2 testing.

For the as-received Type 2 tanks, significant acoustic emission was obtained at a maximum pressure slightly higher than the autofrettage pressure. This result is consistent with the observation that a structure does not produce acoustic emission until it is loaded beyond the previous maximum load. This behavior, called the Kaiser Effect, was originally defined based on the response of metallic structures, which typically exhibit a Kaiser Effect. Composite structures do not exhibit a Kaiser Effect as completely as metallic structures. A composite structure may produce some residual acoustic emission at a load below its previous maximum load. For example, a composite specimen loaded to 400 pounds in tension would produce acoustic emission. Upon reloading, much less acoustic emission would occur until the second load exceeded 400 pounds. (A metallic specimen would typically produce no acoustic emission below 400 pounds.) If the composite specimen was damaged by notching or impacting before reloading, the damage would produce acoustic emission at a load below 400 pounds. According to the Kaiser Effect, Type 2 tanks autofrettaged at 7,100 psig would not be expected to produce significant acoustic emission at a load below 7,100 psig. Testing of as-received Type 2 tanks confirmed this expected response. Only a small amount of acoustic emission was obtained below the 7100 psig autofrettage pressure.

Sources of acoustic emission during pressurization of as-received tanks was attributed to the overwrap and to noise from outside sources. Determination of which signals were from the overwrap and which were from external noise was accomplished through examination of signal arrival times, amplitudes, frequency content, and event duration. Most signals were sorted by their frequency content and duration. A typical waveform and its FFT for a signal attributed to mechanical noise is shown in Figure 87. The duration of the waveform is very long, a characteristic of mechanical noise. The FFT of the waveform shows that the waveform consists entirely of low frequency components below 100 kHz, another mechanical noise characteristic. A

typical waveform attributed to the overwrap in an as-received Type 2 tank is shown in Figure 88. The arrival times, indicated by the arrows, suggest that the source for the acoustic emission is on the bottom of the tank, between sensors four and six. The FFT of the waveform, shown in Figure 88b, exhibits a broad low frequency content to 500 kHz but little high frequency content above 1 MHz. Another typical waveform recorded during pressurization of an as-received Type 2 tank is shown in Figure 89. The signals shown in Figures 88 and 89 are representative of the signals associated with the response of the overwrap. No waveforms were recorded with significant high frequency content, which is characteristic of fiber breakage. Visual inspection of the tanks after initial pressurization revealed that the autofrettage cracks were more prominent. This observation combined with the acoustic emission data support the conclusion that the acoustic emission events obtained during pressurization of as-received Type 2 tanks were generated by matrix cracking.

A typical waveform and FFT from pressurization of the as-received Type 4 tank is shown in Figure 90. As with the Type 2 tanks, the recorded acoustic emission events were consistent with matrix cracking. No waveforms with high frequency components characteristic of fiber breakage were obtained.

6.3.2 Damaged Tanks

After being subjected to damage, either by impact or saw cut, tanks were again pressurized and the modal acoustic emission recorded. In all cases, the damaged tanks produced acoustic emission at a lower pressure than the as-received state. The emissions from the damaged tanks were attributed to the presence and growth of the inflicted damage.

Typical waveforms from the pressurization of a Type 2 tank with a saw cut and impact damage are shown in Figures 91 and 92, respectively. The waveforms recorded from these damaged tanks were similar to each other. In addition, the waveforms were not significantly different from the waveforms produced by the as-received tanks, which were attributed only to matrix cracking. No signals were attributed to fiber breakage. Post-pressurization visual inspection of the damaged tanks revealed circumferential cracks in the overwrap originating from the ends of the saw cut and the impact damaged area. These matrix cracks were consistent with the acoustic emissions from the tanks.

A typical waveform produced during the pressurization of the damaged Type 4 tank is shown in Figure 93. The impact damage area was identified as the primary source of acoustic emission events during the post-damage pressurization. Over 80% of the signals recorded originated in the damaged area. No high frequency waveforms indicative of fiber breakage were recorded. Visually, no changes were observed in the damaged Type 4 tank following pressurization. However, matrix cracking could have occurred within the overwrap without being detected on the surface of the tank.

The damaged tanks produced significant acoustic emission at lower pressures than the as-received tanks. The typical waveforms recorded from both impact and saw cut tanks contained primarily small amplitude, low frequency components, which is consistent with matrix cracking

events. No signals with the high frequency components characteristic of fiber breakage were obtained. The acoustic emission data and visual inspections support the conclusion that matrix cracking was the primary mechanism of damage growth in the tanks.

6.3.3 Fatigue Tests

Tanks were subjected to cyclic pressure loading to determine the effect of repeated pressurizations on damage growth and lifetime. Acoustic emissions from Type 2 tanks included a large number of fretting and rubbing events. A typical fretting event signal, which is characterized by long duration and low frequency components, is shown in Figure 94. This signal was identified as a fretting event, in part, because of the number of times that it was repeated during the fatigue testing. In some cases, the identical waveform was generated in the overwrap during more than 50 consecutive fatigue cycles. Physically, fretting was associated with crack growth in the damaged area, as cracked and delaminated surfaces of the overwrap plies rubbed against each other. A signal from a noise event, which was also repeated over a large number of consecutive pressurization cycles, is shown in Figure 95. Acoustic emission events, similar to those shown in Figures 88 and 89, were interspersed in the noise data and attributed to matrix cracking. No signals indicative of fiber breakage were found in the acoustic emission during fatigue testing of the Type 2 tanks. The acoustic emission events indicated that fretting and matrix cracking were the primary mechanisms of damage growth during fatigue testing.

During fatigue testing of the Type 4 tank, two types of signals were recorded. The small amplitude signal from sources all over the tank is shown in Figure 96. These signals were likely produced by small cracks in the matrix. The signals that originated in the damaged area of the tank, which are likely from matrix cracking, are shown in Figure 97. On single channels, a few high frequency events were recorded. These events were similar to those seen during tow testing and attributed to fiber breakage. Just before failure of the Type 4 tank, a large increase in the number of events per cycle occurred. The majority of the events, similar to the event in Figure 97, was associated with matrix cracking in the impact damaged area. Just prior to failure, low amplitude, high frequency events, such as the waveform shown in Figure 98, were recorded.

The failure of the Type 4 tank occurred at the impact site in the transition between the cylindrical section and dome of the tank. In this area, fiber orientations are changing rapidly. Much of the load is carried in shear, in which the load is transferred between fibers through the matrix and the fiber-matrix interface. Therefore, behavior of the tank in this area is very matrix dependent. The presence of acoustic emissions characteristic of matrix cracking during fatigue testing of the tank was not surprising. The absence of high amplitude, fiber breakage signals was somewhat surprising, because catastrophic failure of the tank during fatigue testing must have necessarily included fiber breakage. Some indication of fiber breakage was seen in the acoustic emission data, such as the waveform shown in Figure 98. This low amplitude, high frequency signal is similar to those observed in the tow tests. The heavily damaged area of the tank may have attenuated or prevented the propagation of high amplitude signals associated with fiber breakage, which may explain why these high amplitude signals were not recorded just prior to failure.

6.3.4 Pressurization After Fatigue

After each set of 3,000 pressure cycles, tanks were pressurized to 4,500 psig and held at that pressure for 100 seconds. A typical waveform generated in a Type 2 tank during a pressure hold is shown in Figure 99. Waveforms recorded under these constant pressure conditions were similar to the waveforms recorded from damaged tanks (Section 6.3.2). For Tank 013, a plot of the number of acoustic emission events versus time following 6,000 pressure cycles is shown in Figure 100. This plot is typical of the response of Tank 013 during the pressure holds.

A plot of acoustic emission events recorded during each pressure hold for Tank 013 is shown in Figure 101. With the exception of the data point following 12,000 fatigue cycles, the amount of acoustic emission generated during a hold increases with the number of fatigue cycles. The data at 12,000 cycles is in question and was not included in the data analysis. This data is different from all of the other pressure hold data for all tanks. The invalid data point may have been caused by a software problem, which occurred just prior to the completion of the 12,000 cycles.

Tank 014, which was undamaged prior to fatigue testing, was pressurized following 3,000 pressure cycles. The overwrap did not produce a significant number of acoustic emission events until the pressure approached the autofrettage pressure, which is similar to the response of the as-received Tank 014. This result indicates that the fatigue cycles introduced no new damage to the as-received tank.

For Tank 018, a plot of the number of acoustic emission events during pressure holds versus the number of fatigue cycles is presented in Figure 102. Data for 3,000 cycles is missing, because the high rate of acoustic emission events saturated the A/D boards. The remaining data points in Figure 102 approximate a constant number of events with fatigue cycles. This response may be explained by the physical condition of the tank caused by propagation of the slit during pressurization. Visual examination of the tank early in the fatigue testing revealed that the hoop cracks from the ends of the slit and the delamination under the slit had propagated around the entire circumference of the tank. Consequently, the band of material associated with the slit was completely separated from the underlying liner and from the adjacent overwrap. Therefore, no further damage and associated acoustic emission would occur during subsequent pressure cycling. The recorded acoustic emission events may be from the portion of the overwrap on either side of the slit, which was still bonded to the liner.

For Tank 003, the Type 4 tank, a plot of the number of acoustic emission events during pressure holds versus the number of fatigue cycles is shown in Figure 103. Data were obtained following 3,000 and 6,000 pressure cycles before the tank failed. The number of events at pressure hold increases with fatigue cycles, as it did in Tank 013. However, the rate of increase is much greater for Tank 014. This acoustic emission response is consistent with the progressive failure exhibited by Tank 014, leading to catastrophic failure of the tank during fatigue testing.

7.0 DISCUSSION

This project addressed two questions concerning in-service inspection of NGV fuel tanks:

1. Will the NGV fuel tank perform satisfactorily if the composite overwrap is damaged?

2. Can acoustic emission inspection detect the presence of damage in an NGV fuel tank?

In this section, these questions will be answered based on the results of the project. First, some general observations can be made:

- Very few tanks were tested in this project. Only five Type 2 tanks of three different designs and one Type 4 tank were evaluated. This is a limited database that provides an initial evaluation but cannot support general conclusions.

- A great deal of testing was performed. Tanks were subjected to a variety of damage, from no damage to significant impact loads and saw cuts. As-received and damaged tanks were subjected to monotonic and cyclic pressure loads, including 15,000 service pressure cycles.

- Extensive testing was performed to evaluate the potential acoustic emission inspection of NGV fuel tanks. With one exception, acoustic emission data was obtained from each test performed on each tank in its as-received and damaged condition during monotonic and cyclic pressure testing. Acoustic emission inspection was performed following every 3,000 pressure cycles, as a simulation of fuel tank inspection every three years of service.

- Acoustic emission was used to characterize not only the response of the NGV fuel tanks, but also the response of the composite material used in the overwrap. Fiber tow tests provided an independent measure of composite material response. The tow test results were then used to better interpret and understand the acoustic emission data obtained from the tank testing.

7.1 Damage Tolerance of the NGV Fuel Tanks

The damage tolerance of the NGV fuel tanks was evaluated based on the ability of a damaged tank to complete the ANSI/NGV2 fatigue design lifetime of 15,000 service pressure cycles. The test results were highly dependent upon the tank design. Three of the Type 2 tanks were subjected to significant damage from impact loading and saw cuts. However, none of the damaged Type 2 tanks failed during 15,000 fatigue cycles. The one Type 4 NGV fuel tank, which sustained damage from a 5-foot drop test, did fail following 8,146 fatigue cycles (54% of the design lifetime).

7.1.1 Type 2 Tanks

Performance of the Type 2 tanks raises a question about the fatigue capability of the steel liner alone and the role of the overwrap. FaAA's understanding was that the liner was unable to sustain the 15,000 service pressure cycles without the overwrap. However, even when half the length of the overwrap was completely cut, the tank did not fail prematurely. Therefore, the amount of overwrap required to ensure satisfactory performance of the tank is not known. The margin of safety may be large enough to accommodate the loss of half of the fibers. Fatigue testing of the liner alone and additional damage tolerance testing of Type 2 tanks would provide data required to address this question.

Response of the damaged overwrap to cyclic pressurization was the same in the three damaged Type 2 tanks. Circumferential cracks initiated and propagated from both the pyramid impactor damage and the slits. Under cyclic loading, cracks grew circumferentially until they went completely around the tank. The band of overwrap within the slit also delaminated from the underlying material. Under pressure cycling, the delamination propagated around the entire circumference of the tank. The primary difference in the response of the tank to the impact damage and the slits was the amount of overwrap affected by the damage. The pyramid impactor damage was localized to a small region surrounding the impact site. The amount of material affected by the slit was defined by the length and depth of the slit.

Damage from both the pyramid impactor and the slit was detectable by acoustic emission and visual inspection. For the flat impactor, which was applied with an impact energy ten times greater than the pyramid impactor, no change in acoustic emission was detected between the pre- and post-impacted tank. Although the flat impactor left noticeably visible marks on the tank immediately following the impact, the marks were difficult to see one month after testing. With the pyramid impactor, the impact load was locally concentrated, whereas the load was distributed over a large area with the flat impactor. These results illustrate the influence of the impactor shape on the resulting impact damage in the composite overwrap and the difficulty that may arise in evaluating NGV tanks based on a visual examination.

The effect of the impact damage and slit on the tanks was associated with matrix cracking, based on both acoustic emission inspection and visual examination of the Type 2 tanks. Changes in damage during pressure cycling were also detected by acoustic emission inspection of the tanks. The acoustic emission signals during fatigue testing were attributed to circumferential cracking of the matrix and delamination, both of which were observed on the tanks.

Insight into the behavior and relative importance of damage can be obtained by examining the response of Tanks 013 and 018 to fatigue testing. Tank 013 contained two slits and two impact damaged areas. During fatigue testing, Tank 013 exhibited an increase in acoustic emission events with an increasing numbers of cycles. This increase in emissions provides an indication of the presence of the damage. However, acoustic emissions from Tank 018 remained approximately constant during fatigue testing, in spite of the fact that Tank 018 contained a slit that was much larger than the slits in Tank 013. The acoustic emission response of Tank 018 could lead to an erroneous conclusion that little or no damage was present, when in fact, a large

slit in the overwrap was present and the overwrap was completely separated from the remainder of the tank. In fact, the acoustic emission response of Tanks 013 and 018 is explained by the observed physical changes in the tanks. However, these results illustrate the need for additional work to understand the behavior and failure of damaged tanks, and the ability of acoustic emission to accurately detect different types of damage in NGV fuel tanks.

7.1.2 Type 4 Tanks

The Type 4 tank sustained sufficient damage from the drop test to cause premature failure of the tank during subsequent fatigue testing. The tank was dropped on its "shoulder," at the transition from the cylindrical section to the dome. The transition region and the dome are recognized as being the most susceptible to impact damage in Type 4 tanks, because of the fiber orientation in these locations which requires the load to be carried in shear. Because shear strength is a matrix-dominated property, the load carrying capability of the tank in the transition region and the dome can be significantly reduced by matrix damage. By contrast, the cylindrical region of the tank is better able to withstand impact loading, because the properties are fiber dominated, which are more damage tolerant than the matrix.

7.2 Acoustic Emission Inspection of NGV Fuel Tanks

Acoustic emission inspection of NGV fuel tanks was evaluated based on technical capabilities and practical considerations.

7.2.1 Technical Capabilities

Technically, acoustic emission was able to measure the response of the tanks to damage and loading. The presence or absence of damage and damage growth during fatigue was detected in both the Type 2 and Type 4 tanks, which is a requirement for an NGV fuel tank in-service inspection method. The characterizations of the acoustic emission signals, such as matrix cracking events, were verified by visual examination of the tank. For the Type 2 tanks, significant acoustic emission was not obtained until the test pressure exceeded the autofrettage pressure, which reflects the Kaiser Effect in composite structures. Because the Type 2 tanks did not fail in fatigue, the current state of damage, as detected by acoustic emission could not be related to the expected lifetime of the tank. An in-service NGV fuel tank inspection method needs this capability to support accurate and reliable criteria for removing damaged tanks from service.

The acoustic emission results for the Type 4 tank indicate that the tank damage was associated with matrix cracks, which grew under cyclic loading until the tank failed. A number of signals in the acoustic emission data indicated that the Type 4 tank was beginning to fail during fatigue testing. Because these signals occurred shortly before catastrophic failure of the tank, they did not provide a sufficiently early warning of future tank failure. Although fibers necessarily failed during the tank failure process, high frequency acoustic emission signals characteristic of fiber breakage were not obtained. One explanation is that the high frequency signals were attenuated

by the presence of the cracked matrix in the damaged area. For Type 4 tanks, additional work is needed to characterize the failure of damaged tanks and to evaluate the ability of acoustic emission to detect the presence of significant damage during periodic inspections of in-service tanks.

In both the tow tests and the tank tests, the acoustic emission results were consistent with the visually observed response of the test specimens. Both the types and locations of acoustic emission sources were identified in the tow tests. In the damaged tank tests, the predominance of matrix cracking signals reflected the observed circumferential cracking and delamination in the overwrap. In some cases, such as Tank 004, discrimination between signals from two different sources (slits) in the acoustic emission data was possible.

7.2.2 Practical Considerations

From a practical standpoint, the acoustic emission inspection was relatively easy to implement. Sensors were easy to apply with the hot glue, and they stayed on the tank during the various load cycles. Complete coverage of the overwrap was provided using 4 to 6 sensors. Once the sensors were in place and the response of the system calibrated, the inspection itself was a highly automated process under computer control. Admittedly, the most difficult part of acoustic emission inspection is the interpretation of the data, which makes it similar to other inspection methods. However, once the methodology for a specific tank design is established, the acoustic emission inspection lends itself to automated, computerized implementation, with little human intervention. During the testing at FaAA's Phoenix Test and Engineering Center, the FaAA engineers and technicians learned how to perform acoustic emission inspection of NGV fuel tanks from the Digital Wave experts. After a few days, the FaAA personnel were sufficiently capable and comfortable with the acoustic emission inspection technology and procedures to perform the testing themselves. They were able to conduct all of the acoustic emission testing of the Type 4 tank without the presence of the Digital Wave expert. This experience provides a measure of the practicality of the acoustic emission inspection method for NGV tanks.

7.2.3 Acoustic Emission Inspection Methods for NGV Fuel Tanks

The modal acoustic emission technique used in this project provided the capability to detect and characterize the damage and the location of the damage in the composite overwrap of the tanks. As a result, a direct correspondence between the acoustic emission inspection data and the physical condition of the tank, which is a prerequisite for a valid in-service inspection method, was achievable. This correspondence was not always exact, as in the case of Tank 018, in which the large separation of the overwrap was not detected by acoustic emission. The potential applicability of modal acoustic emission to in-service inspection of NGV fuel tanks was supported by the results of this project. However, many questions remain. For example, this project did not address the ability of acoustic emission inspection to detect defects in the liner of the fuel tank. Additional work is required before a practical inspection method can be developed and qualified.

Results of the modal acoustic emission inspection performed in this project can be compared with the acoustic emission inspection method in the proposed ASTM standard. The relationship between the condition of the tank and the acoustic emission inspection data is only indirect in the proposed standard. In the proposed inspection method, acoustic emission events (counts) are detected and the number of counts are used to disposition the tanks. The source and location of the events are not identified, and the importance of the detected events to the failure of the tank are not taken into consideration. These apparent limitations of the proposed ASTM acoustic emission inspection method raise questions about the ability of the method to accurately and reliably inspect NGV fuel tanks of different designs that contain different types of damage.

REFERENCES

1. "Basic Requirements for Compressed Natural Gas Vehicle (NGV) Fuel Containers," ANSI/ AGA NGV2-1992.

2. "Practice for Continuous Monitoring of Acoustic Emission from Metal Pressure Boundaries," Standard E1139-92, American Society for Testing and Materials, 1992.

3. "Practice for Leak Detection and Location Using Surface-Mounted Acoustic Emission Sensors," Standard E1211-87, American Society for Testing and Materials, 1992.

4. "Standard Test Method for Examination of Seamless, Gas Filled, Pressure Vessels, Using Acoustic Emission," Standard E1419-91, American Society for Testing and Materials, 1991.

5. "Acoustic Emission Monitoring of Fiberglass Reinforced Plastic Resin (FRP) Tanks/ Vessels, Standard E1067-89, American Society for Testing and Materials, 1991.

6. "Acoustic Emission Examination of Fiber Reinforced Plastic Pressure Vessels," Section V, Article 11, *Boiler and Pressure Vessel Code*, American Society of Mechanical Engineers.

7. "Design and Test of Composite Pressure Vessels," RTP-1, Section X, *Boiler and Pressure Vessel Code*, American Society of Mechanical Engineers.

8. "Recommended Practice for Acoustic Emission Testing of Fiberglass Reinforced Plastic (FRP) Tanks/Vessels," The Composites Institute of the Society of the Plastics Industry.

9. G.S. Bhuyan, "Leak-Before-Break and Fatigue Crack Growth Analysis of All-Steel On-Board Natural Gas Cylinders," *Fracture Mechanics: Twenty-Third Symposium*, ASTM STP 1189, American Society for Testing and Materials, 1993.

10. M.P. Connolly, "Inspection of Steel (Type NGV2-1) Compressed Gas Cylinders for Natural Gas Vehicles Using Source Location Acoustic Monitoring (SLAM)," Journal of Non-Destructive Evaluation, 1995.

11. S.J. Hudak, M.P. Connolly, J. Hanley, and S. Lukezich, "Development and Validation of a Prototype Acoustic Emission System for Inspection of Metal NGV Fuel Cylinders," Report 06-1566, Gas Research Institute, 1995.

12. "Standard Test Method for Examination of Gas-Filled Filament-Wound Composite Pressure Vessels Using Acoustic Emission," Draft ASTM Standard, June 20, 1995.

13. J.R. Mitchell and N. Newhouse, "Techniques for Using Acoustic Emission to Produce Smart Tanks for Natural Gas Vehicles," AECM-5, Fifth International Symposium on

Acoustic Emission for Composite Material, Sundsvall, Sweden, American Society of Nondestructive Testing, July 10-14, 1995.

14. J.R. Mitchell, "Standard Test to Quantify the Knee in the AE vs. Load as a Material Parameter for Composites," TR-107-69-5/89, Physical Acoustics Corporation.

15. M.A. Hamstad, J.W. Whittaker, and W.D. Brosey, "Correlation of Residual Strength with Acoustic Emission from Impact Damaged Composite Structures under Constant Biaxial Load," Journal of Composite Materials, **26**(2), 1992.

16. M.R. Gorman, "Burst Prediction by Acoustic Emission in Filament-Wound Pressure Vessels," Journal of Acoustic Emission, **9**(2).

17. B.W. Rosen, "Tensile Failure of Fibrous Composites," AIAA Journal, **2**(11), 1964.

18. S.L. Phoenix, E.M. Wu, "Statistics for the Time Dependent Failure of Kevlar-49/Epoxy Composites: Micromechanical Modeling and Data Interpretation," *Mechanics of Composite Materials/Recent Advances*, Hashin and Herakovich (eds), Pergamon Press:New York, 1983.

19. M. Tasnon and C. Roy, "Damage Tolerance in Graphite-Epoxy Composite: Comprehensive Monitoring Method," Polymer Composites, **8**(5), 1987.

20. E.V.K. Hill, "Burst Pressure Prediction in 45.7 cm (18 inch) Diameter Graphite/Epoxy Pressure Vessels Using Acoustic Emission Data," 36th International SAMPE Symposium, April 1991.

21. K.S. Downs, "A Discussion of Existing Specifications for Acoustic Emission (AE) Testing and/or Composite Overwrapped Pressure Vessels (COPVs)," Lockheed Martin Astronautics, June 1996.

22. M.R. Gorman, "Burst Prediction by Acoustic Emission in Filament-Wound Pressure Vessels," Journal of Acoustic Emission, **9**(2), 1990.

23. W.H. Prosser, K. Jackson, et al., "Advanced Waveform-Based Acoustic Emission Detection of Matrix Cracking in Composites," Materials Evaluation, 1995.

24. M.R. Gorman and W.H. Prosser, "AE Source Orientation by Plate Wave Analysis," Journal of Acoustic Emission, **9**(4), 1990.

25. S.M. Ziola and M.R. Gorman, "Source Location in Thin Plates Using Cross-Correlation," Journal of the Acoustical Society of America, **90**(5), 1991.

26. M.R. Gorman, "Plate Wave Acoustic Emission," Journal of the Acoustical Society of America, **90**(1), 1991.

27. W.H. Prosser and M.R. Gorman, "Plate Mode Velocities in Graphite/Epoxy Plates," Journal of the Acoustical Society of America, **96**(2), 1994.

28. W.H. Prosser and J. Dorighi, "Extensional and Flexural Waves in a Thin-Walled Graphite/ Epoxy Tube," Journal of Composite Materials, **26**(14), 1992.

29. M.R. Gorman, "New Technology for Wave Based Acoustic Emission and Acousto-Ultrasonics," AMD, **188**, 1994.

30. M.R. Gorman, "Wave Propagation and Signal Analysis," Short Course, 38th US AEWG Meeting, NASA Langley Research Center, May 1, 1995.

31. "Composite Overwrap Pressure Vessel Testing," Report to Brunswick Corporation, Lincoln, NE, 1993.

32. S.M. Ziola and M.R. Gorman, "Transverse Cracking and Longitudinal Splitting in Graphite/Epoxy Tensile Coupons as Determined by Acoustic Emission," Journal of Acoustic Emission, **8**(3).

33. S. Kantwell and J. Morton, "Impact Resistance of Composites/A Review," Composites, **22**(5), 1991.

34. A. Abrate, "Impact of Laminated Composite Materials," Applied Mechanics Reviews, **44**(4), 1991.

35. C. Poe and W. Illg, "Hidden Impact Damage in Thick Composites," 12th Annual QNDE Conference, 1986.

36. C. Poe, "Simulated Impact Damage in a Thick Graphite/Epoxy Laminate Using Spherical Indenters," NASA TM-100539, Jan. 1988.

37. S. Swanson, D. Cairns, et al., "Compression Fatigue Response for Carbon Fiber with Conventional and Toughened Epoxy Matrices with Damage," Journal of Engineering Materials and Technology, Transactions of the ASME, **115**(1), 1993.

38. "Guidelines for Visual Inspection and Requalification of Fiber Reinforced High Pressure Cylinders," CGA C-6.2-1988, Compressed Gas Association, 1988.

39. "Compressed and Liquefied Gases in Portable Cylinders," NFPA 55, National Fire Protection Association, ANSI/NFPA 55, 1993.

40. "Basic Requirements for Compressed Natural Gas Vehicle (NGV) Fuel Containers," ANSI/ AGA NGV2-1992, American National Standard, 1992.

41. G.K. Knight, "Residual Strength of Carbon/Epoxy Pressure Vessels Subjected to Low Velocity Impacts," ANTEC '89 Conference, Society of Plastics Engineers, 1989.

42. D.A. Thomas, "Long-Life Assessment of Graphite/Epoxy Materials for Space Station Freedom Pressure Vessels," Journal of Propulsion, **8**(1), Jan.-Feb. 1992.

43. R.C. Haddock, E.E. Morris, and F.J. Darms, "Safety of Filament Wrapped Graphite/Epoxy Composite Pressure Vessels for Aerospace Applications," AIAA/ASME/SAE/ASEE 27th Joint Propulsion Conference, June 24-26, 1991, Sacramento, CA.

44. C.A. Braun and R.C. Haddock, "Manufacturing Process Controls for High Reliability Carbon Filament-Wound Seamless Aluminum Lined Composite Pressure Vessels," AIAA/ ASME/SAE/ASEE 28th Joint Propulsion Conference and Exhibit, July 6-8, 1992, Nashville, TN.

45. D.B. Tiller, G.B. Khawand, C.F. Murray, and R.E. McClellan, "Design and Qualification of a Carbon Overwrapped, Aluminum Lined Pressurant Tank for the INTELSAT VII Satellite," AIAA/ASME/SAE/ASEE 27th Joint Propulsion Conference, June 24-26, 1991, Sacramento, CA.

46. C.F. Murray, N.L. Newhouse, and G. Khawand, "All-Composite Pressurant Tanks for Aerospace Applications," AIAA/ASME/SAE/ASEE 29th Joint Propulsion Conference and Exhibit, June 28-30, 1993, Monterey, CA.

47. R.B. Veys, A.R. Cederberg, and J.D. Schimenti, "Fatigue Analysis Techniques for Composite Tankage with Plastically Operating Aluminum Liners," AIAA/ASME/SAE/ ASEE 27th Joint Propulsion Conference, June 24-26, 1991, Sacramento, CA.

48. M.P. Connolly, "The Detection of Impact Damage in Composite Pressure Vessels using Source Location Acoustic Monitoring," 31st AIAA/ASME/SAE/ASEE Joint Propulsion Conference and Exhibit, July 10-12, 1995, San Diego, CA.

49. M.P. Connolly, S.J. Hudak, T.S. Grant, S. Roy, and C.H. Parr, "Assessment of Design and Durability Issues for Composite NGV Fuel Cylinders," GRI-92/0401, Gas Research Institute, Feb. 1994.

50. "GRI's Cylinder Safety Task Force Research Program and Recommendations to NGV Users," Gas Research Institute, Nov. 1994.

51. M.P. Connolly, J.J. Hanley, and V.D. Aaron, "Field Study of Composite NGV Fuel Cylinders," GRI-94/0341, Gas Research Institute, Sept. 1994.

52. J.T. Herridge, D.R. Stephens, et al., "Identification of Service Environment of NGV Fuel Cylinders," GRI-94/0203, Gas Research Institute, Jul. 1994.

53. J. Wong, C. Webster, and L. Gambone, "Environmental Damage of Fiberglass Fully-Wrapped NGV Cylinders Due to Moisture and Road Salt Exposure," GRI-94/0399, Gas Research Institute, Oct. 1994.

54. C. Blazek, S. Chao, et al., "Coating Systems for NGV Composite Cylinders," GRI-94/0359, Gas Research Institute, Sept. 1994.

55. T.A. Williams, "Failure Modes in Fiber-Reinforced Plastic Materials," GRI-94/0212, Gas Research Institute, Sept. 1994.

56. M.P. Connolly and S.J. Hudak, "Fracture Mechanics Analysis of NGV Fuel Cylinders, Part II: Metal Cylinder Liners," GRI-93/0120, Gas Research Institute, Mar. 1994.

57. J.B. Chang, H.D. Beeson, M.R. Cain, W.L. Ross, and D.D. Davis, "Experimental Evaluation of Space Flight Composite Overwrapped Pressure Vessels," Presentation at Joint Structural and Mechanical Behavior Committee of JANNAF, 1994.

58. J.B. Chang, H.D. Beeson, M.R. Cain, W.L. Ross, and D.D. Davis, "Space Flight Graphite/Epoxy Composite Overwrapped Pressure Vessels Evaluation," PVP 318, *Structural Integrity of Pressure Vessels, Piping and Components*, ASME 1995.

59. S.T. Chiu, J.C. Shu, and J.B. Chang, "Evaluation of Analysis Methods for Composite Overwrapped Pressure Vessels," Presentation at Joint Structural and Mechanical Behavior Committee of JANNAF, 1994.

60. J.D. Shu, S.T. Chiu, and J.B. Chang, "An Enhanced Analysis Method for Composite Overwrapped Pressure Vessels," AIAA, 1995.

61. J.P. Nokes and E.C. Johnson, "Inspection Techniques for Composite Overwrapped Pressure Vessels," PVP 318, *Structural Integrity of Pressure Vessels, Piping and Components*, ASME 1995.

62. J.P. Nokes, F. Izaguirre, J.R. Hribar, R.L. Ruiz, and E.C. Johnson, "Nondestructive Evaluation of Gr/Ep Composite Overwrapped Pressure Vessels," Presentation at Joint Structural and Mechanical Behavior Committee of JANNAF, 1994.

63. Military Standard 1522A (USAF), "Standard General Requirements for Safe Design and Operation of Pressurized Missile and Space Systems," Notice 3, 04 Sept. 1992.

64. Handouts from the 8th COPV Program Review, White Sands Test Facility, Jan. 24, 1996.

65. K.S. Downs and MA. Hamstad, "High Sensor Density Acoustic Emission Monitoring of Graphite/Epoxy Pressure Vessels," AECM-5, Fifth International Symposium on Acoustic Emission from Composite Material, July 10-14, 1995, Sundsvall, Sweden.

66. M.A. Hanstad and K.S. Downs, "On Characterization and Location of Acoustic Emission Sources in Real Size Composite Structures - A Waveform Study," Journal of Acoustic Emission, **13**(1/2), 1995.

67. K.S. Downs and MA. Hamstad, "Differences in Generation and Detection of Acoustic Emission Based on a Large Number of AE Sensors on Graphite/Epoxy Pressure Vessels," AECM-5, Fifth International Symposium on Acoustic Emission from Composite Material, July 10-14, 1995, Sundsvall, Sweden.

68. "CGA C-6.2: Guidelines for Visual Inspection and Requalification of Fiber Reinforced High Pressure Cylinders," Compressed Gas Association, 1988.

69. R.S. Frankle and H.F. Wachob, "Investigation of the Failure of an SCBA Cylinder," Report FaAA-SF-R-96-06-16, Failure Analysis Associates, Inc., Menlo Park, CA, 1996.

70. D. Eitzen, F.R. Breckenridge, "Acoustic Emission Sensors and their Calibration," *Nondestructive Testing Handbook (2nd ed.) Vol. 5*, P. McIntire (ed.), American Society for Nondestructive Testing, 1987.

Table 1. Comparison of Candidate NGV Fuel Tank Inspection Methods

Features	Inspection Methods									
	visual-optical	penetrant	magnetic particle	ultrasonics	X-ray	acoustic emission	therm-ography	shear-ography	eddy current	microwave
Application										
all steel tank	Yes	Yes	Yes	Yes	Yes	Yes	No	Yes	Yes	No
carbon/glass fiber overwrap	Yes	No	No	Yes	Yes	Yes	Yes	Yes	No	No
carbon fiber overwrap	Yes	No	No	Yes	Yes	Yes	Yes	Yes	No	No
carbon fiber hoop wrap	Yes	No	No	Yes	Yes	Yes	Yes	Yes	No	No
Technical										
detects surface defects	Yes	Yes	Yes	Yes	Yes	Yes	Yes	Yes	Yes	Yes
detects subsurface defects	No	Some	Some	Yes	Yes	Yes	Yes	Yes	Yes	Yes
quantifies defect size	Yes	Yes	Yes	Yes	Yes	No	Yes	Yes	Yes	Yes
quantifies defect depth	No	Yes	No	Yes	No	No	No	No	Yes	No
Maturity										
NGV experience	Yes	Yes	Yes	Yes	No	Yes	No	No	No	No
experience with similar structures	Yes	Yes	Yes	Yes	Yes	Yes	Yes	Yes	Yes	Yes
state-of-the-art	Mature	Mature	Mature	Mature	Mature	New	New	New	New	New
Practical Application										
suitable for in-service application	Yes	Yes	Yes	No	No	Yes	No	No	No	No
operator importance	High	High	High	Mod	Mod	Low	Mod	Mod	Mod	Mod
sophisticated equipment required	No	No	No	Yes	Yes	Yes	Mod	Mod	Mod	Mod
can be easily automated?	Optical	No	No	Yes	No	Yes	Yes	Yes	Yes	Yes
inspect multiple tanks at once?	No	No	No	No	No	Yes	No	No	No	No
hazards	No	Yes	No	No	Yes	No	No	No	No	No
inspection speed	Slow	Slow	Slow	Mod	Mod	Fast	Mod	Mod	Mod	Mod
damage potential from inspection	Mod	High	High	High	Mod	Low	Mod	Mod	High	Mod
requires surface preparation	Yes	Yes	Yes	Yes	No	No	Yes	Yes	Yes	Yes
requires tank removal for 100% inspection	Yes	Yes	Yes	Yes	Yes	No	Yes	Yes	Yes	Yes

Note: Mod = moderate

Table 2. Test Matrix for Tow Testing

Test Number	Pull Rate	Tow Notched
1	0.0025 cm/min	No
2	0.005 cm/min	No
3	0.0127 cm/min	No
4	0.0025 cm/min	Yes

FWD settings	Signal	Trigger
High Pass Filter	50 kHz	20 kHz
Low Pass Filter	1.5 MHz	1.5 MHz
Gain	73 dB	70 dB
Threshold	--	0.1 volts
Echo Delay Time	--	0 μ sec

Table 3. Theoretical Arrival Times

Between Sensors	Time Difference -- Longitudinal Mode	Time Difference -- Flexural Mode (2.0 km/sec @ 150 kHz)
1 and 2	~ 7 μ sec	~ 30 μ sec
2 and 3	~ 5 μ sec	~ 25 μ sec
3 and 4	~ 7 μ sec	~ 30 μ sec

Table 4. NGV Fuel Tank Test Specimens

ID	Vendor	Liner	Fiber	Overwrap	Overall Size, inch
012	Pressed Steel Tank	Steel	Carbon	Hoop Wrapped Type 2	61 × 16.4
004	Pressed Steel Tank	Steel	Carbon	Hoop Wrapped Type 2	50 × 11.3
013	Pressed Steel Tank	Steel	Carbon	Hoop Wrapped Type 2	34.4 × 16.2
014	Pressed Steel Tank	Steel	Carbon	Hoop Wrapped Type 2	34.4 × 16.2
018	Pressed Steel Tank	Steel	Carbon	Hoop Wrapped Type 2	34.4 × 16.2
003	Edo Tank	Thermoplastic	Carbon	Fully Wrapped Type 4	36.3 × 17.7

Table 5. Tank Damage

	Impact			
ID	Indenter	Energy, ft-lb	Damage	**Slit Size, in**
012	N/A	N/A	N/A	N/A
004	N/A	N/A	N/A	2 × 0.050 2 × 0.030
013	pyramid pyramid	22.1 221	1.5 inch hoop × 0.5 inch axial; hoop cracks; 2 shallow dents 2.25 inch hoop × 0.5 inch axial; hoop cracks; 0.125 inch deep dent; 1 shallow dent	2 × 0.050 3 × 0.125
014	N/A	N/A	N/A	N/A
018	2 in × 17 in	2,050	N/A	8 × 0.18
003	45° drop e.g., 5 ft above concrete		3 inch diameter; 2.25 inch long crack	N/A

Table 6. Fatigue Testing

	Fatigue Testing						
ID	Ramp Up, sec	Hold, sec	Ramp Down, sec	Hold, sec	Max Pressure, psig	**Cycles**	**Failure?**
012	N/A	N/A	N/A	N/A	N/A	N/A	No
004	15	60	15		3,600 4,500 4,800	5 5 5	No
013	9-10	1	8-9	1	3,600	15,000	No
014	11	1	7	1	3,600	3000	No
018	10	1	8	1	3,600	15,000	No
003	16*	1*	12*	1*	3,600 4,000	6,000 2,146	Yes

* Pressure cycles in fatigue test facility.

Table 7. Acoustic Emission Inspection

ID	No. Sensors	Virgin	Post-Damage	During Fatigue	Fatigue Ramp*
012	8	X	N/A	N/A	N/A
004	6	X	X	X	X
013	8**	X	X	X	X
014	4	X	N/A	N/A	X
018	7	X	X	X	X
003	7	X	X	X	X

* Pressure ramp after fatigue cycling.
** 7 sensors during fatigue testing

Table 8. Results for Tank 013

Condition	Significant AE Pressure, psig	Observations
As-received	7,293	Autofrettage cracks more noticeable
Slit 1 2 × 0.050 inch	5,533	Circumferential cracks emanating from ends of slit
Impact 1 Pyramid-22.1 ft-lbs	5,504	Cracks from slit grown; Edges of slit separated No visible change in damaged area
Impact 2 Pyramid-221 ft-lbs	5,529	Cracks from slit grown No visible change in damaged area
Slit 2 3 × 0.125 inch	4,994	Circumferential cracks emanating from ends of slit
Fatigue 15,000 cycles - 3,600 psig	4,500	Circumferential cracks from slits and damage grow around tank. Slits delaminated from underlying overwrap

Table 9. Results for Tank 014

Condition	Significant AE Pressure, psig	Observations
As-received	7,200	No visible change
Fatigue 3,000 cycles - 3,600 psig	7,200	No visible change

Table 10. Results for Tank 018

Condition	Significant AE Pressure, psig	Observations
Virgin	7,200	Autofrettage cracks more noticeable
Impact 1 2 × 17 inch flat - 2,050 ft-lbs	7,200	No visible change
Slit 8 × 0.18 inch	4,530	Cracks emanate from ends of slit. Cut edges of slit separated
Fatigue 15,000 cycles - 3,600 psig	4,500	Cracks from ends of slit grown around tank Slit delaminated from tank

Table 11. Results for Tank 003

Condition	Significant AE Pressure, psig	Observations
Virgin	6,062	No visible change
Impact 45° Drop c.g., 5 ft above concrete	3,667	No visible change
Fatigue 6,000 cycles - 3,600 psig* 2,146 cycles - 4,000 psig	4,500	Tank failed at impact site after 8,146 cycles

* 230 cycles in the burst test facility and remainder in the fatigue test facility

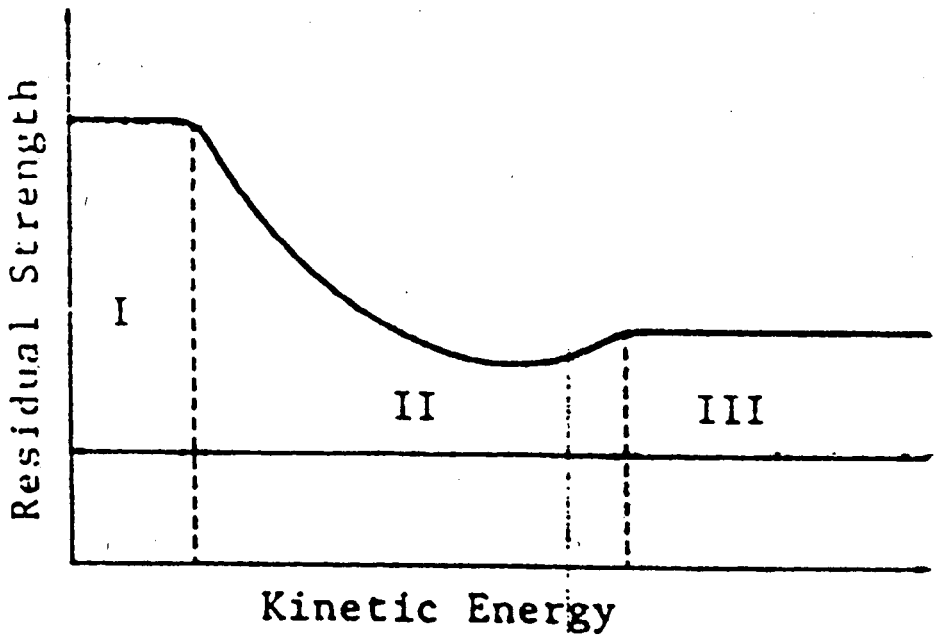

Figure 1. Variation of Residual Tensile Strength with Impact Energy

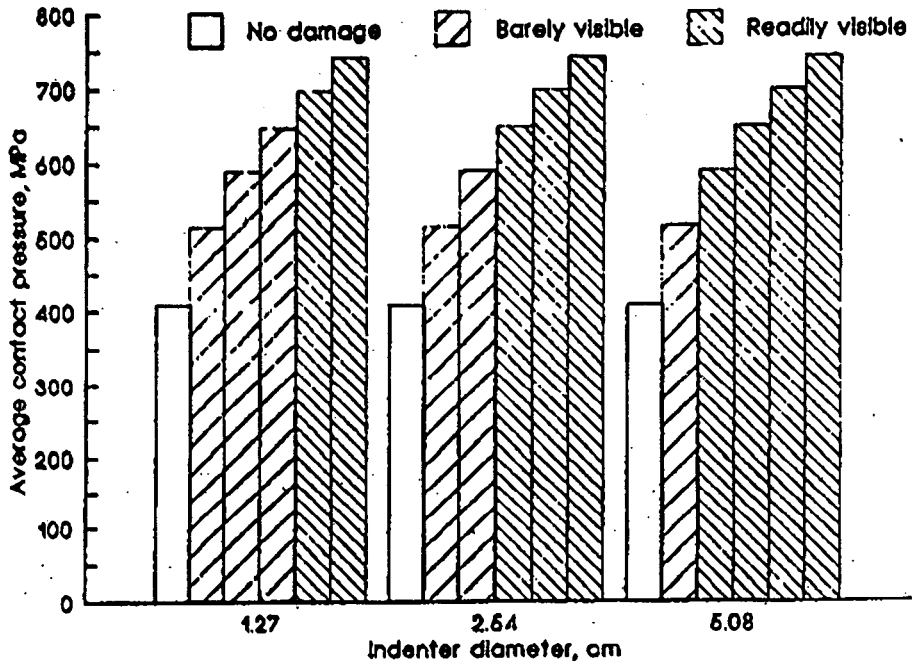

Figure 2. Effect of Indenter on Visibility of Impact Damage

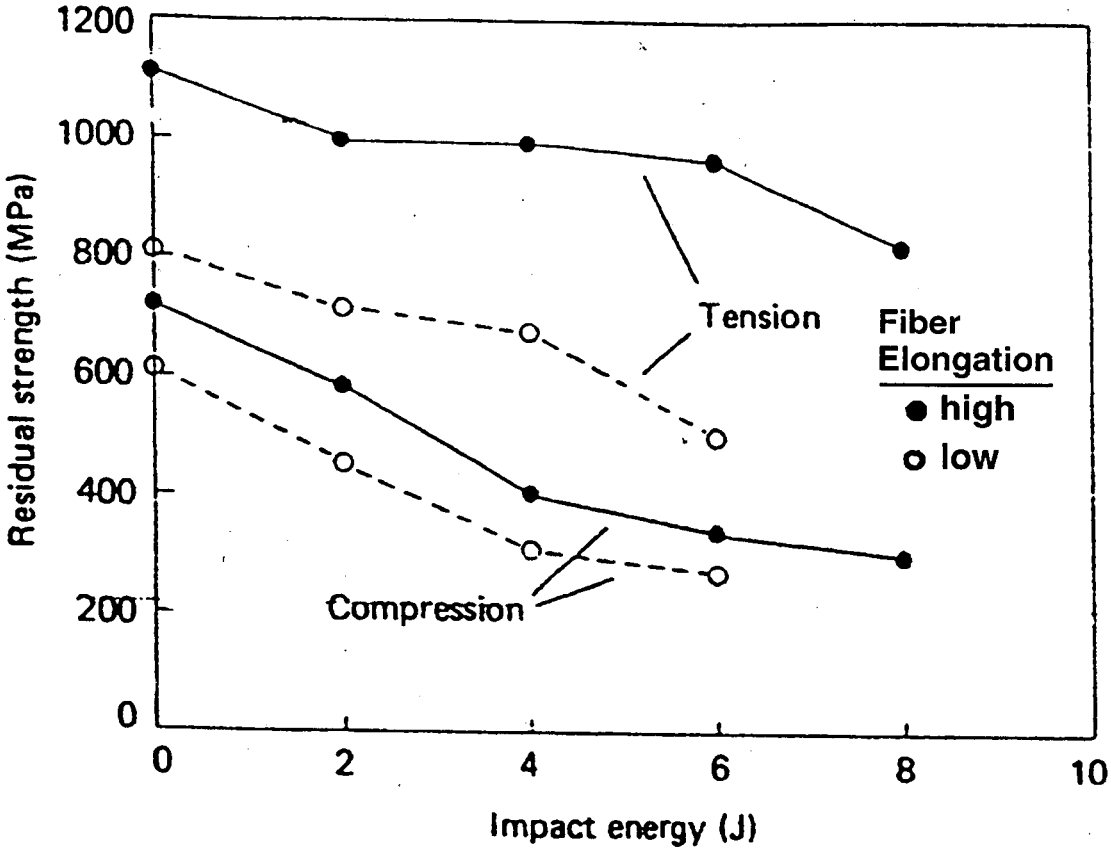

Figure 3. Effect of Fiber Elongation on Post-Impact Residual Strength

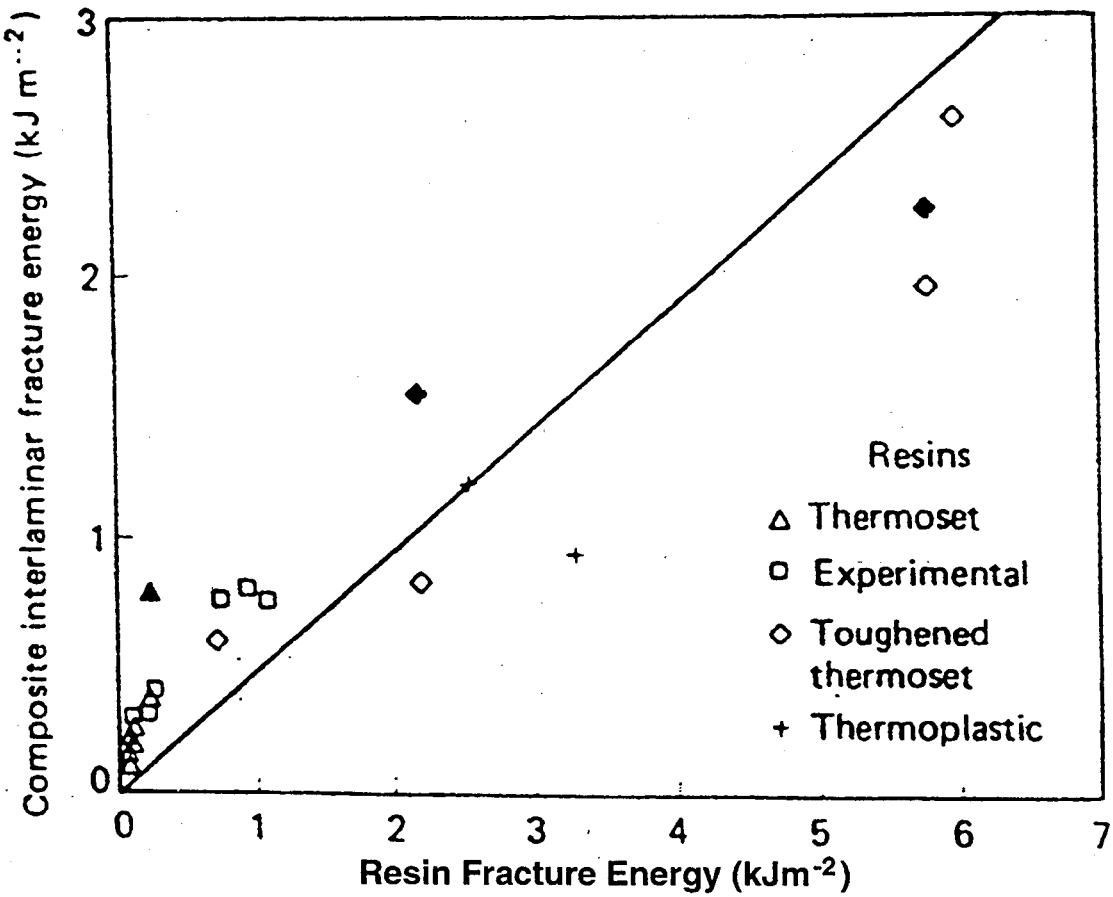

Figure 4. Effect of Resin Fracture Energy on Composite Interlaminar Fracture Energy

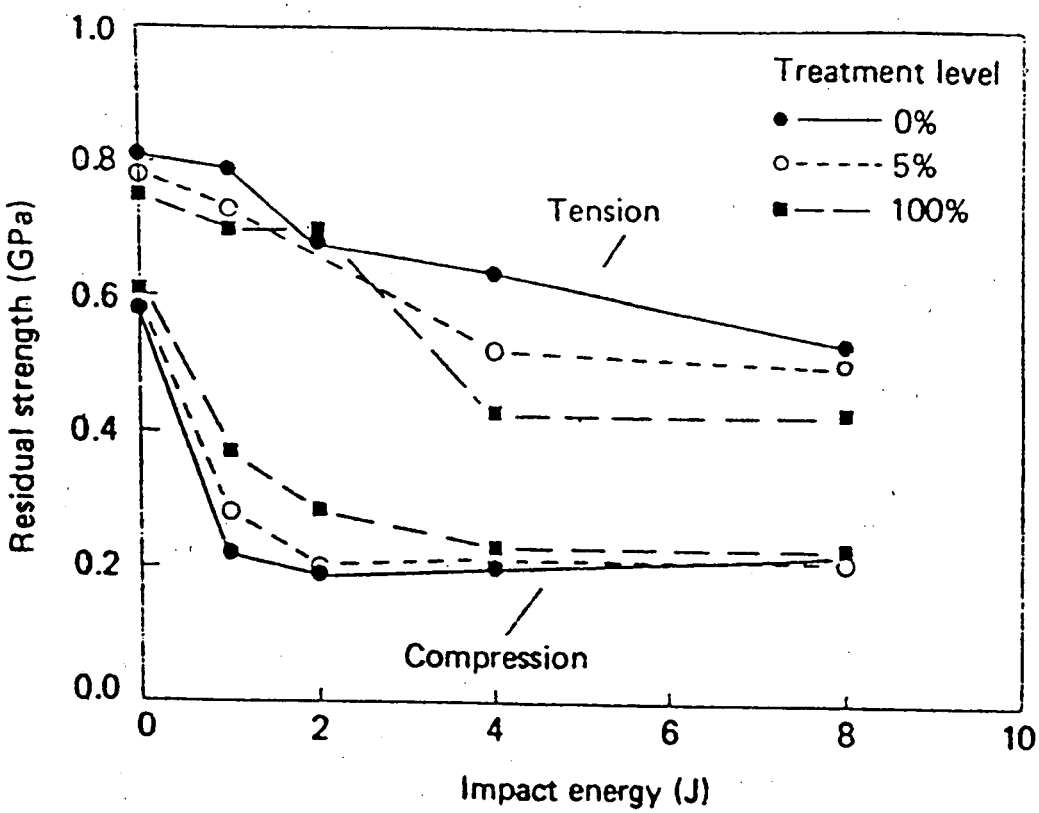

Figure 5. Effect of Fiber Treatment on Post-Impact Residual Strength

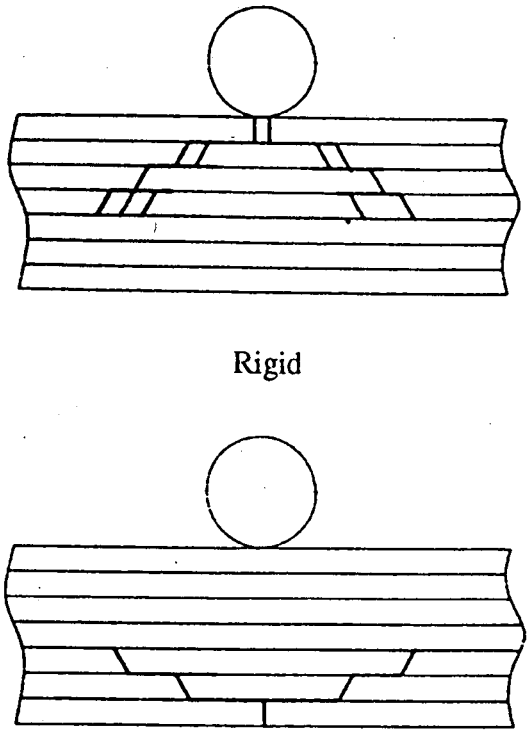

Figure 6. Impact Damage in a Rigid and Flexible Target

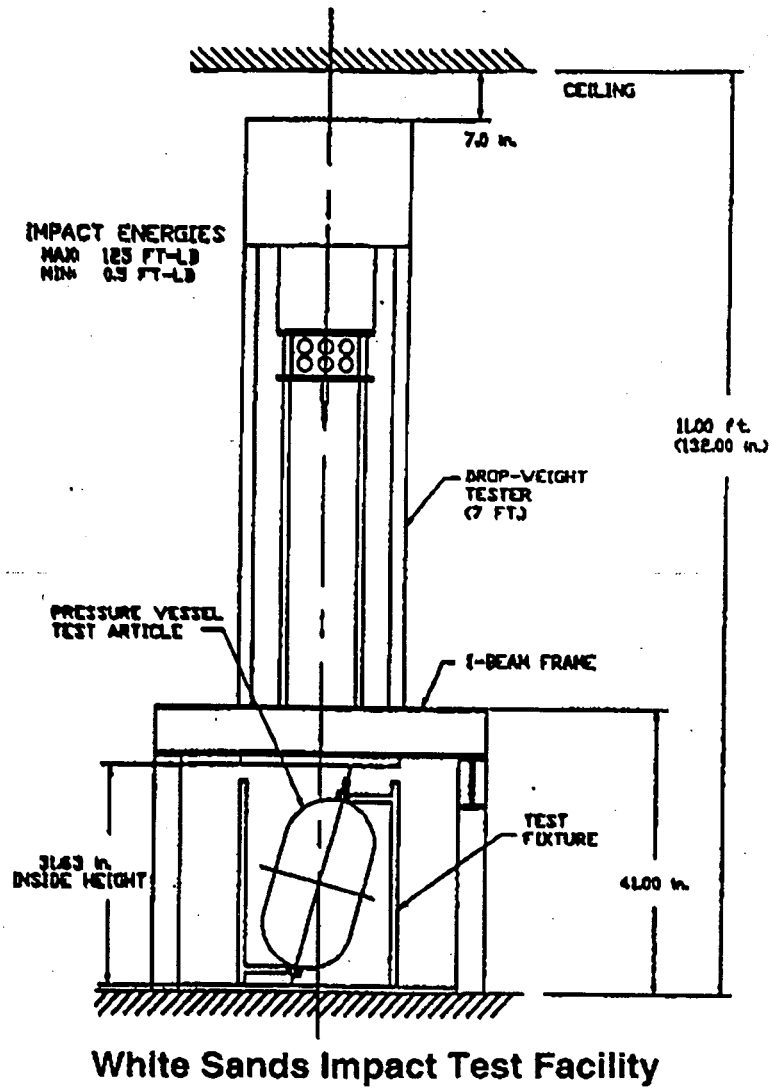

Figure 7. COPV Impact Test Facility at White Sands Test Facility

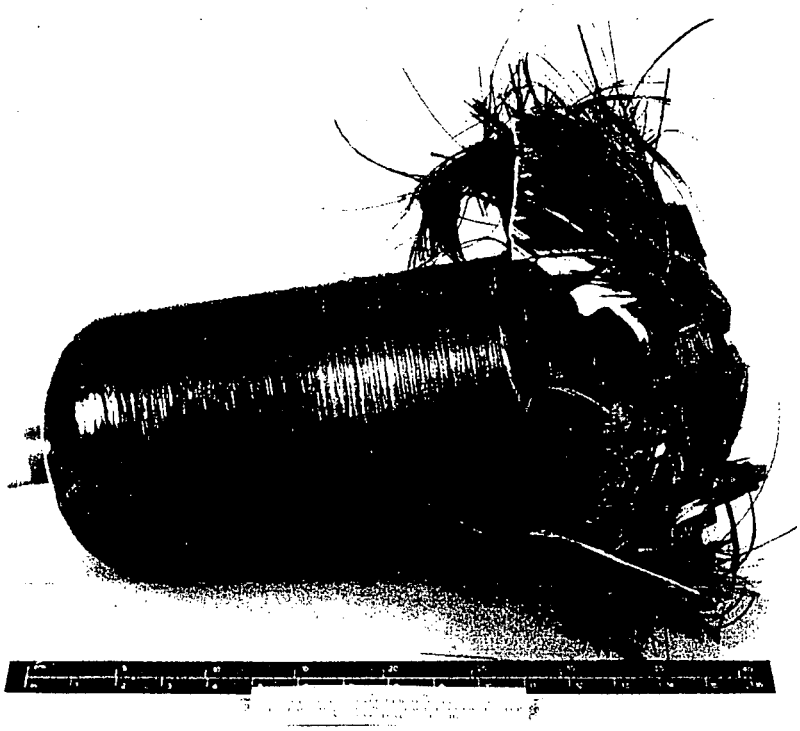

Figure 8. Burst COPV Following Impact

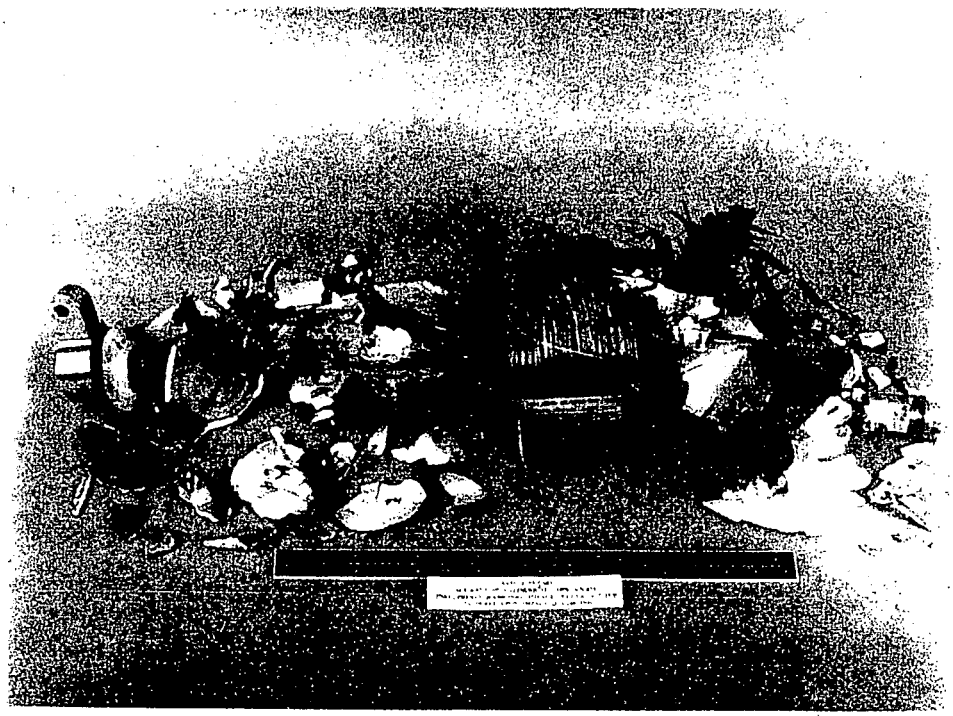

Figure 9. COPV Failed Upon Impact

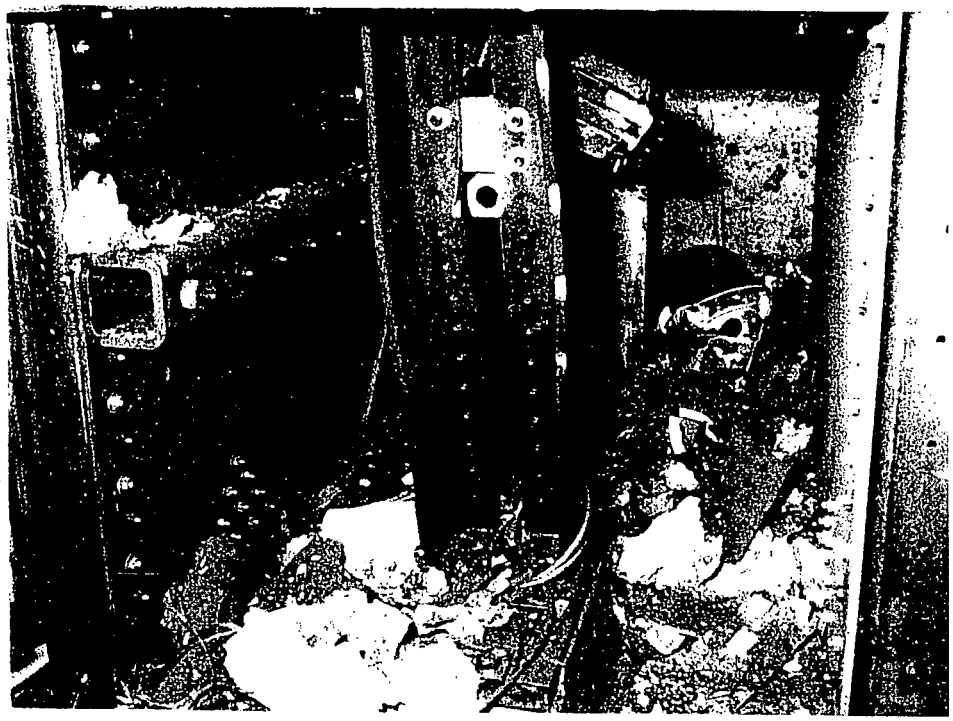

Figure 10. Post-Failure COPV Test Facility

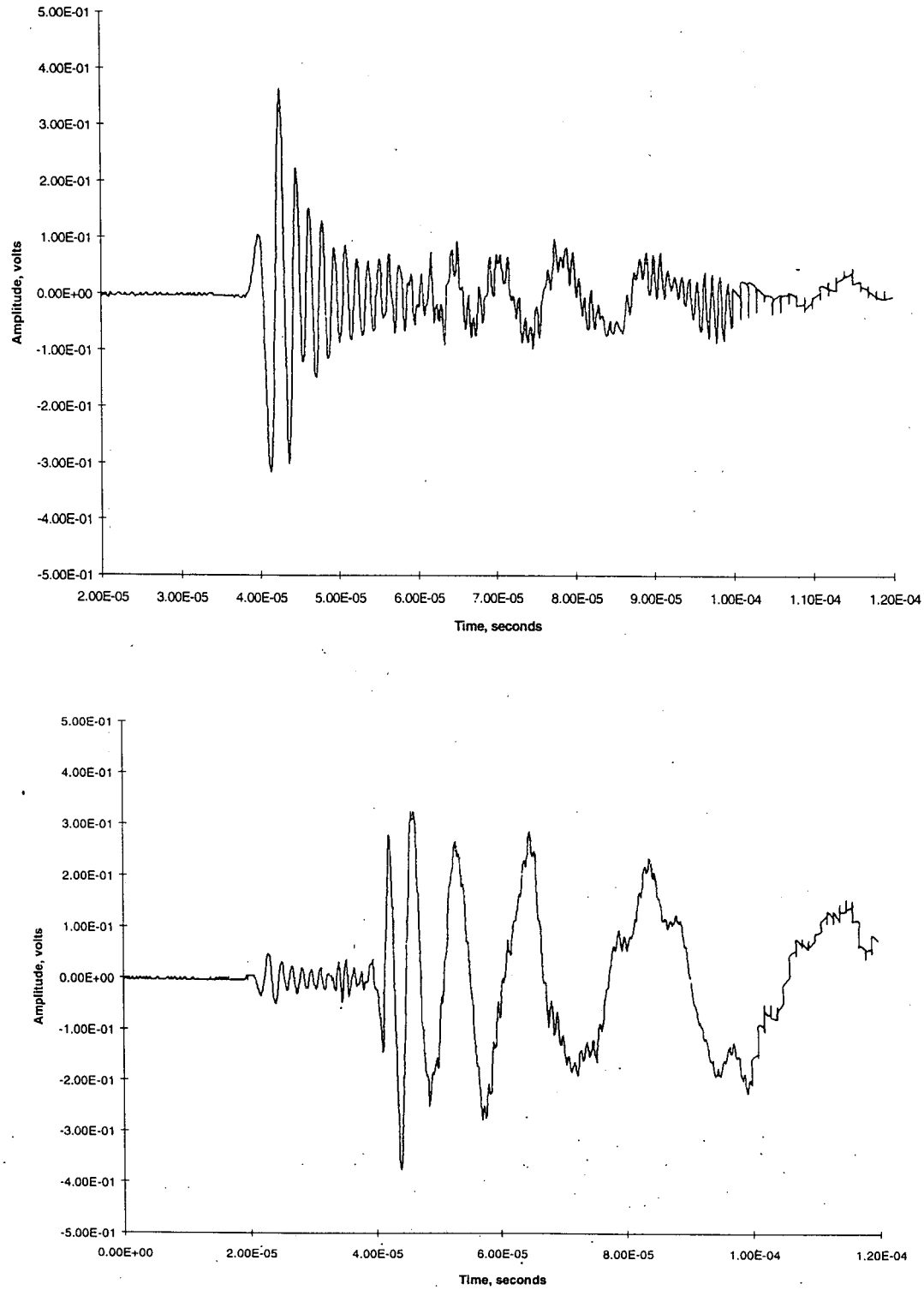

Figure 11. Plate Wave: Extensional Mode on the Top, Flexural Mode on the Bottom

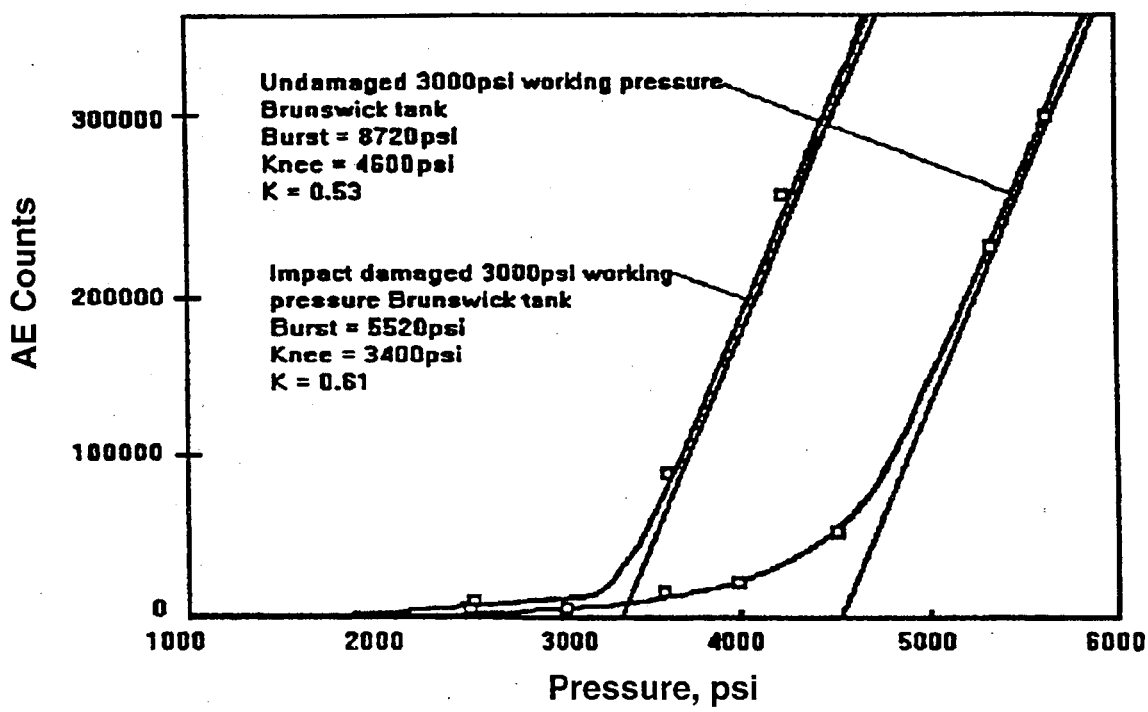

Figure 12. Knee of the Curve [13]

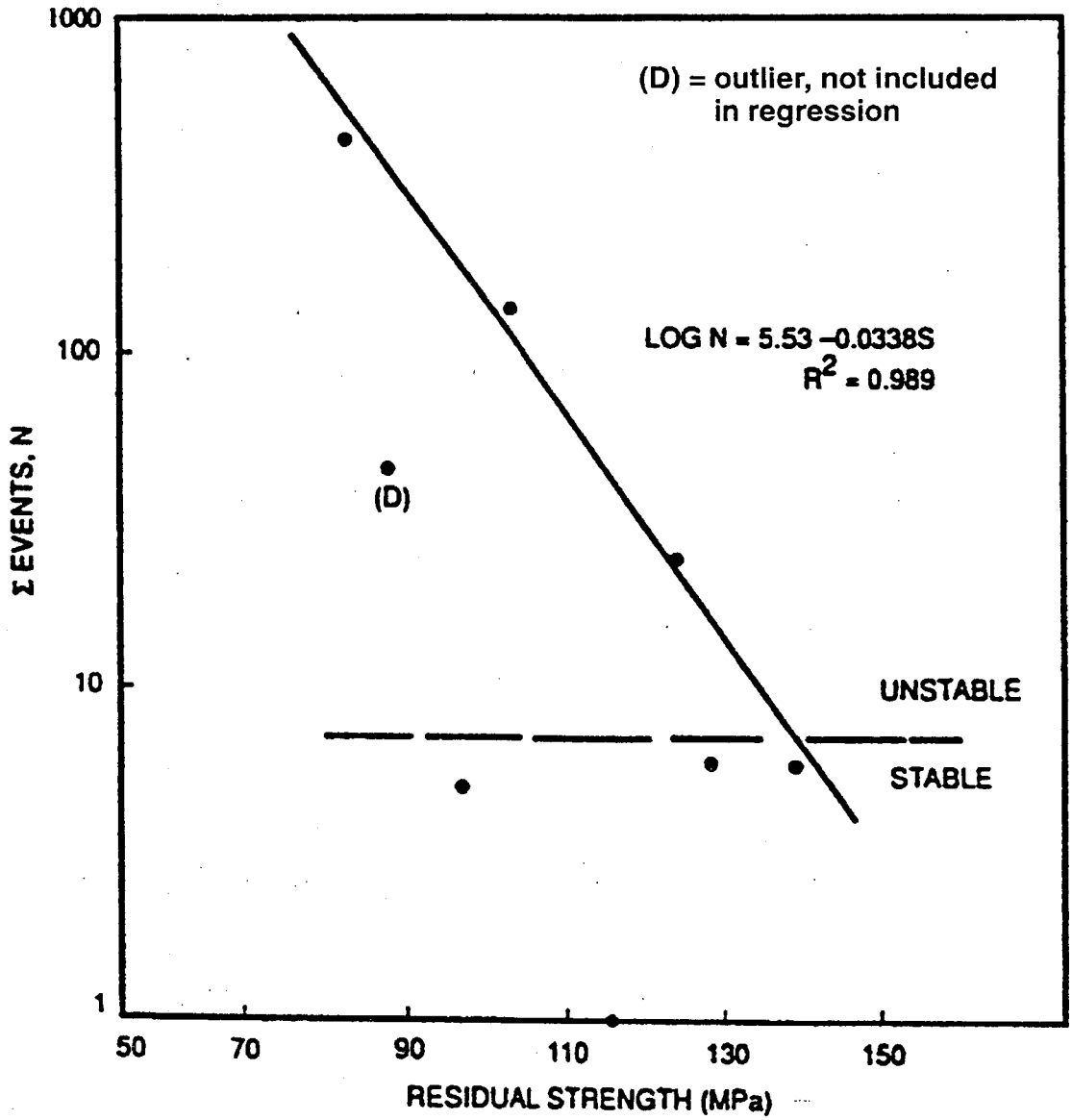

Figure 13. Correlation of Long Duration Events with Residual Strength [15]

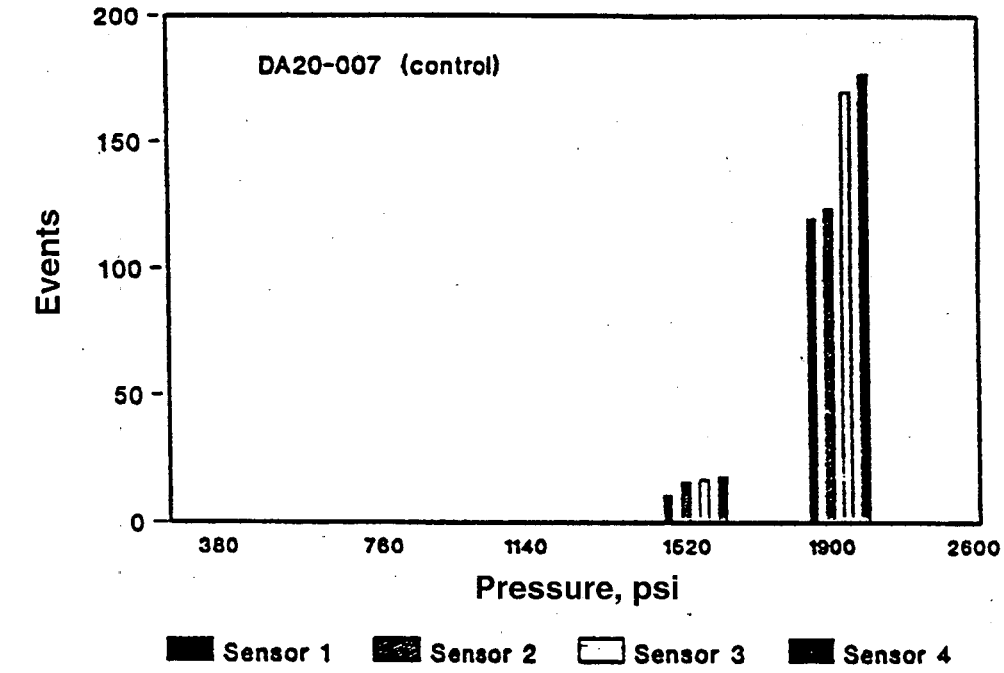

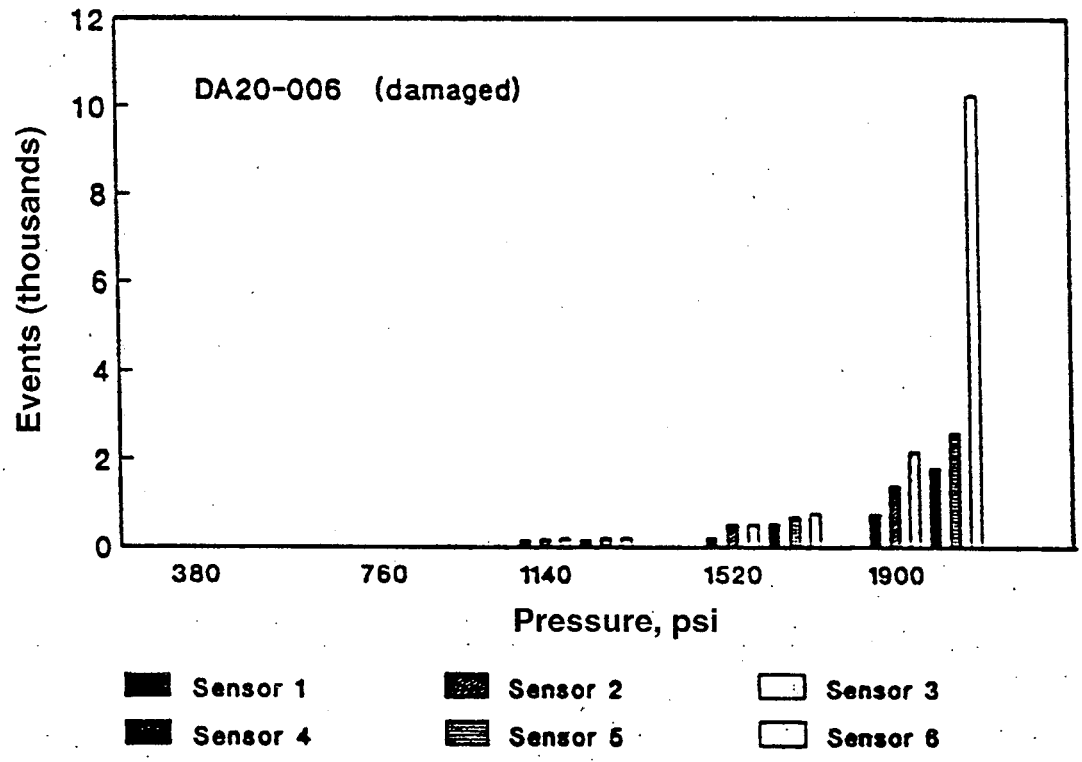

Figure 14. Total Events vs. Burst Pressure for Control (Undamaged) and Damaged Pressure Vessels [16]

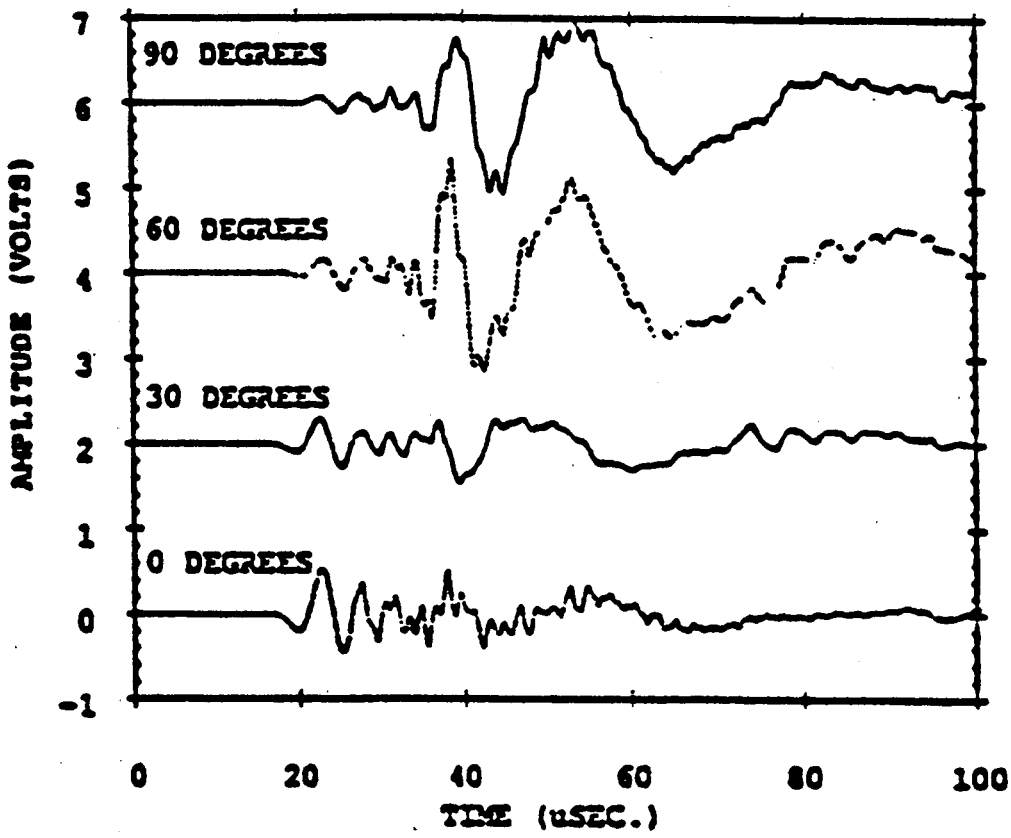

Figure 15. Source Orientation Effects [24]

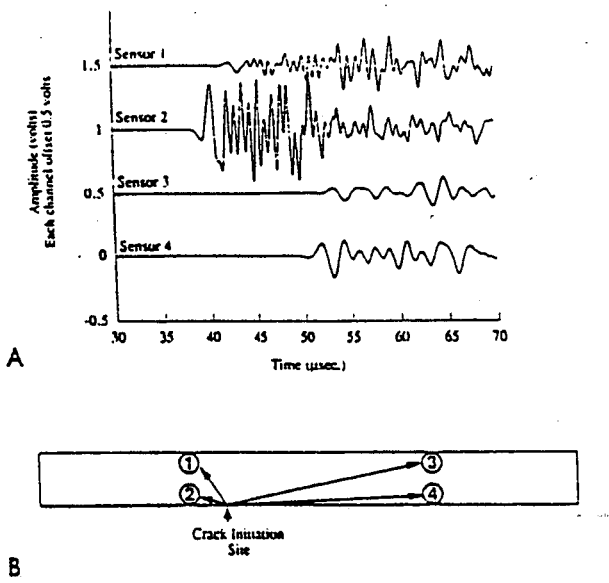

Figure 16. Waveforms Due to Transverse Matrix Cracking [23]

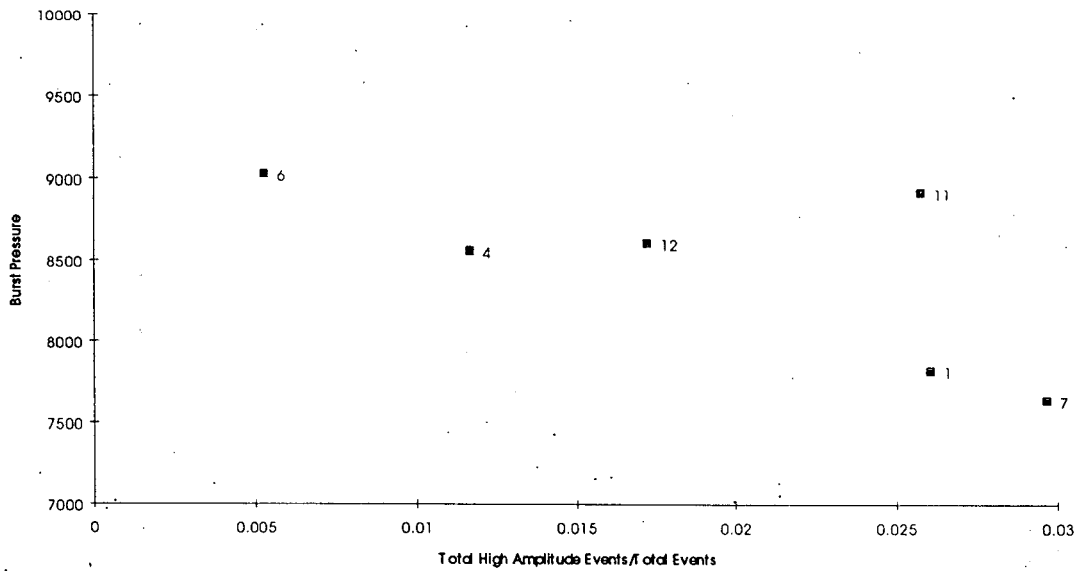

Figure 17. Burst Pressure Correlation for Modal Based AE Analysis [31]

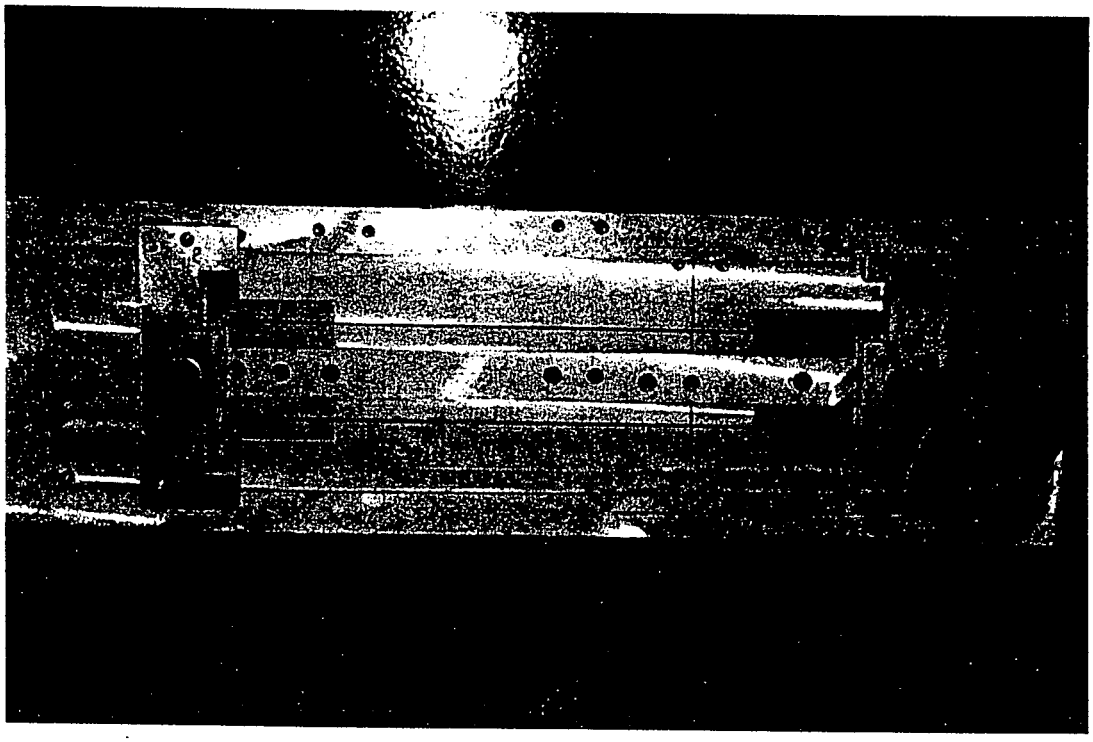

Figure 18. Mounting Tabs on a Tow Test Specimen

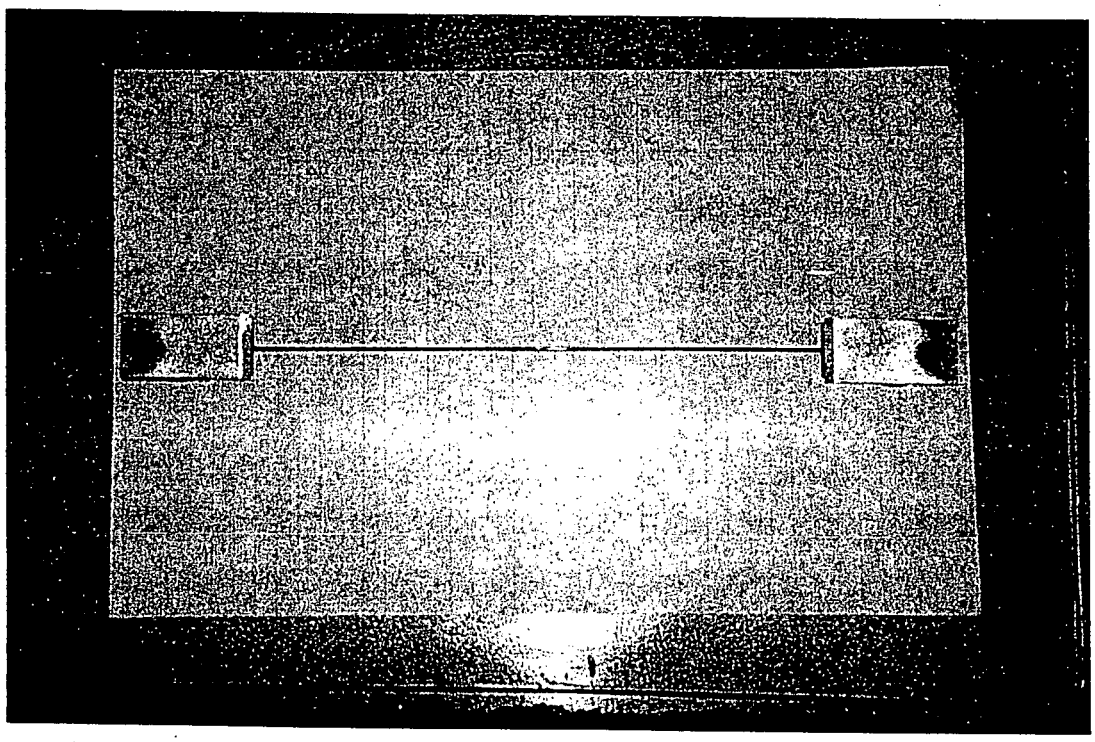

Figure 19. Completed Tow Test Specimen

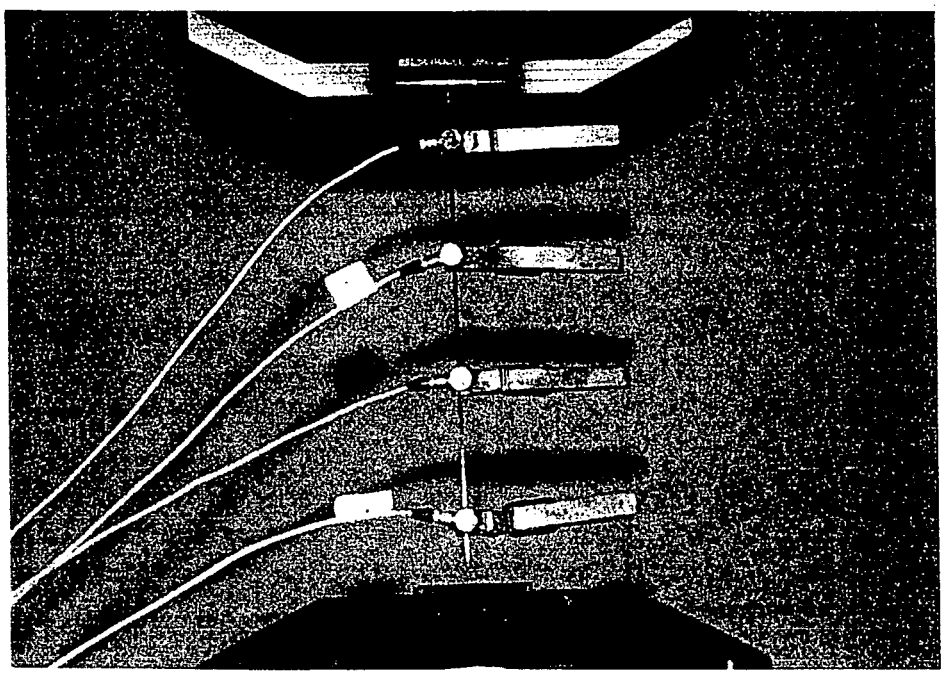

Figure 20. Tow Specimen in Grips of Hydraulic Test Machine

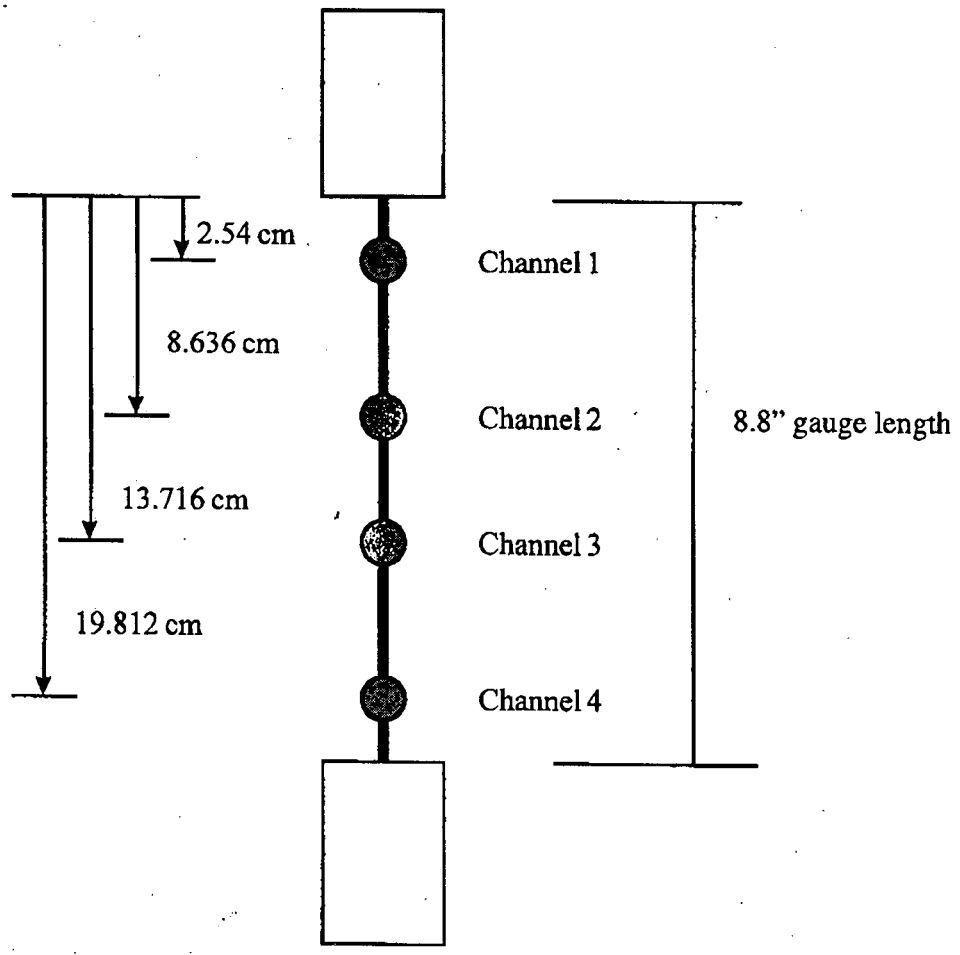

Figure 21. Typical Transducer Mounting Locations on the Tow Test Specimens

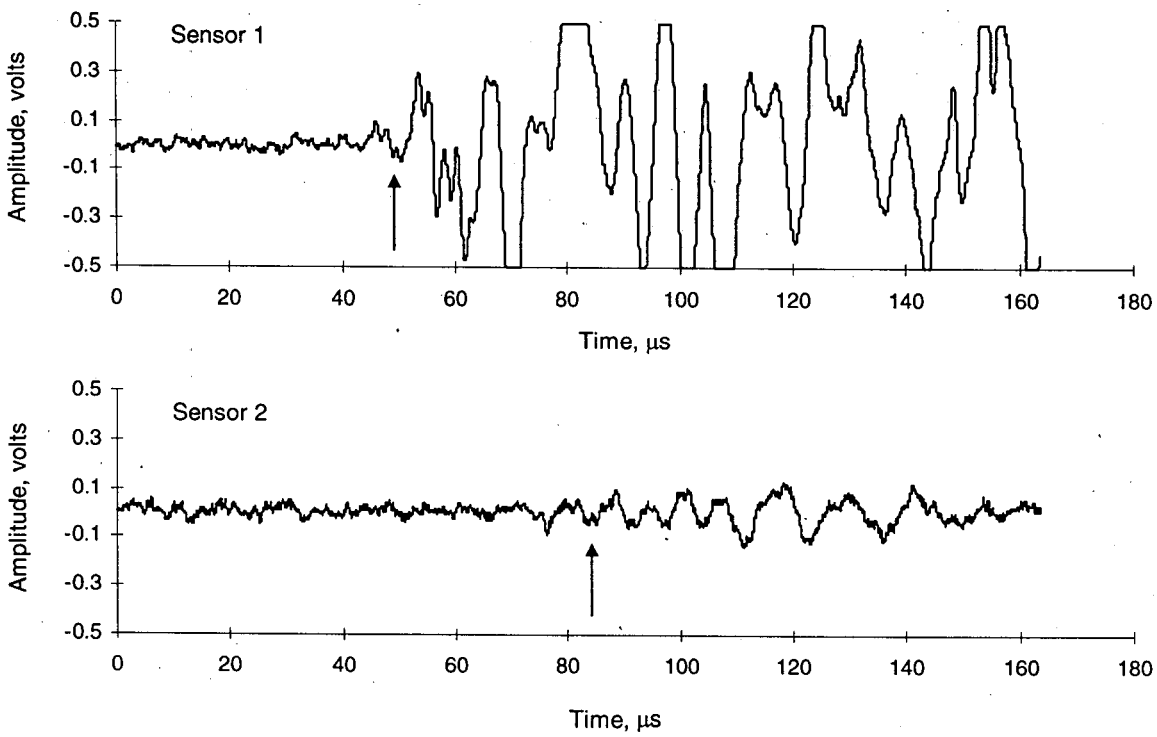

Figure 22. Waveforms from One Event During Tow Test #1 – Flexural Propagation

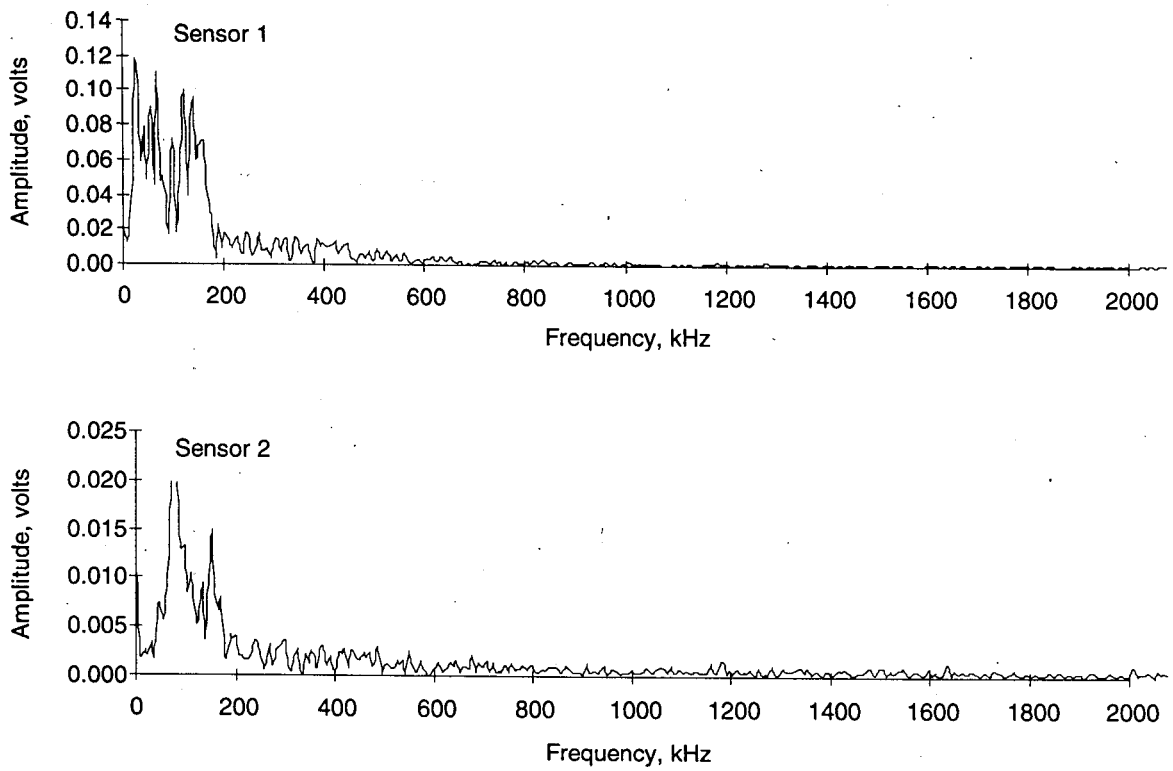

Figure 23. FFT of Waveforms in Figure 20

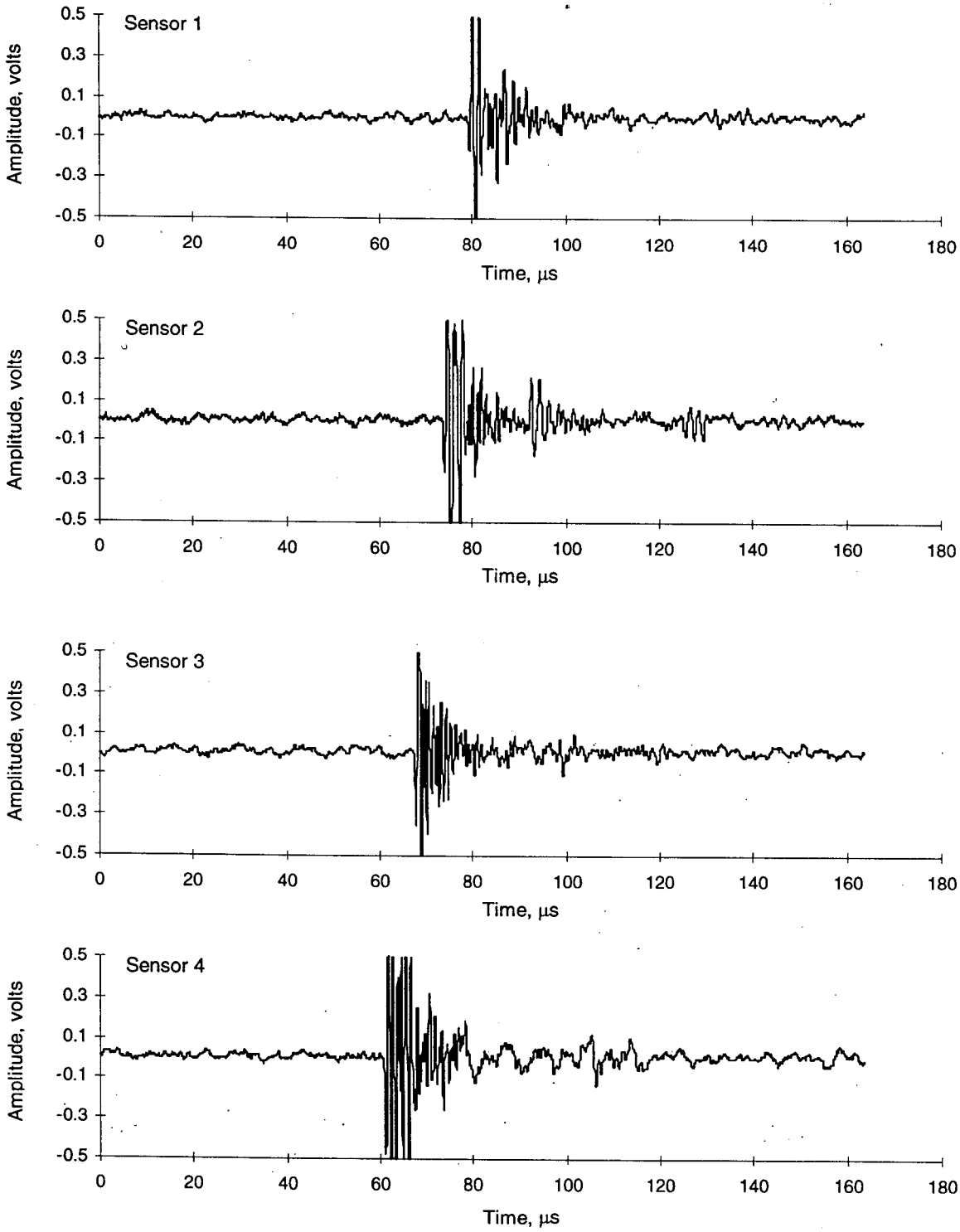

Figure 24. Waveforms from One Event During Tow Test #1 – Extensional Propagation

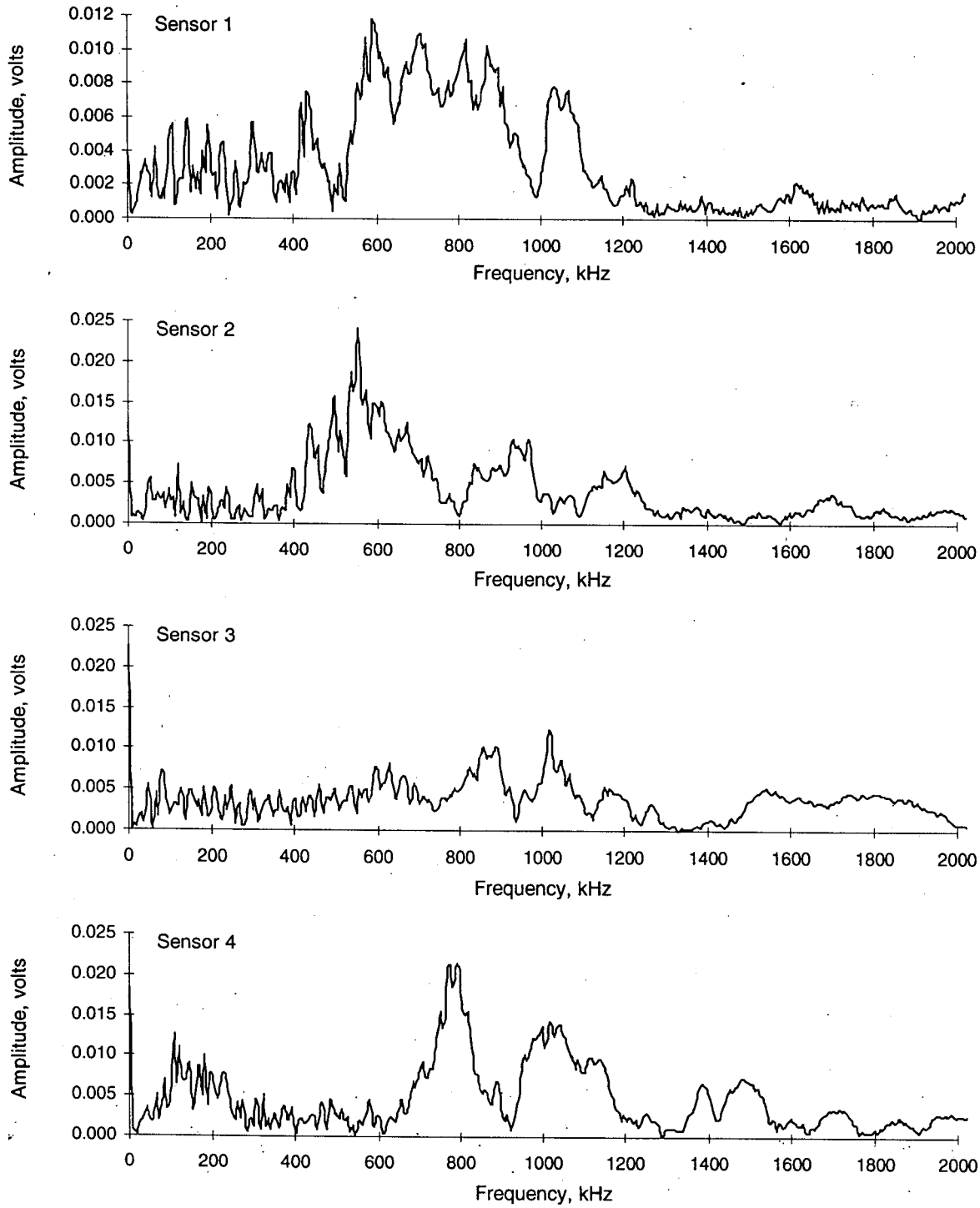

Figure 25. FFTs from Waveforms in Figure 22

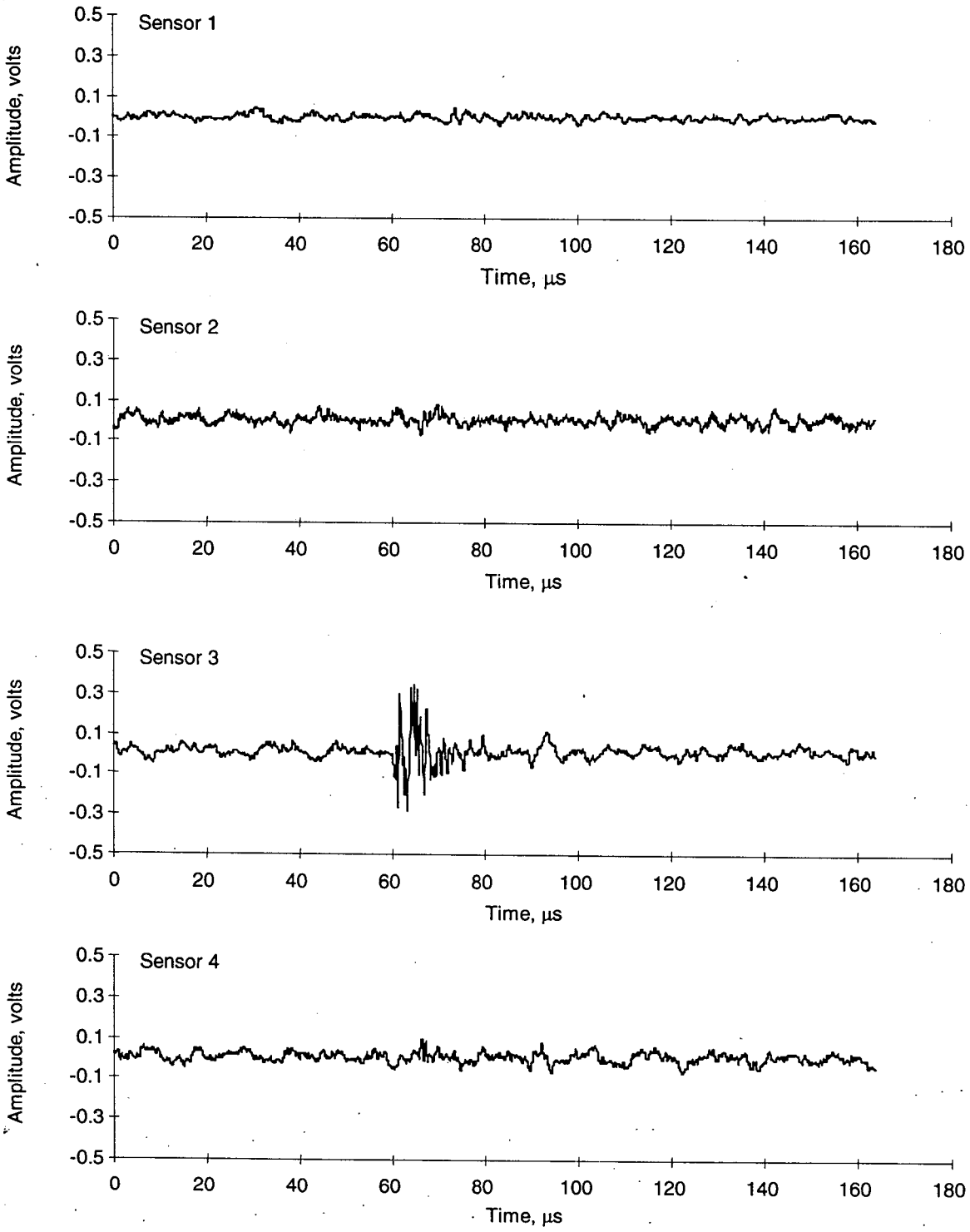

Figure 26. Typical Single Channel Event Recorded During Testing

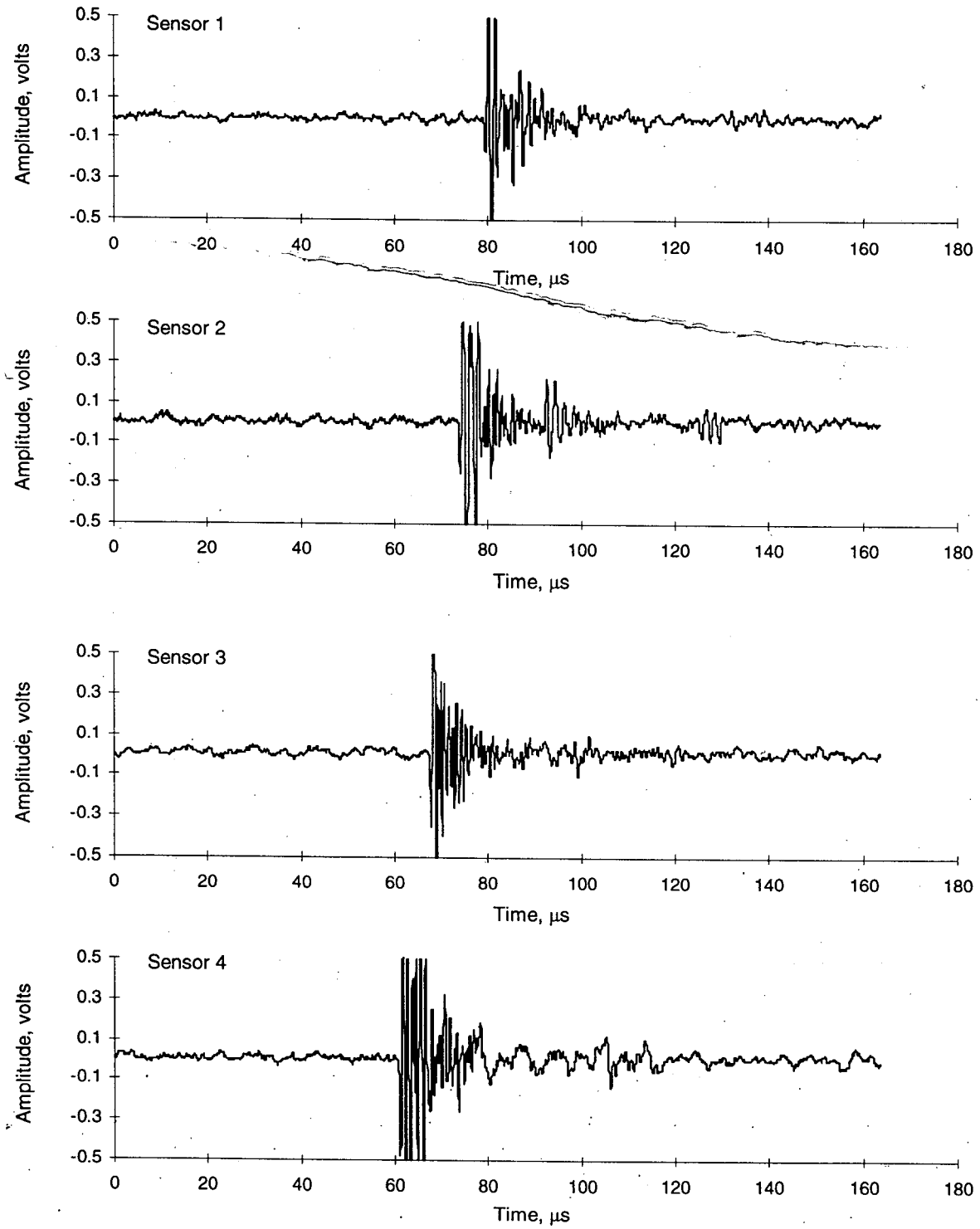

Figure 27. Typical High Frequency, Short Duration Event

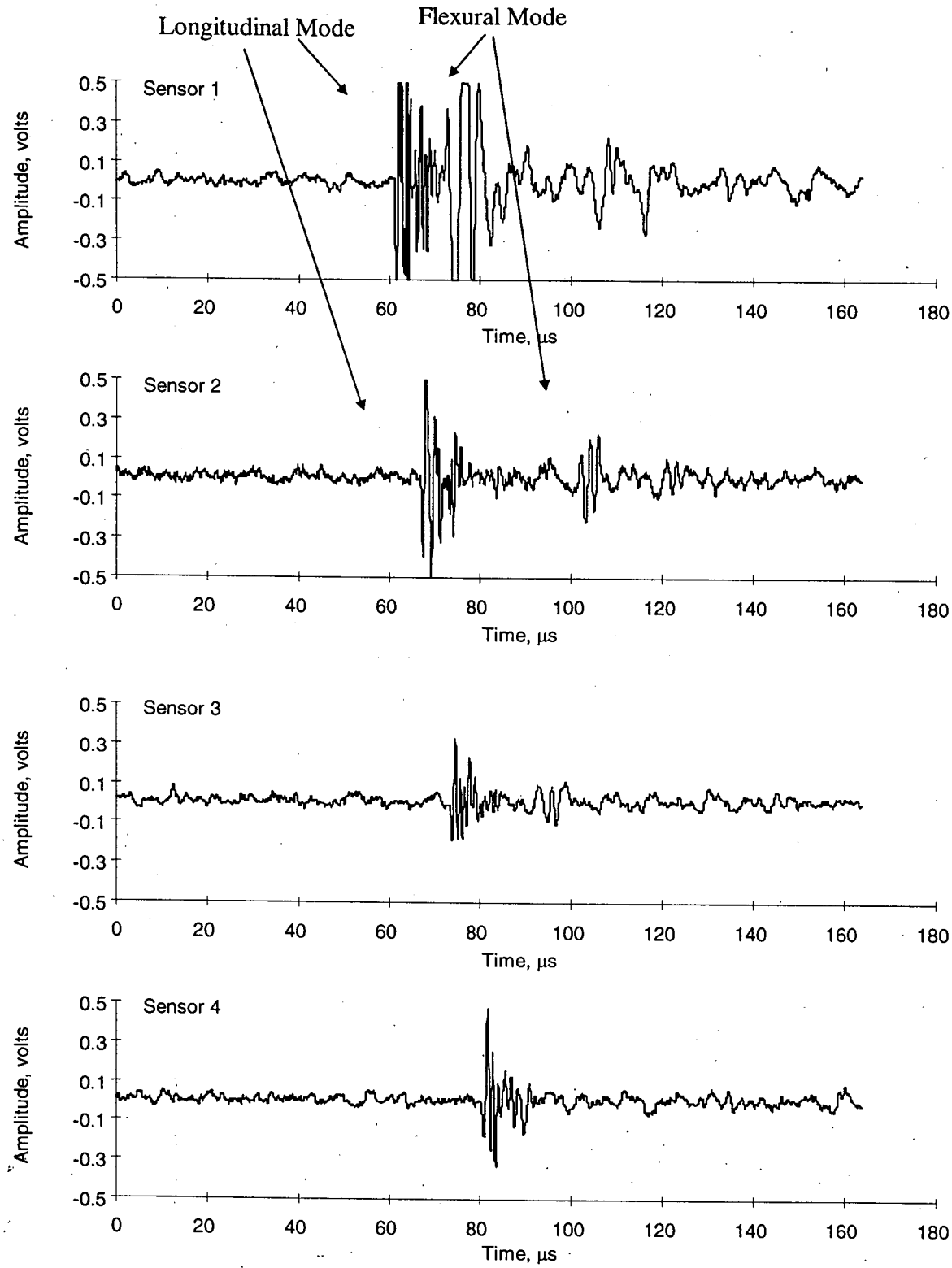

Figure 28. Fiber Break Signal with Flexural Component

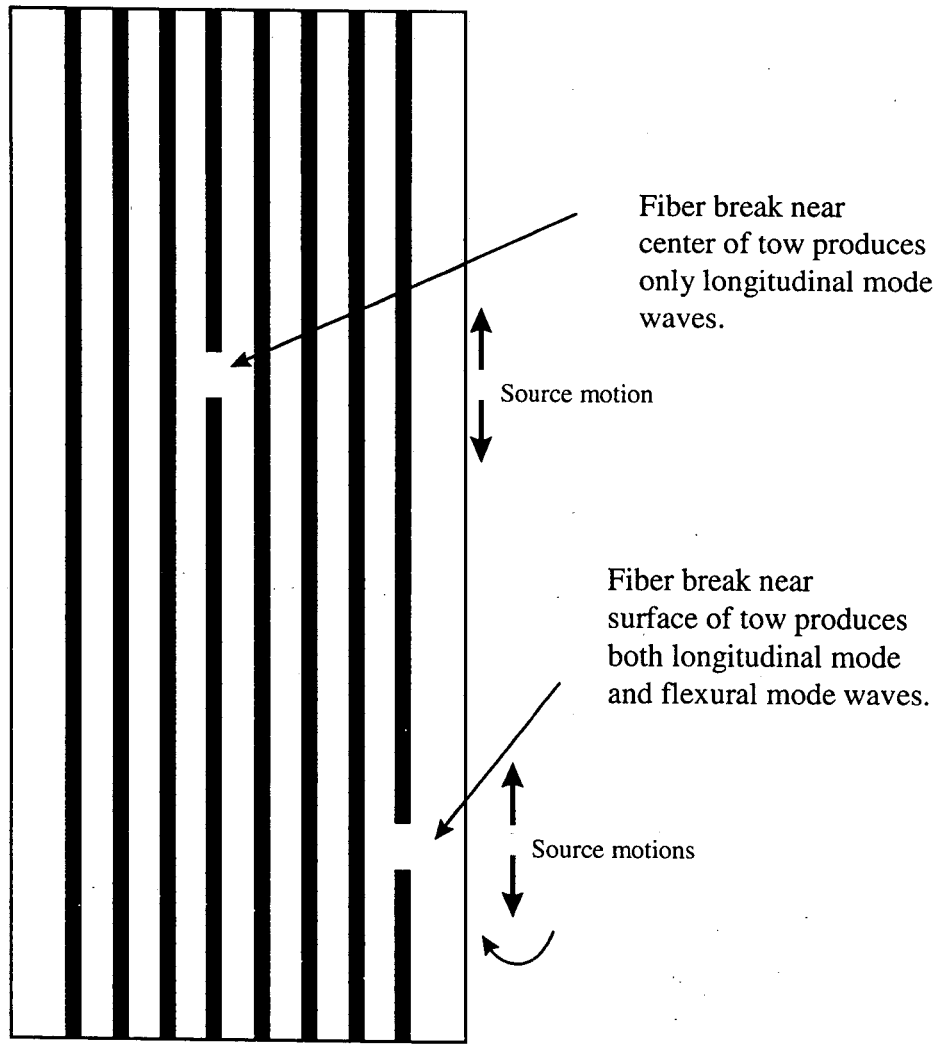

Figure 29. Schematic of Possible Fiber Break Locations in the Tow Test Specimen

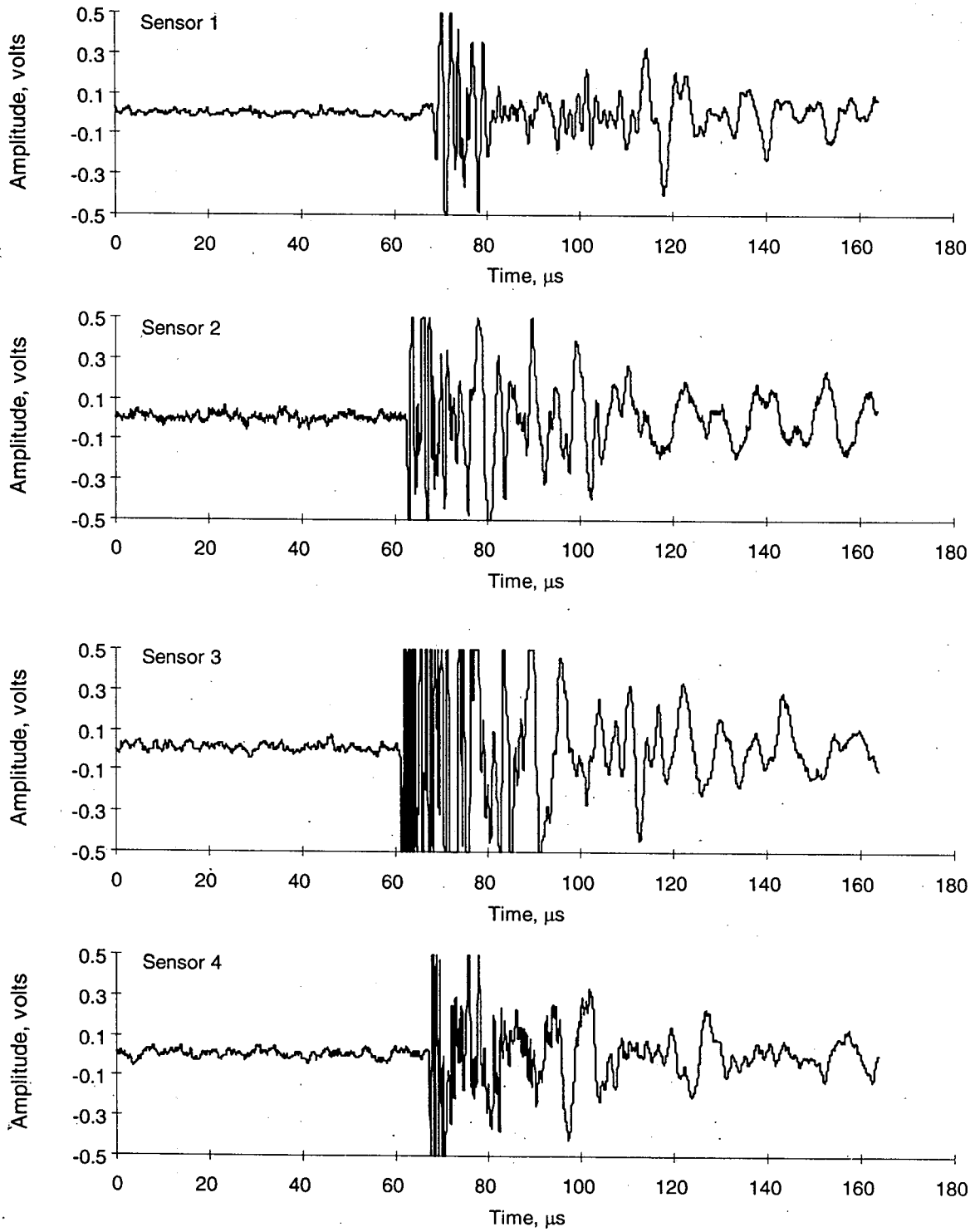

Figure 30. Typical Waveform Used for Source Location

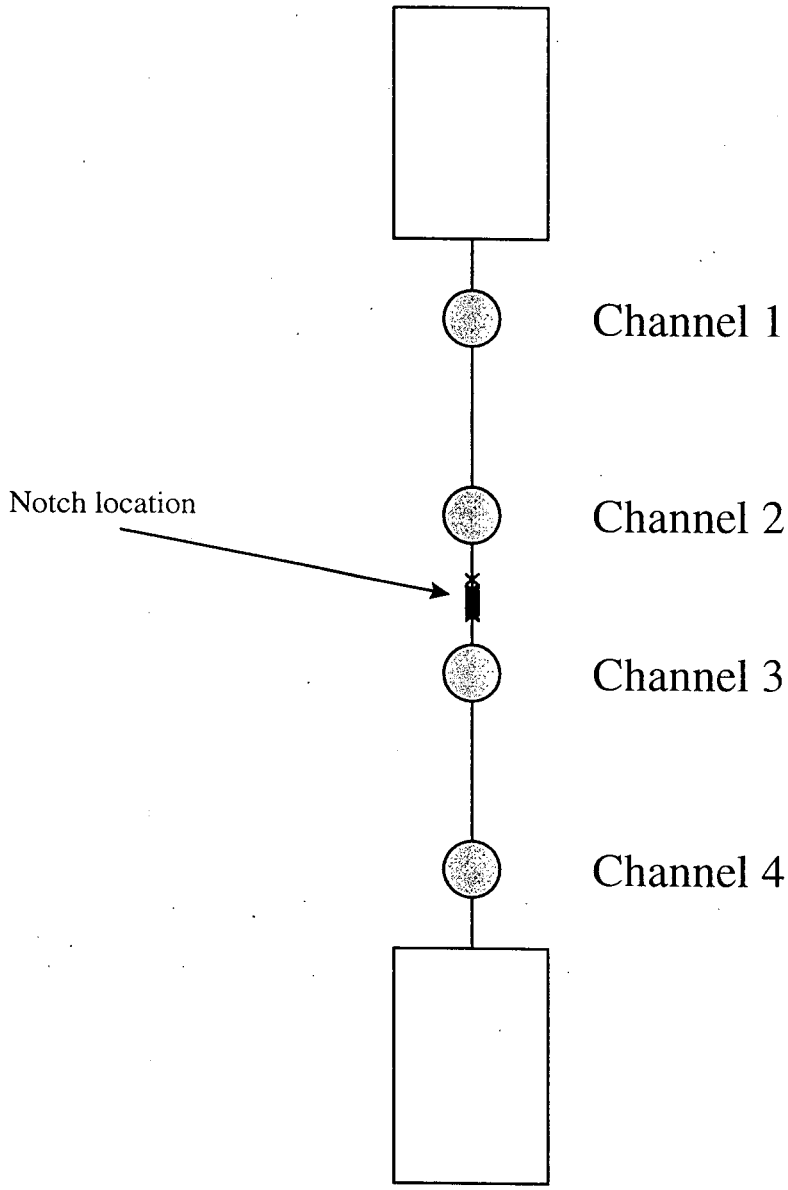

Figure 31. Calculated Source Locations for Tow Test Specimen 4

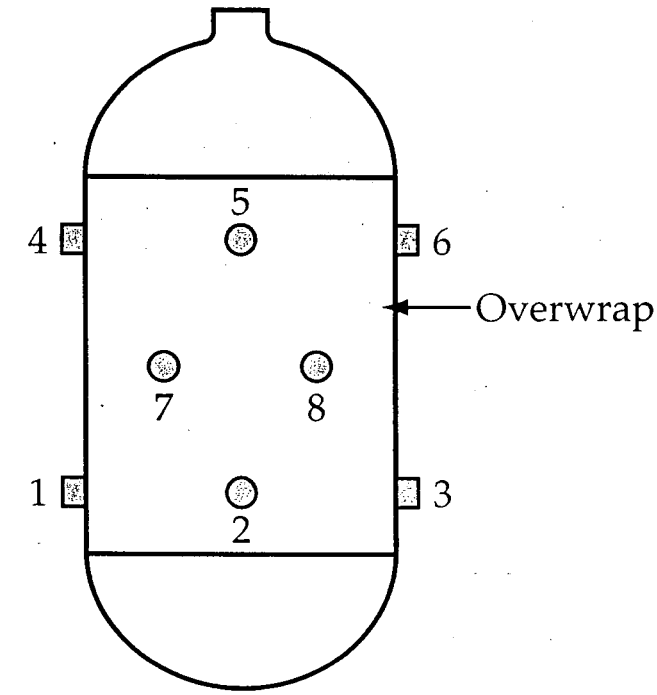

Figure 32. Configuration of Tank 012 Sensors

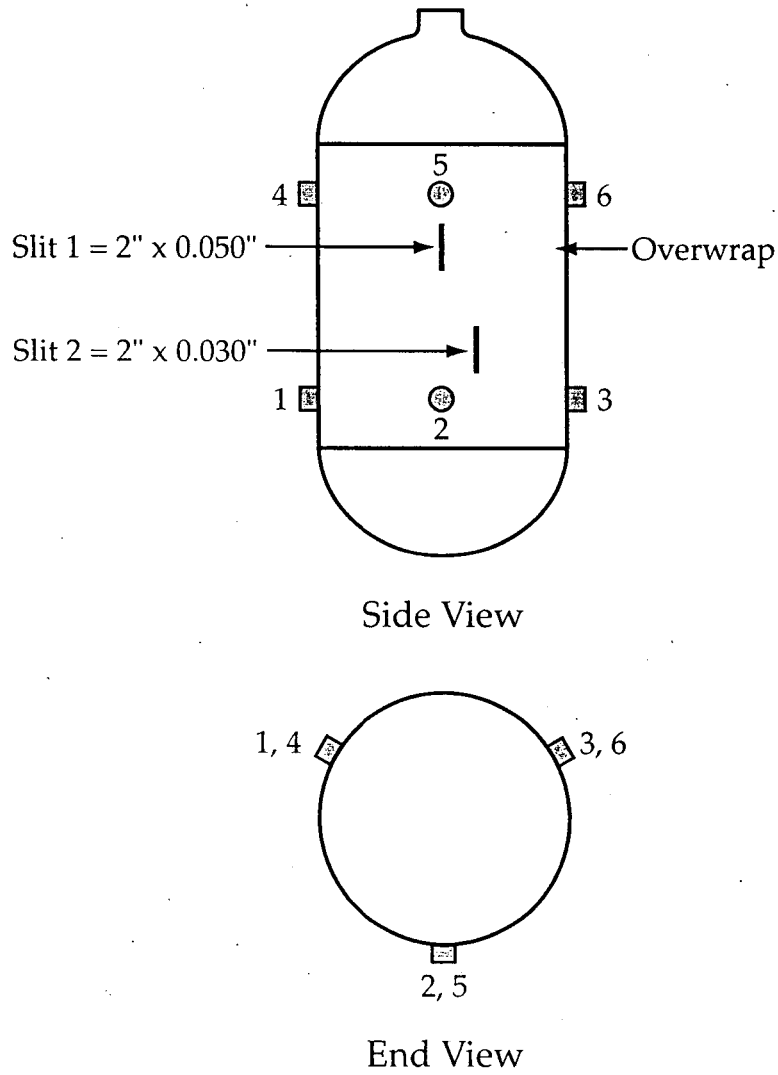

Figure 33. Configuration of Tank 004 Sensors and Damage

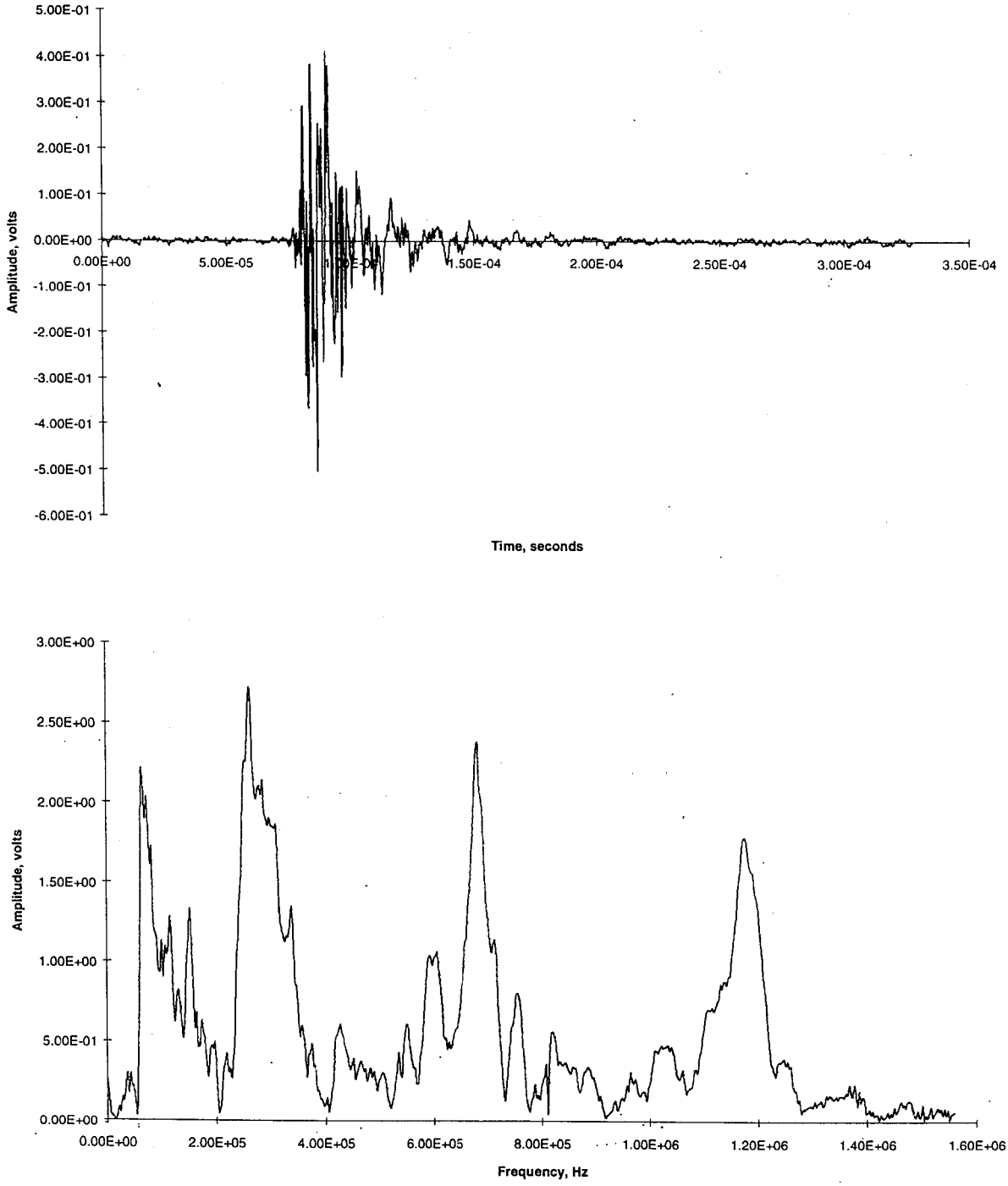

Figure 34. Fiber Break Signal and FFT of Signal – Tank 004

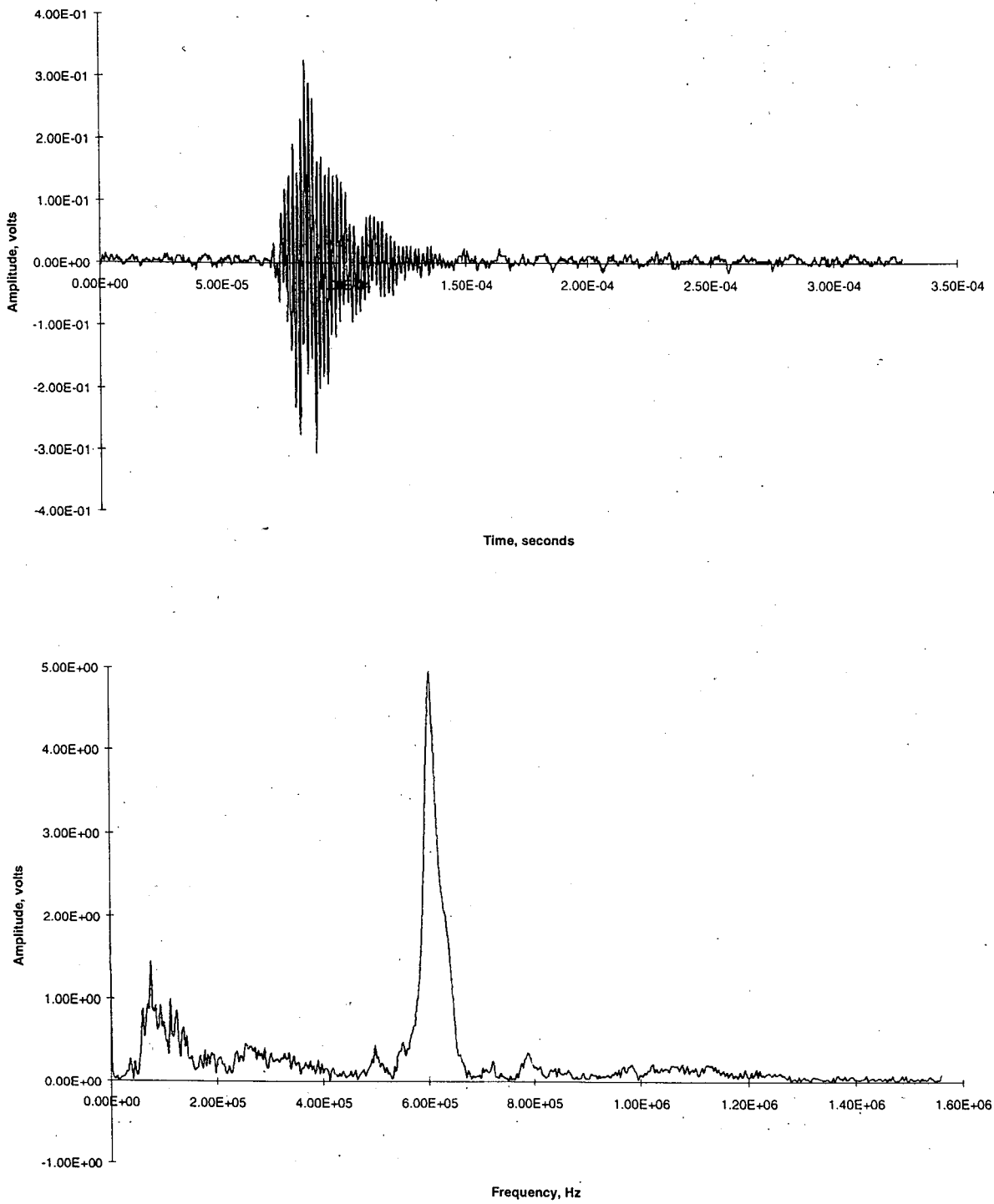

Figure 35. Matrix Cracking Signal and FFT of Signal – Tank 004

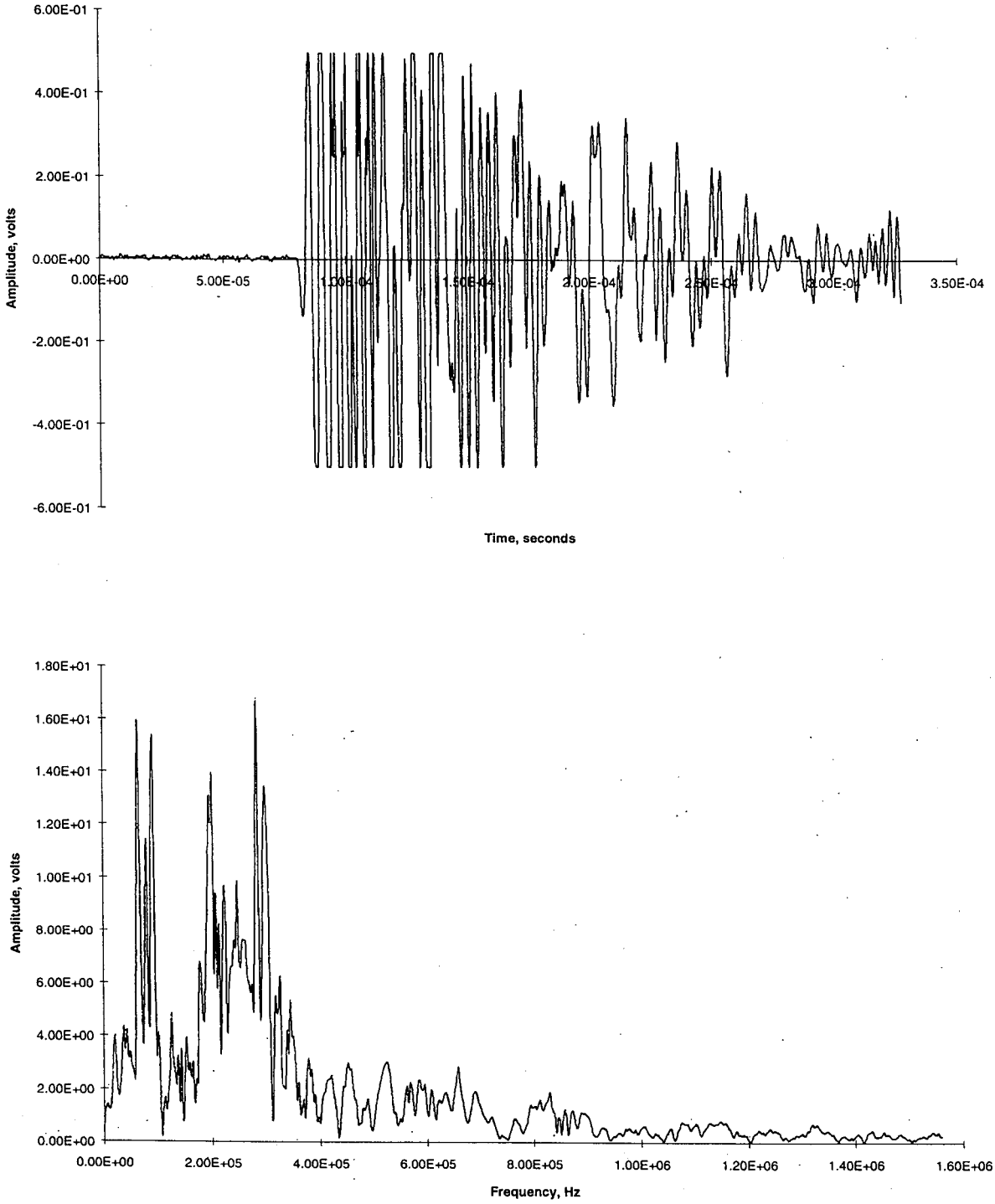

Figure 36. Matrix Splitting Signal and FFT of Signal – Tank 004 with Slits

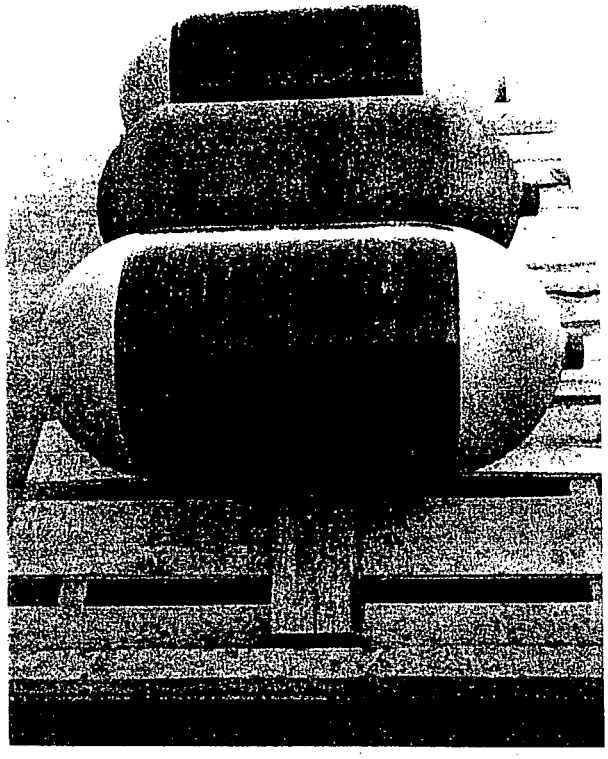

Figure 37. Type 2 Tanks on Pallet

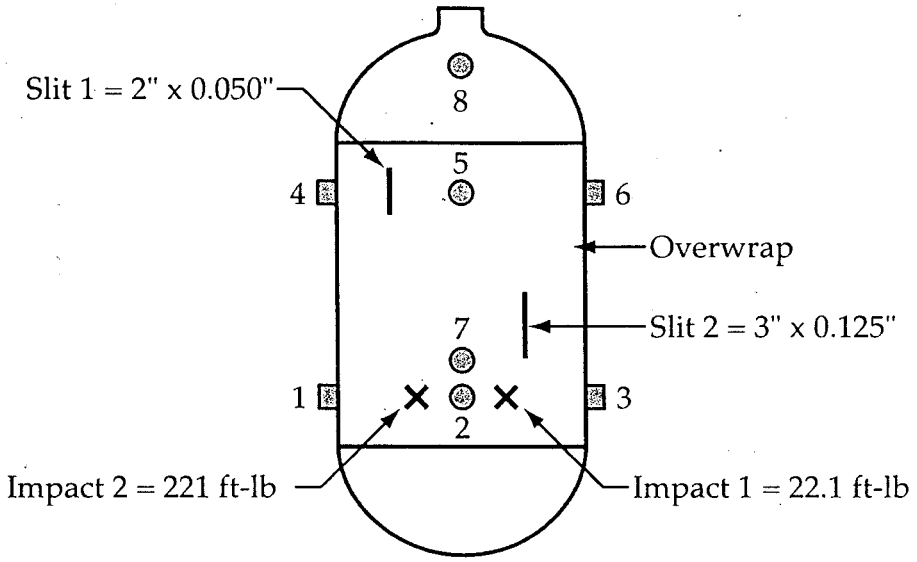

Side View

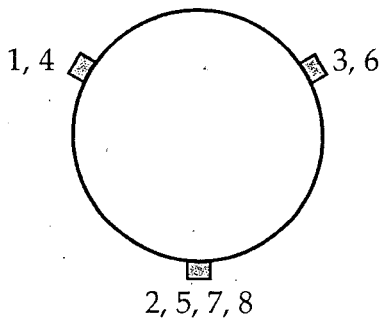

End View

Figure 38. Configuration of Tank 013 Sensors and Damage

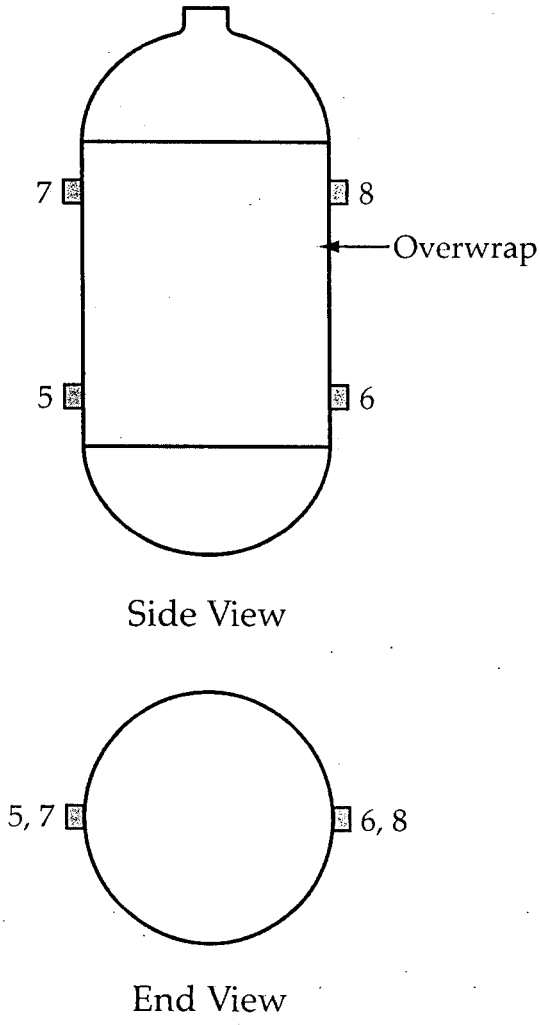

Figure 39. Configuration of Tank 014 Sensors and Damage

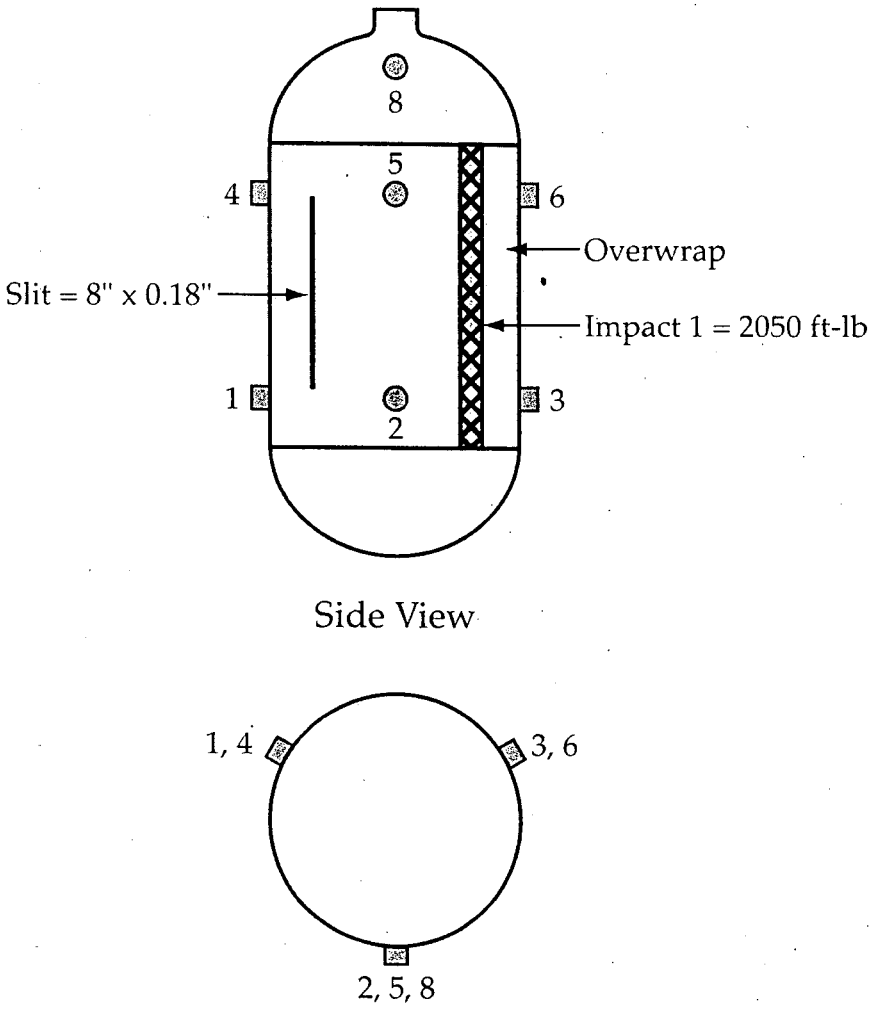

Figure 40. Configuration of Tank 018 Sensors and Damage

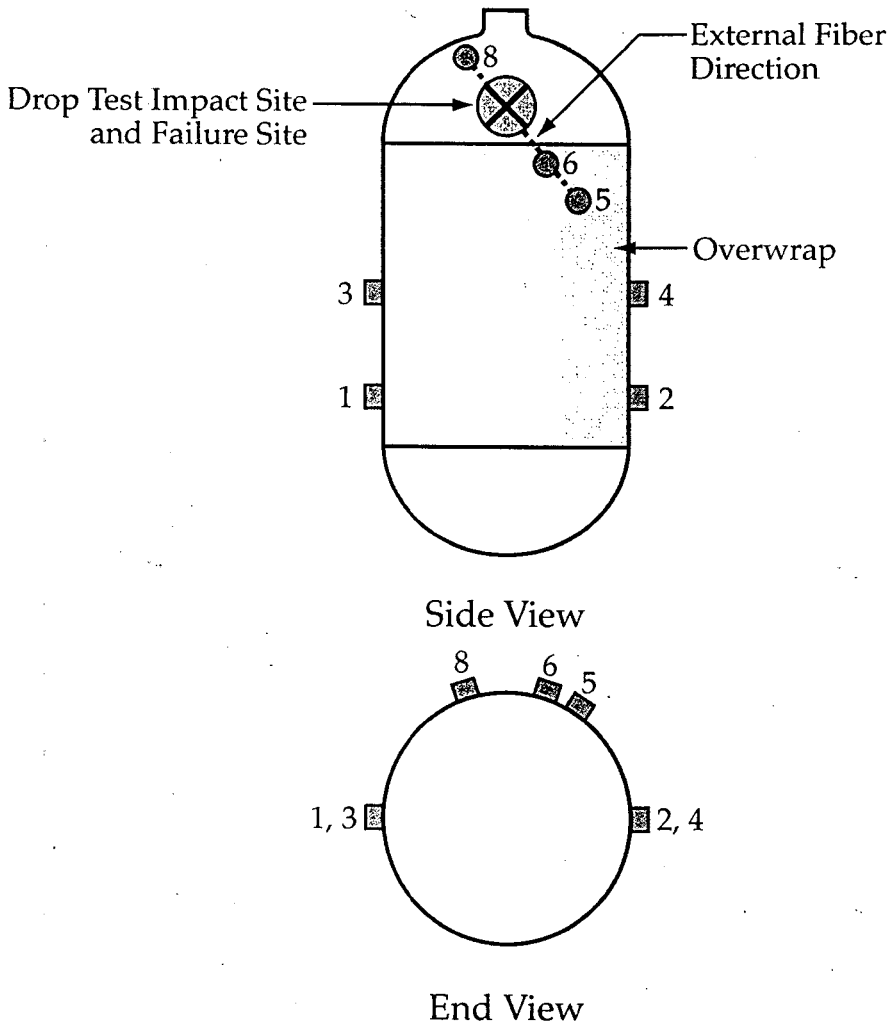

Figure 41. Configuration of Tank 003 Sensors and Damage

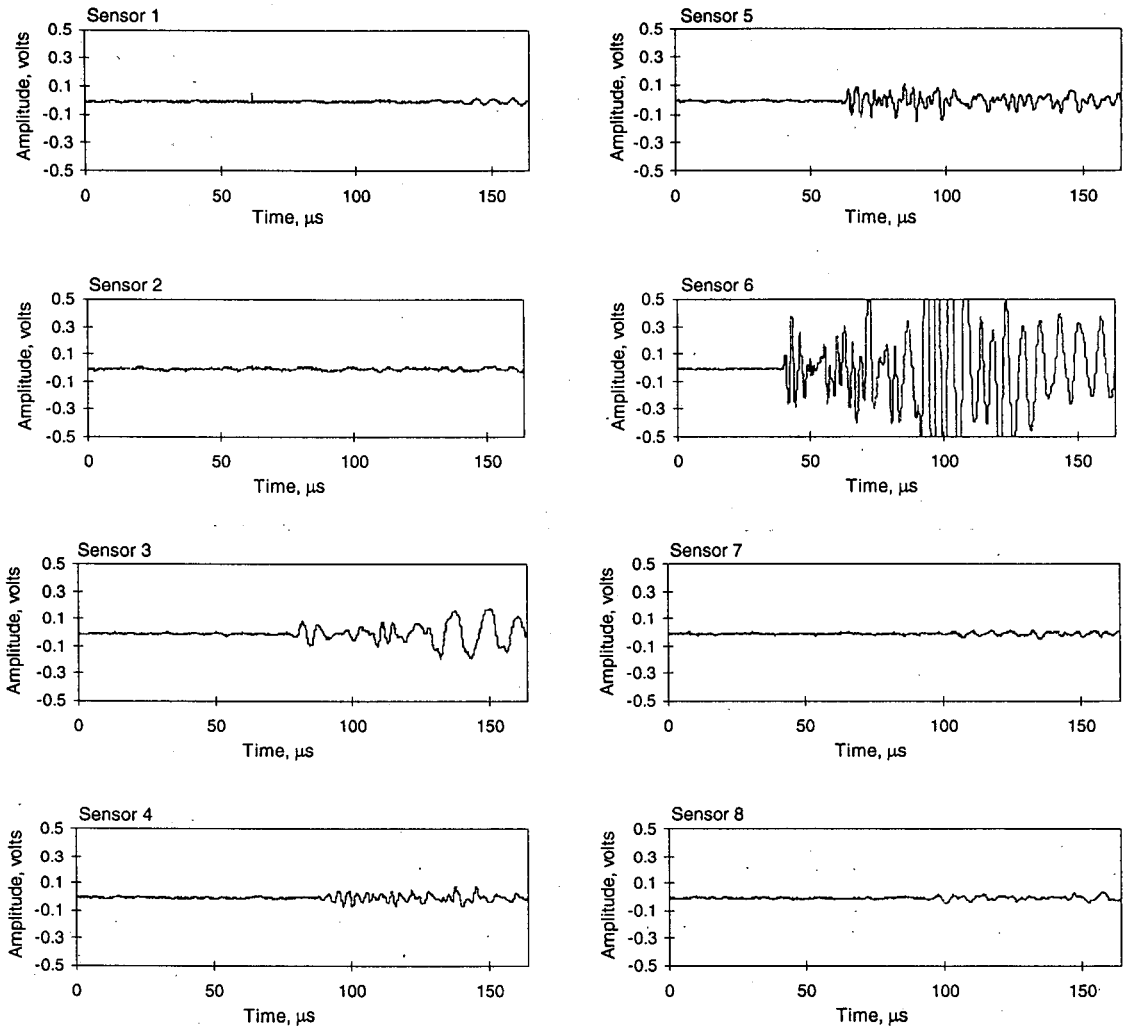

Figure 42. Response from Leadbreak to Check Sensor Coverage of Entire Tank

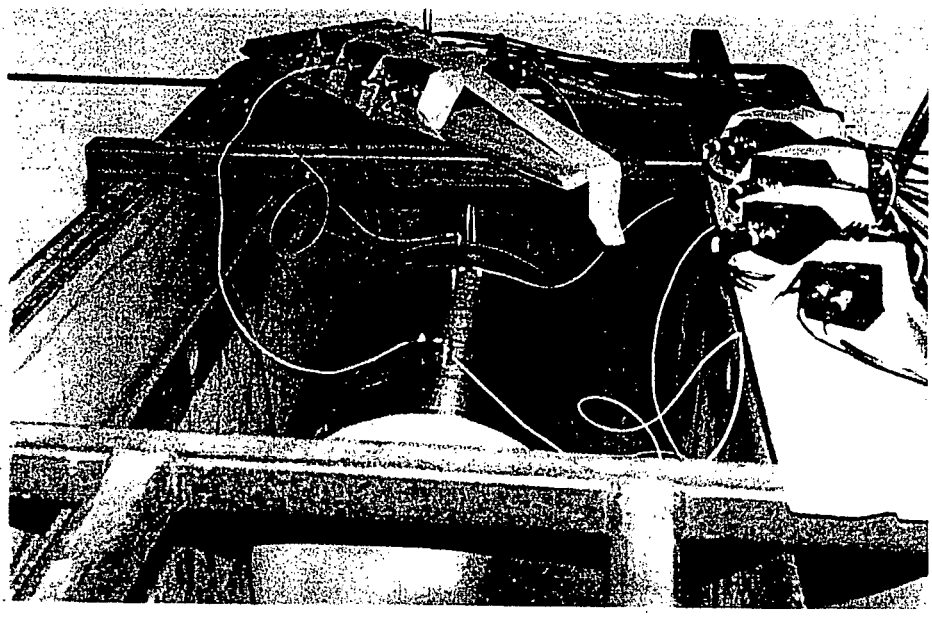

Figure 43. As-Received Tank 013 in the Burst Test Chamber

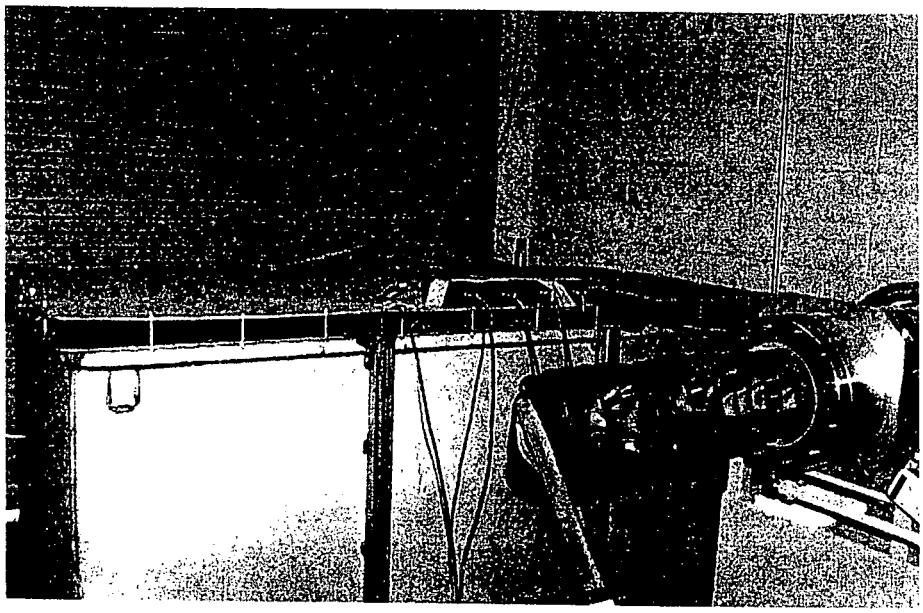

Figure 44. Burst Test Chamber Just Prior to Testing

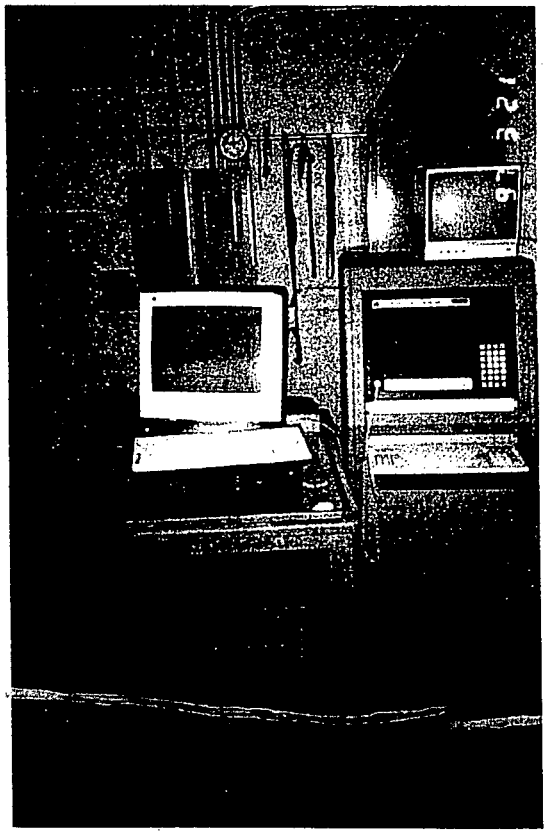

Figure 45. Acoustic Emission Acquisition Equipment

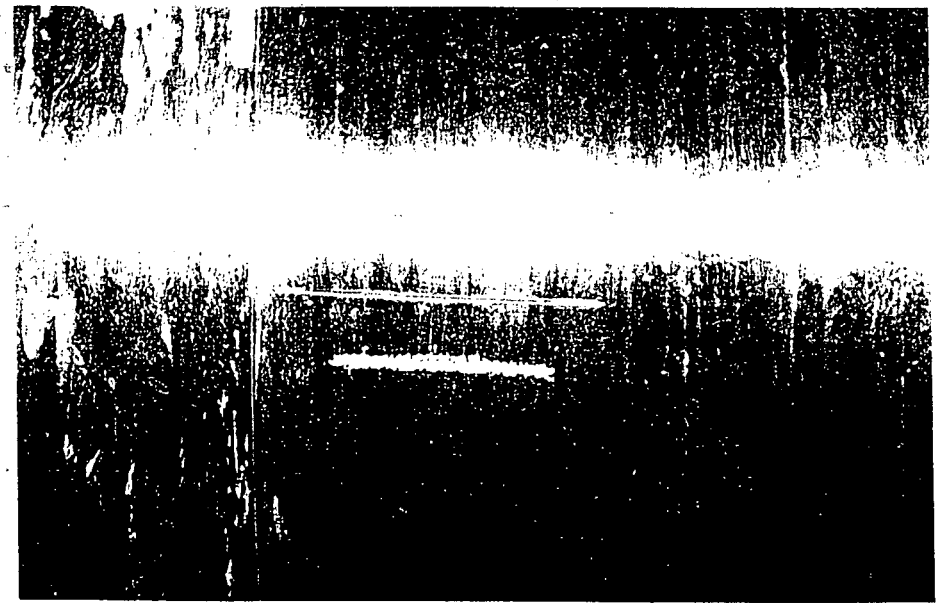

Figure 46. 2-inch Slit in the Overwrap of Tank 013

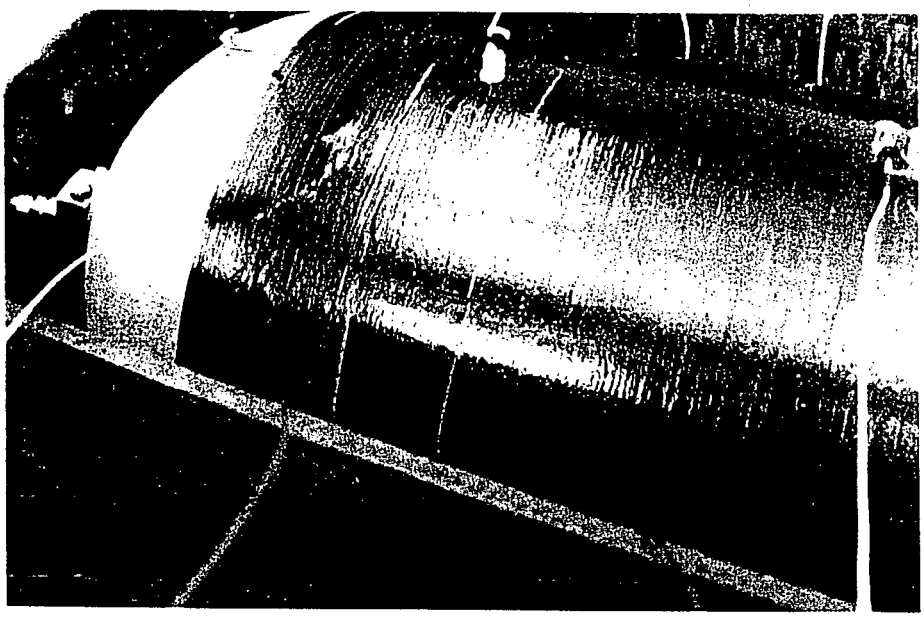

Figure 47. Circumferential Cracks Propagating from the Ends of the 2-inch Slit

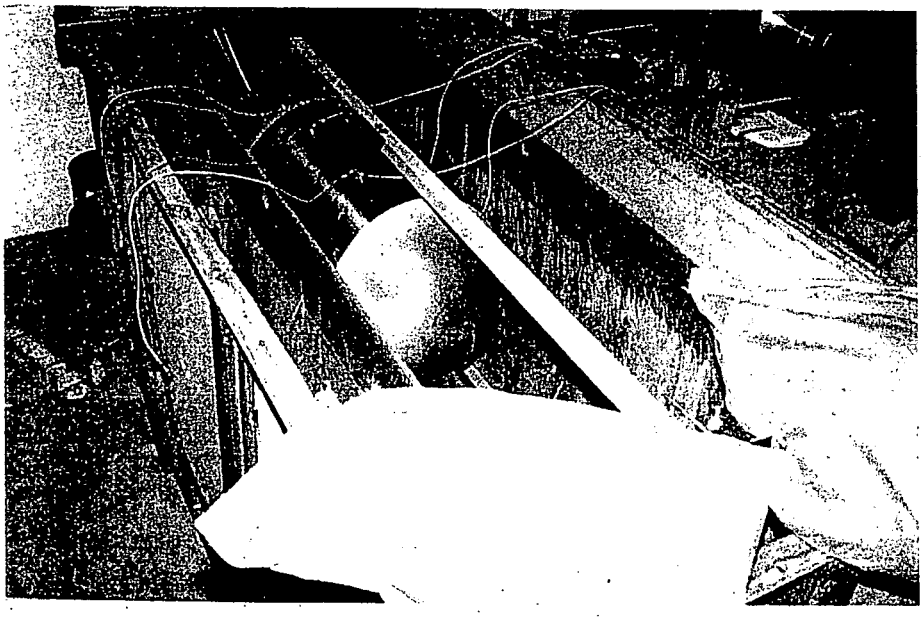

Figure 48. Pendulum Impact Fixture in Burst Test Chamber

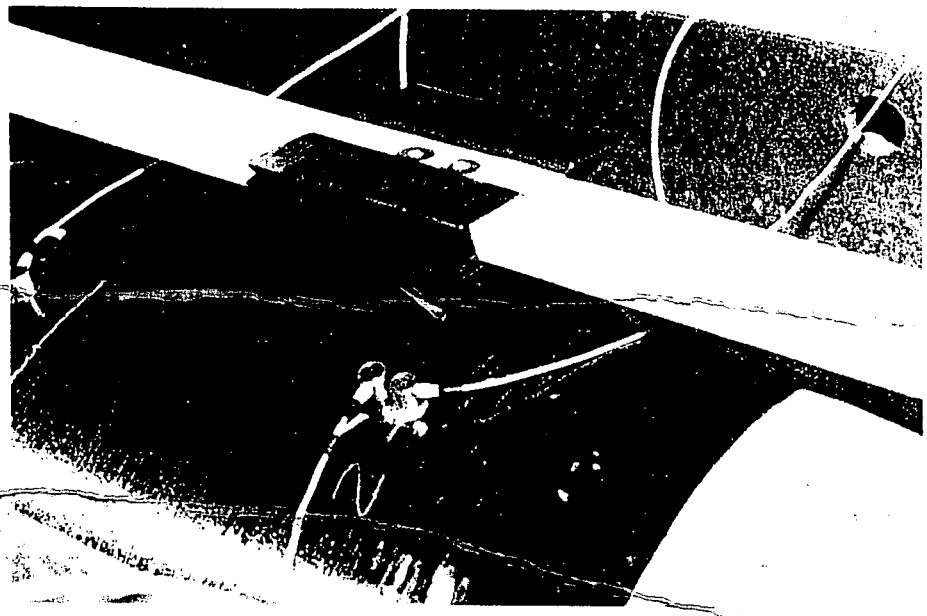

Figure 49. Pyramid-Shaped Impactor

Figure 50. Impact Site Following 22.1 ft-lbs Impact

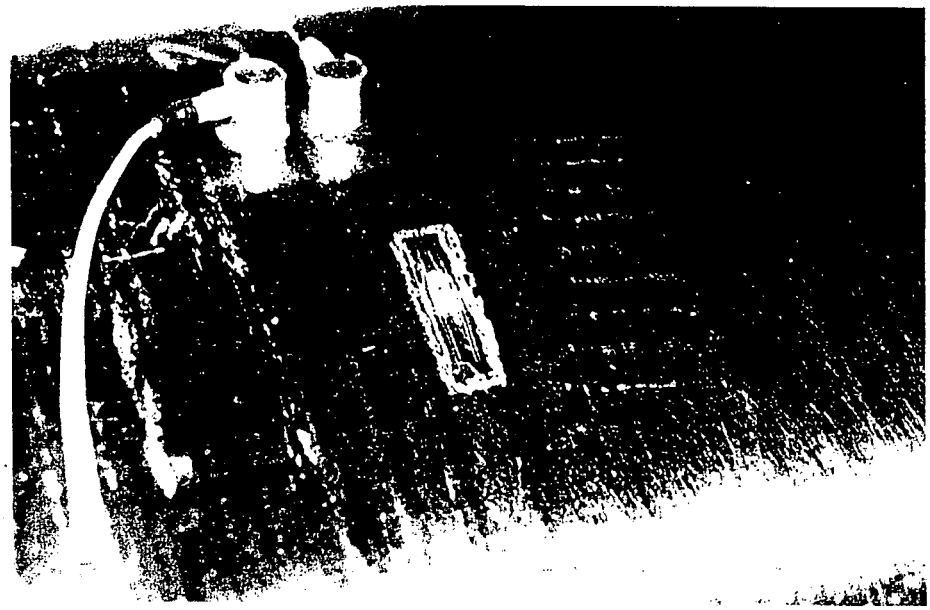

Figure 51. Extent of Damage from 22.1 ft-lbs Impact

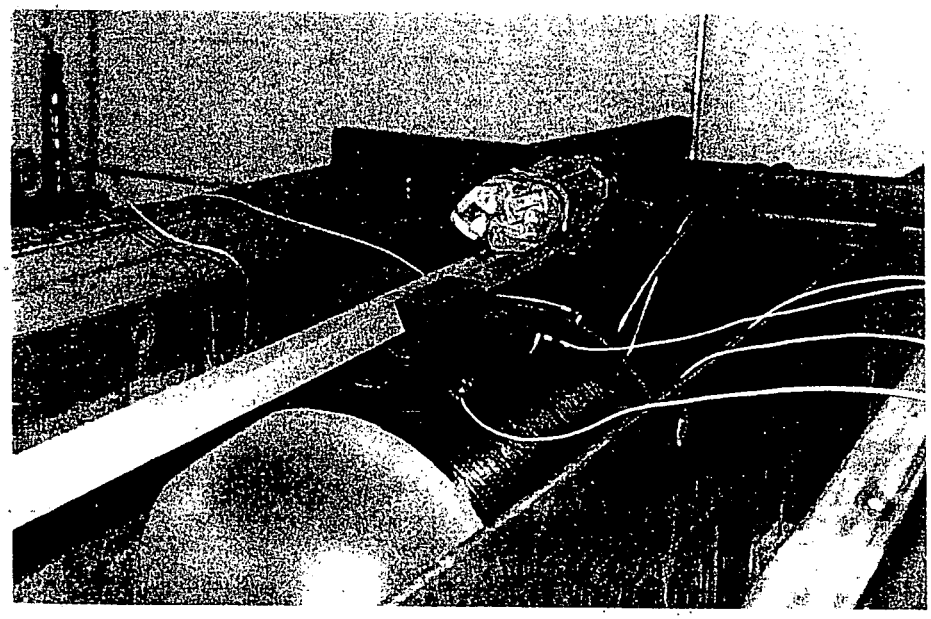

Figure 52. Pendulum Impact Fixture for 221 ft-lbs Impact

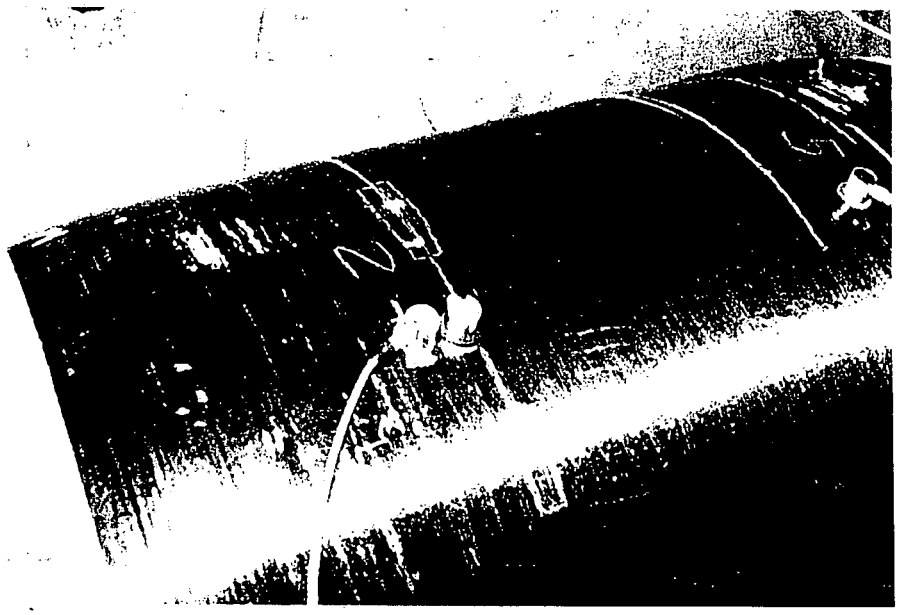

Figure 53. Impact Site Following 221 ft-lbs Impact

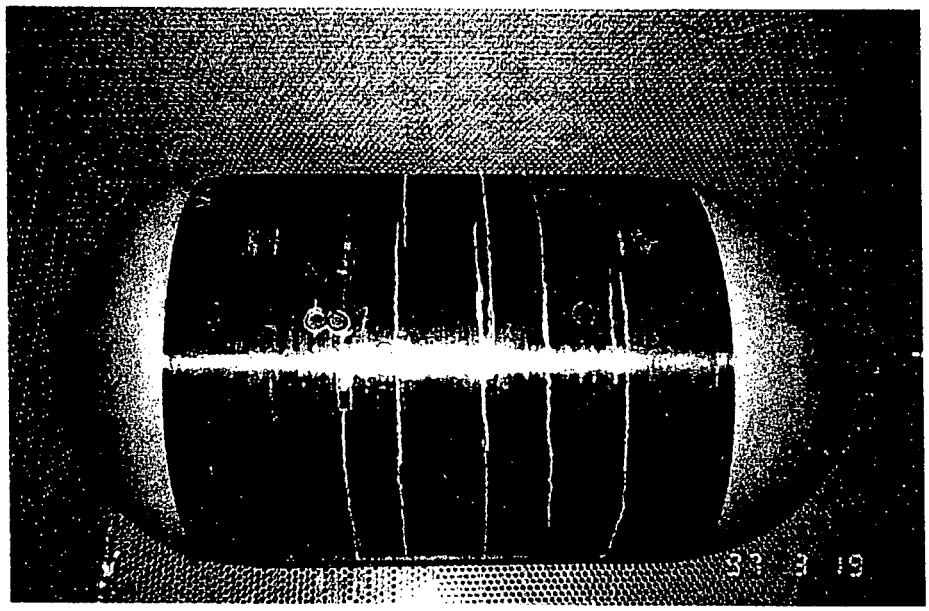

Figure 54. Tank 013 in the Fatigue Test Chamber, 0° View

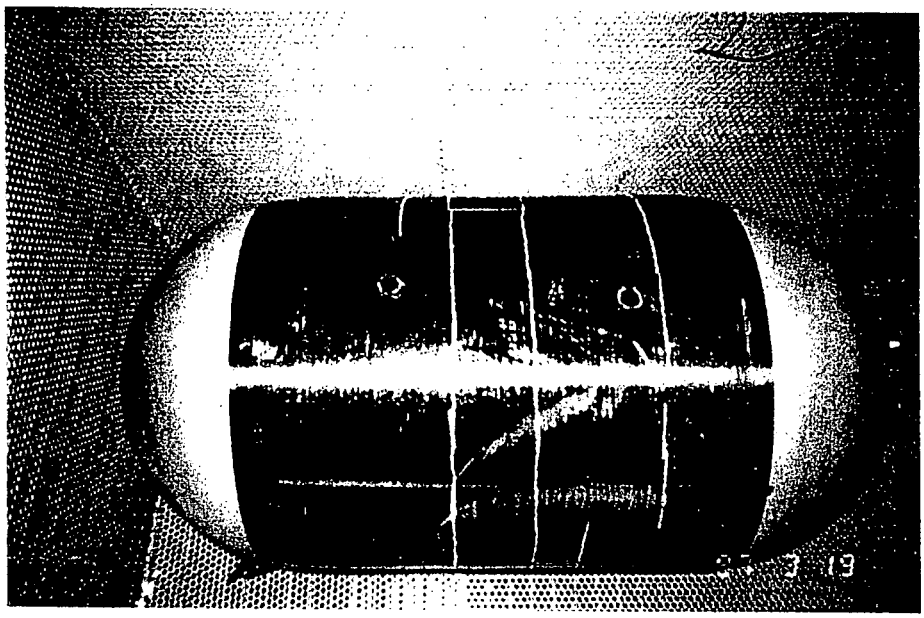

Figure 55. Tank 013 in the Fatigue Test Chamber, 180° View

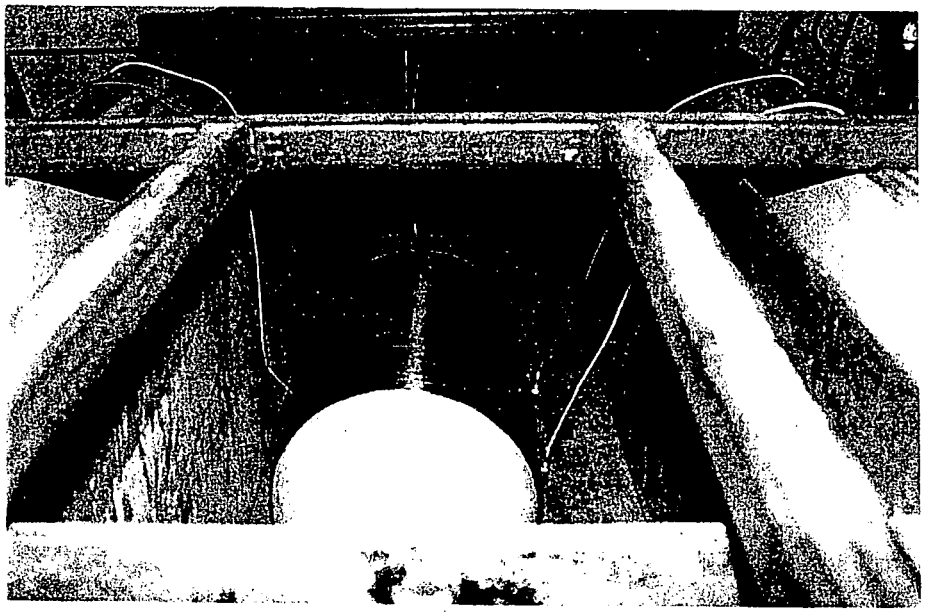

Figure 56. As-Received Tank 014 in the Burst Test Chamber

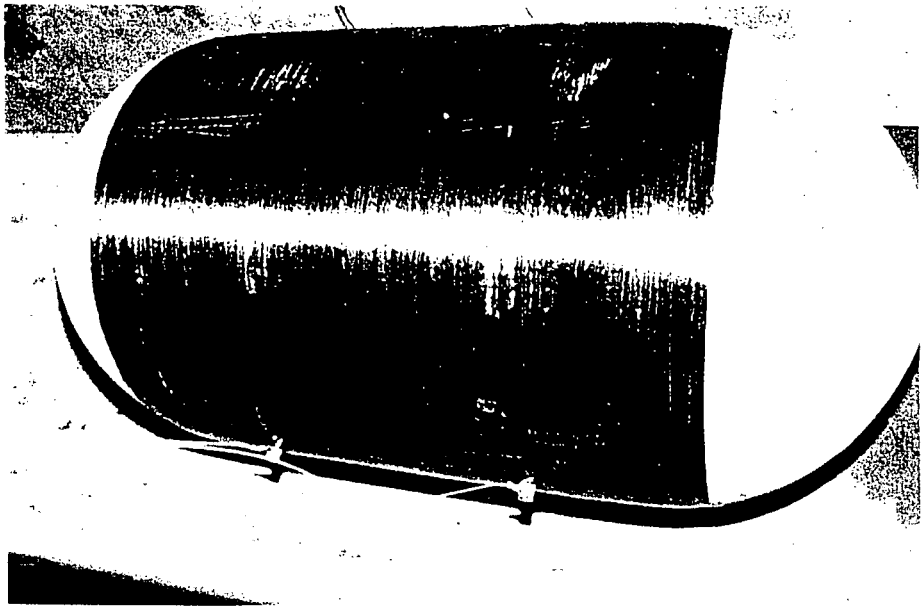

Figure 57. Acoustic Emission Sensors on Tank 014

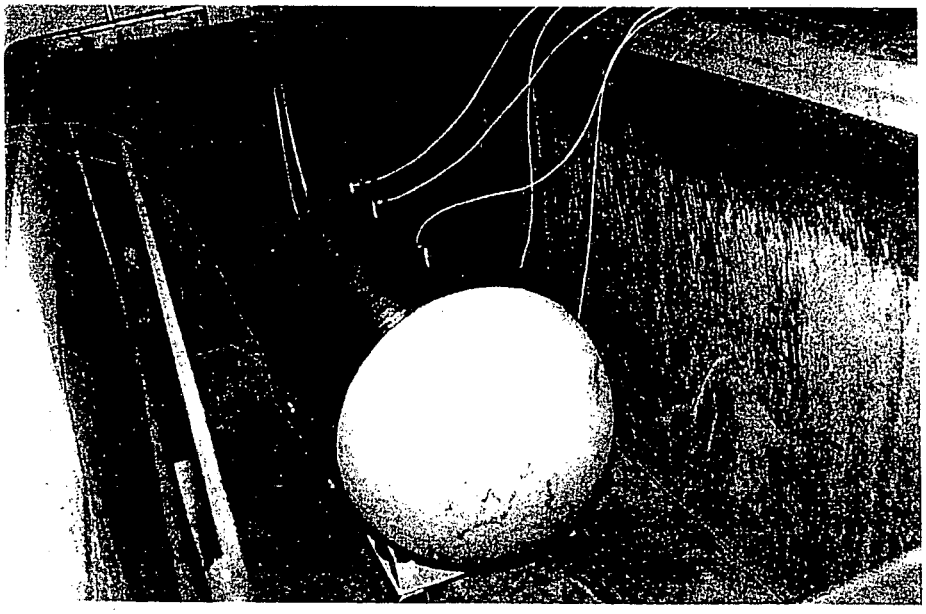

Figure 58. As-Received Tank 018 in the Burst Test Chamber, Left Side View

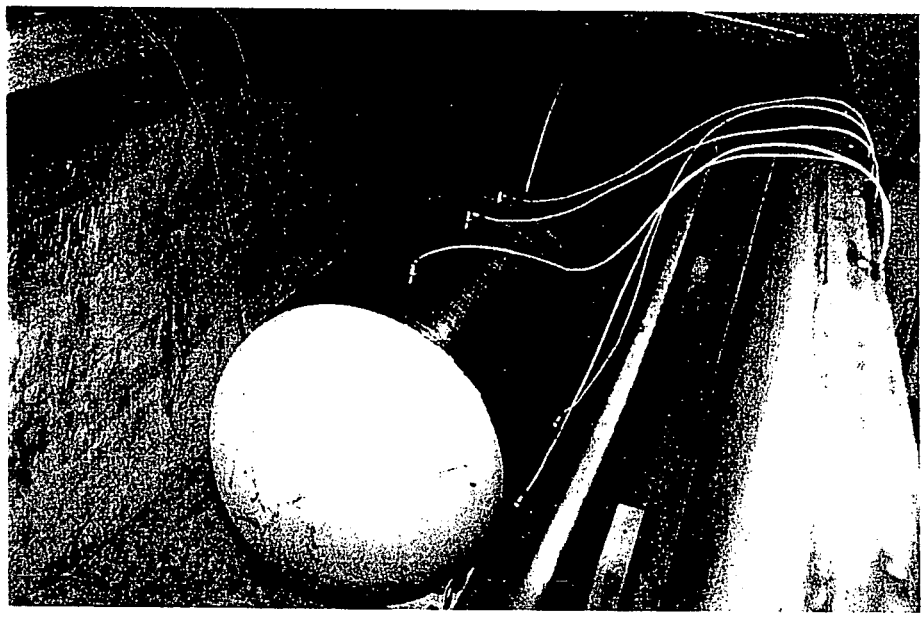

Figure 59. As-Received Tank 018 in the Burst Test Chamber, Right Side View

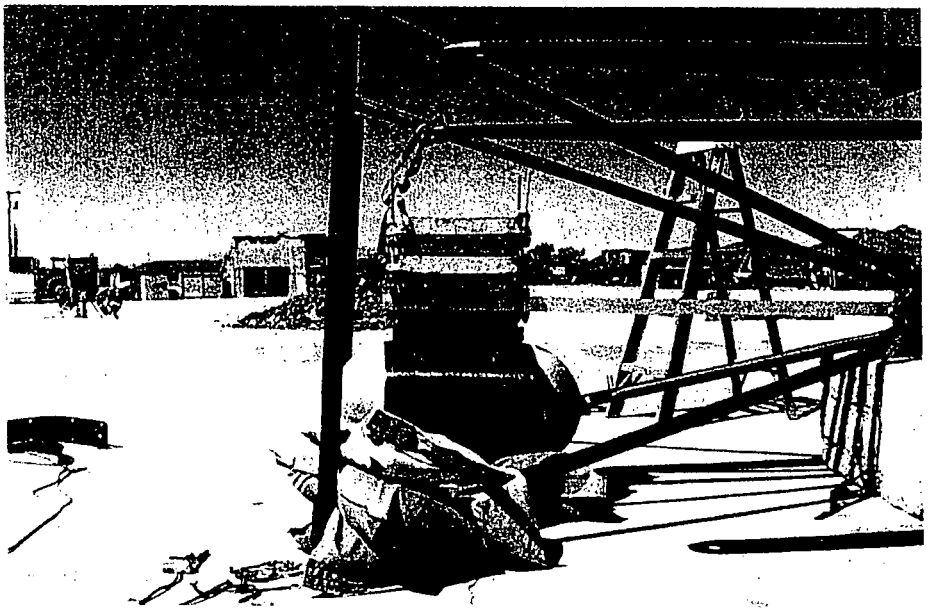

Figure 60. Large Impact Fixture Set-up for Tank 018, Side View

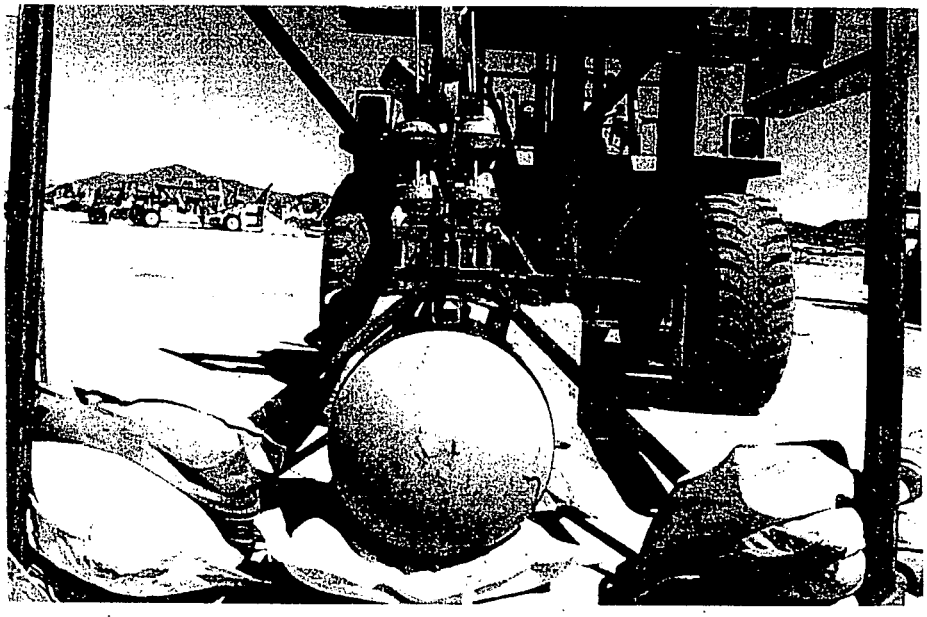

Figure 61. Large Impact Fixture Set-up for Tank 018, End View

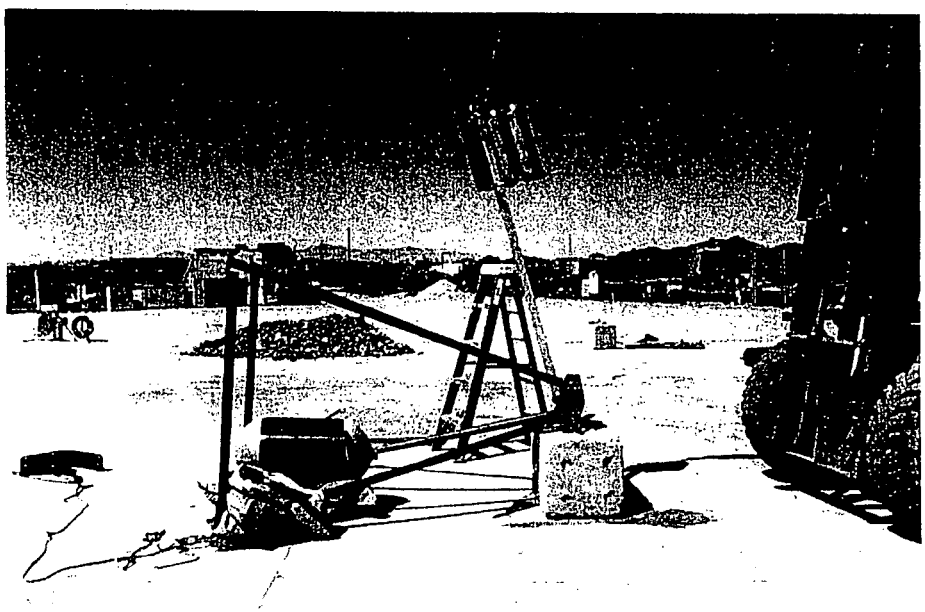

Figure 62. Impact Test Facility Just Prior to Impact of Tank 018

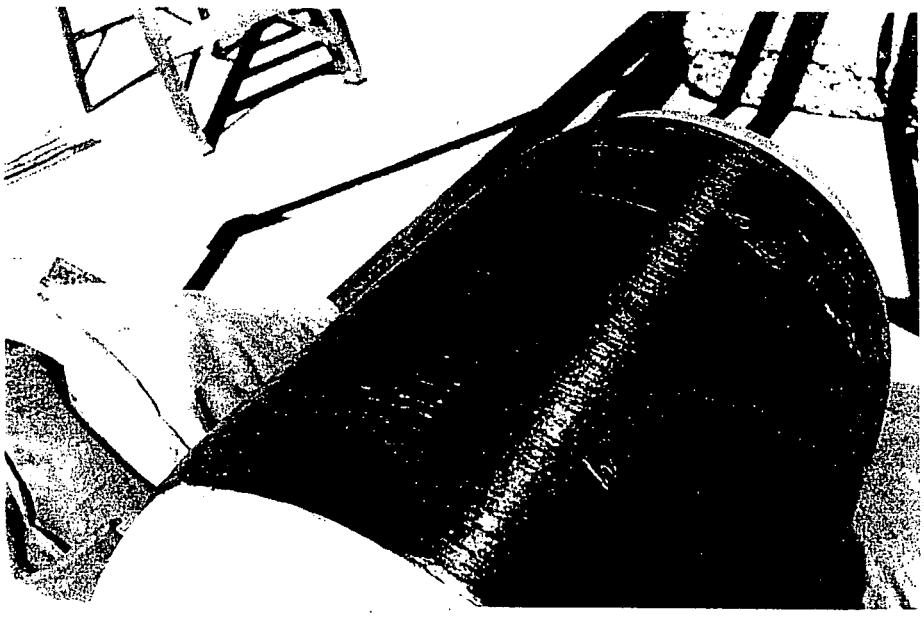

Figure 63. Post-Impact Damage on Tank 018, Overall View

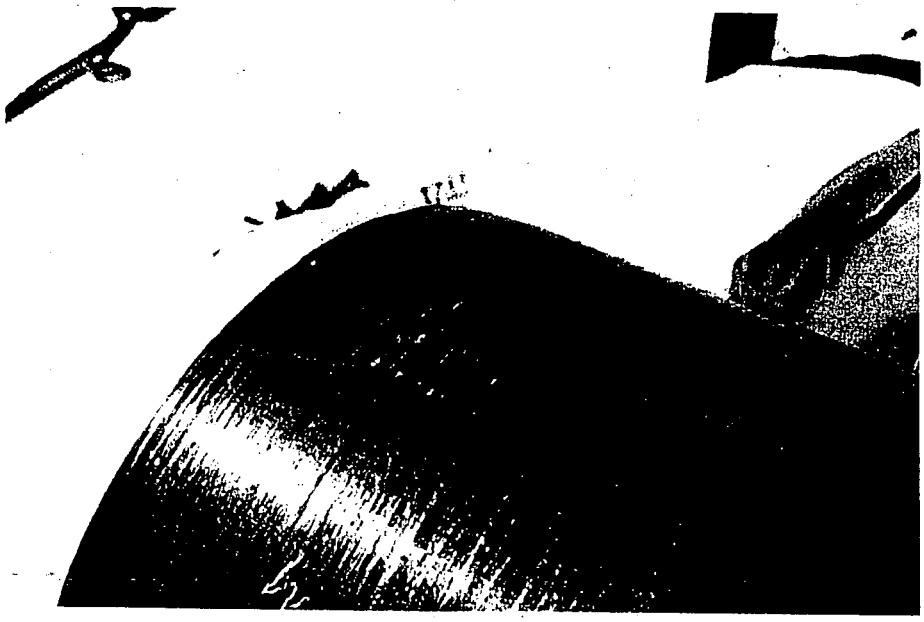

Figure 64. Post-Impact Damage on Tank 018, Close-up

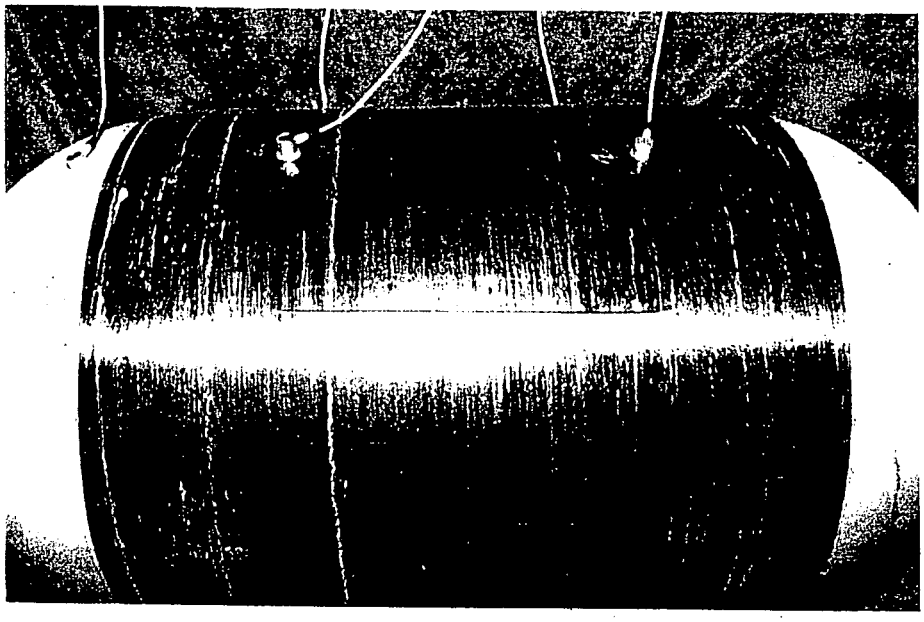

Figure 65. 8-inch Slit Cut in Tank 018

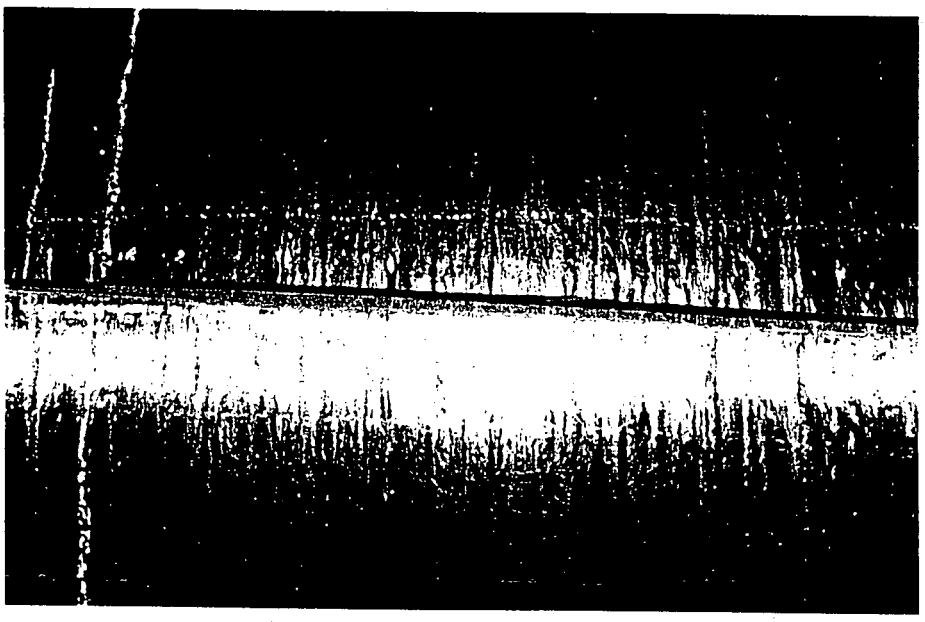

Figure 66. Ends of Slit Separated Following Pressurization

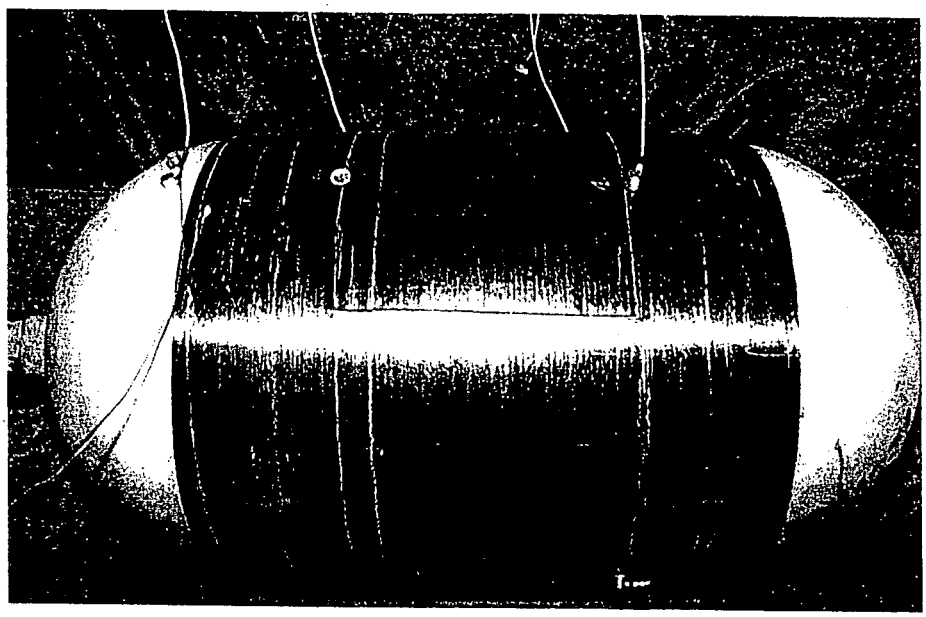

Figure 67. Circumferential Cracks at the Ends of the 8-inch Slit in Tank 018

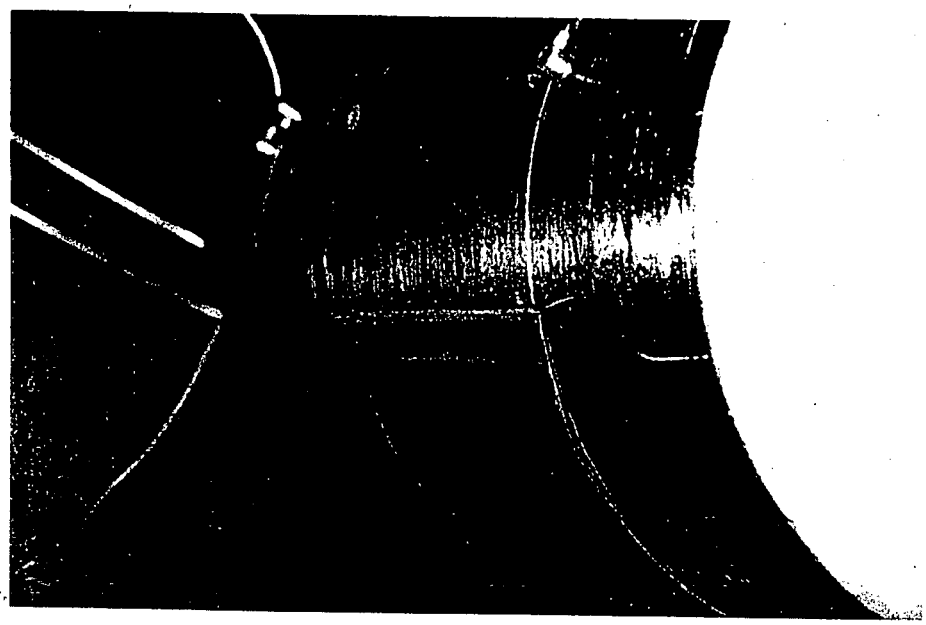

Figure 68. Oblique View of Slit Following Pressurization

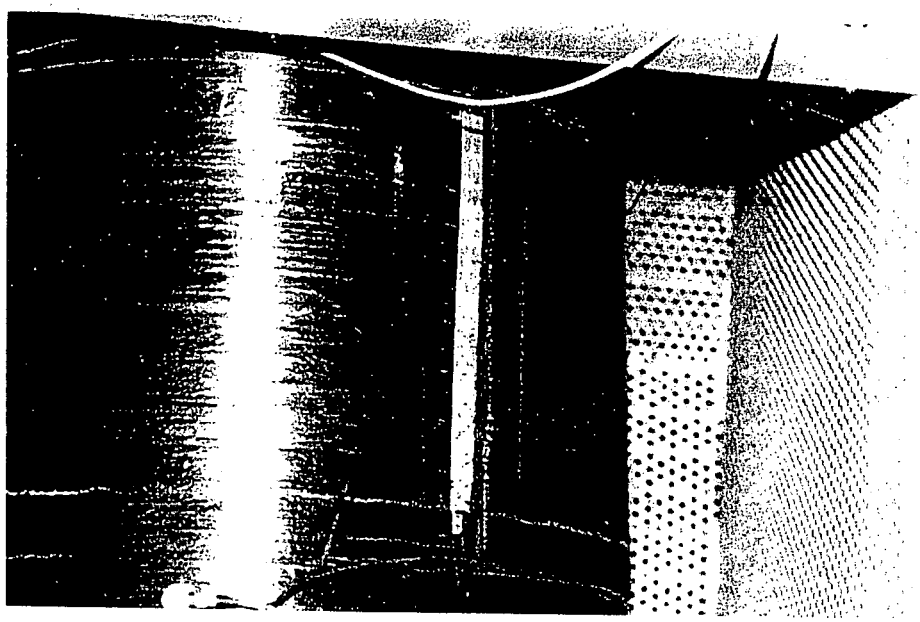

Figure 69. Ends of Slit Separated Following Fatigue Cycling, Overall View

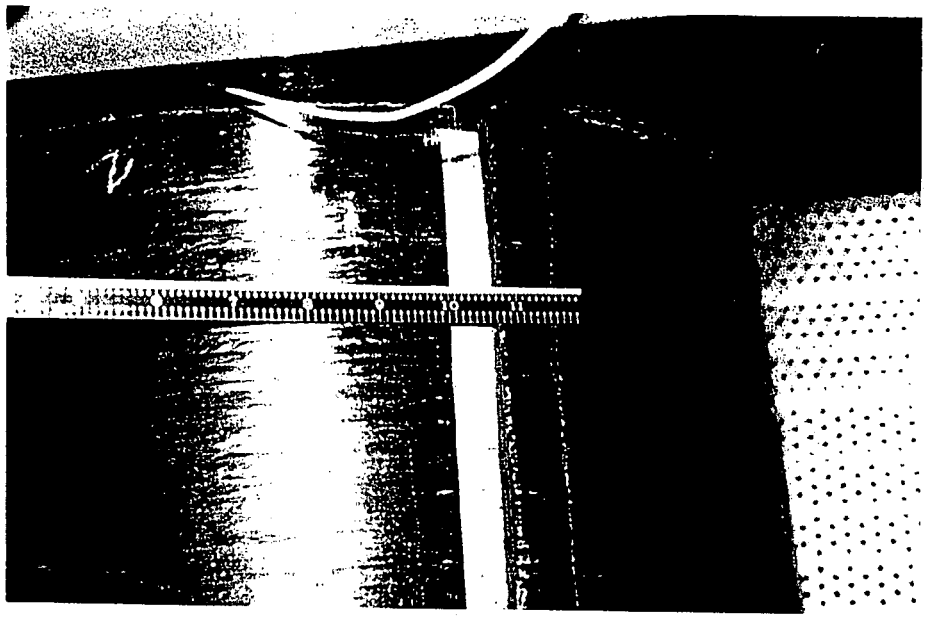

Figure 70. Ends of Slit Separated Following Fatigue Cycling, Close-up

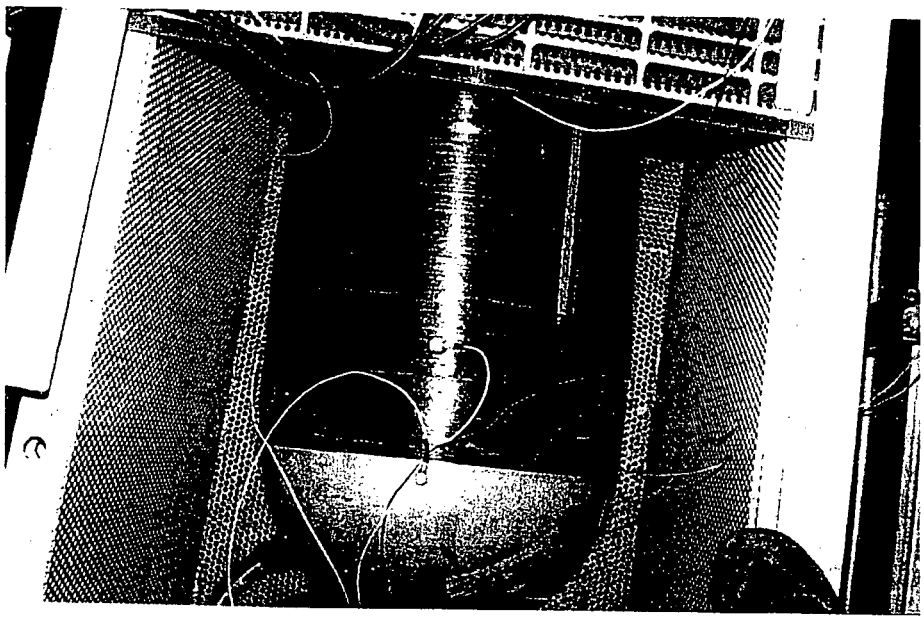

Figure 71. Tank 018 Following 15000 Pressure Cycles

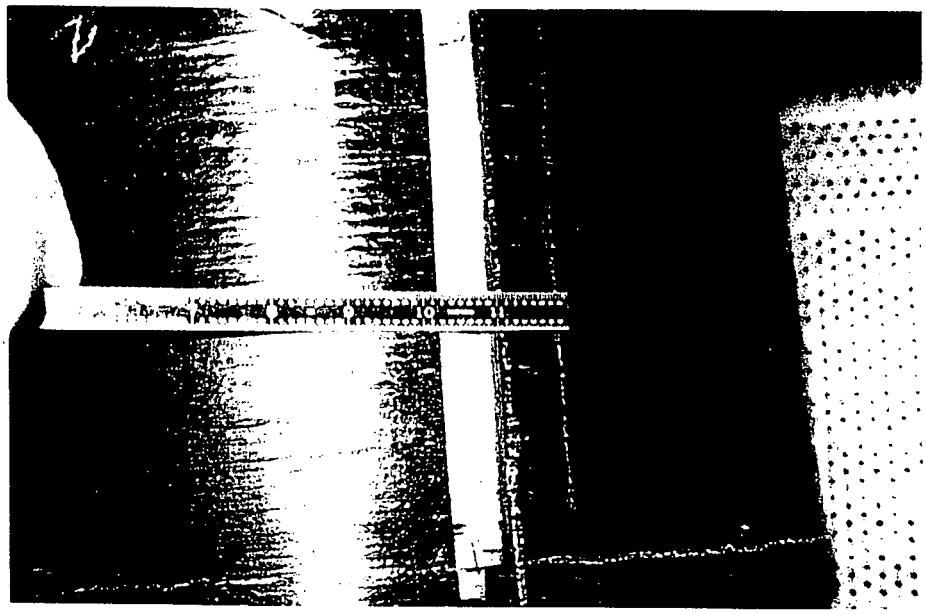

Figure 72. Tank 018 Following 15000 Pressure Cycles, Close-up of Slit

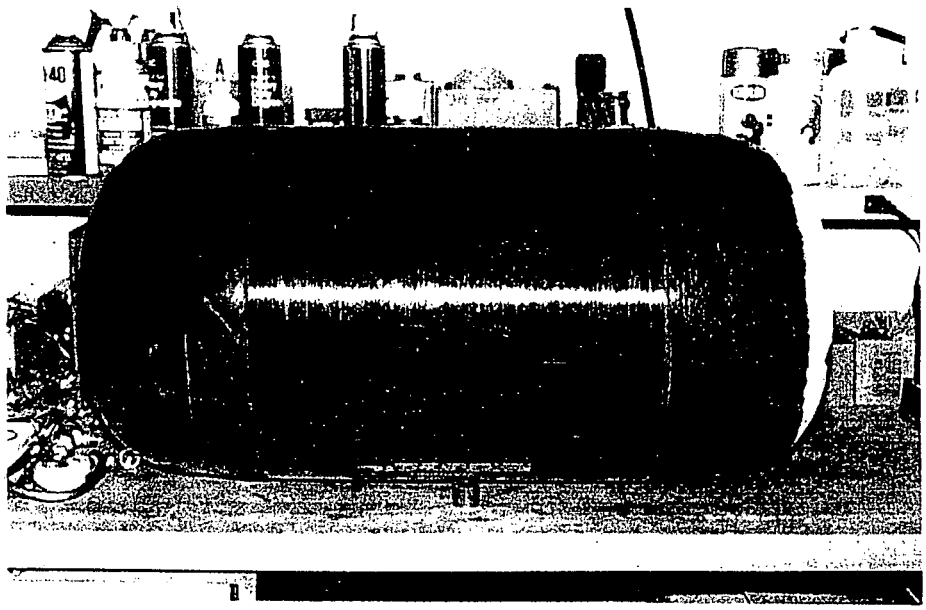

Figure 73. Overall View of Tank 003

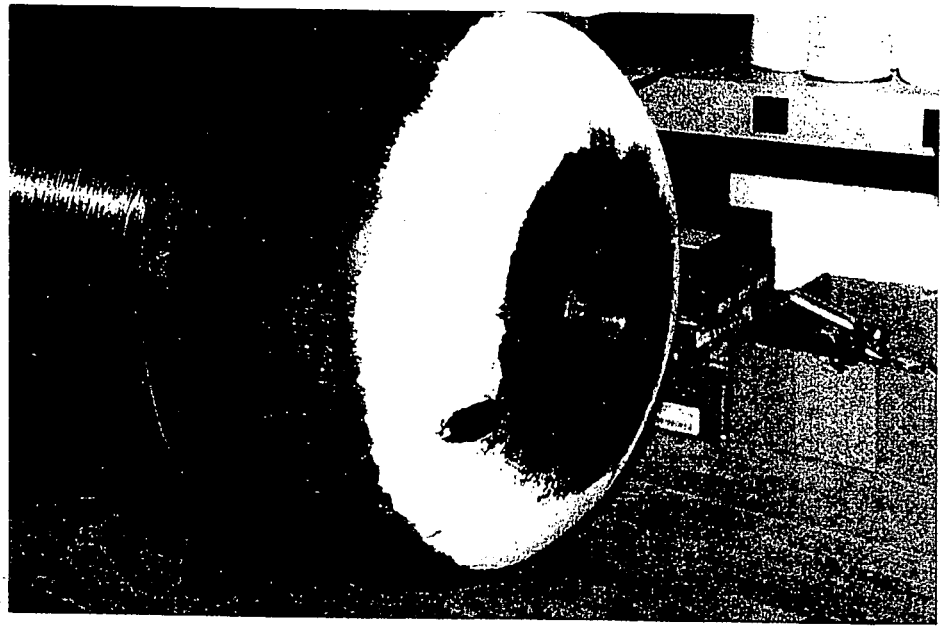

Figure 74. Tank 003 with Rubber Bumper Removed; White Material is Styrofoam

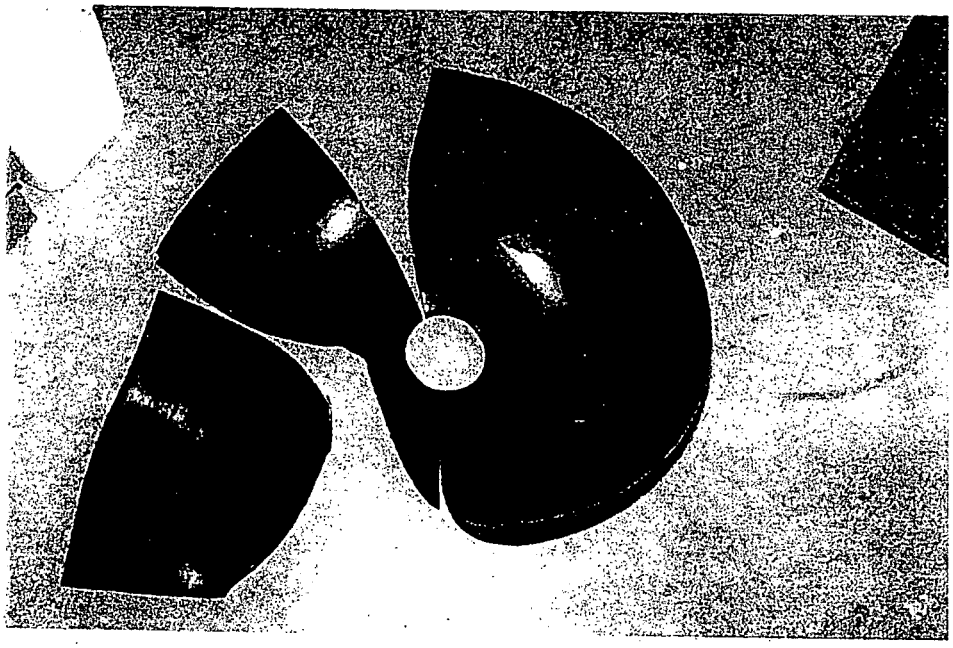

Figure 75. Rubber Bumper Following Removal

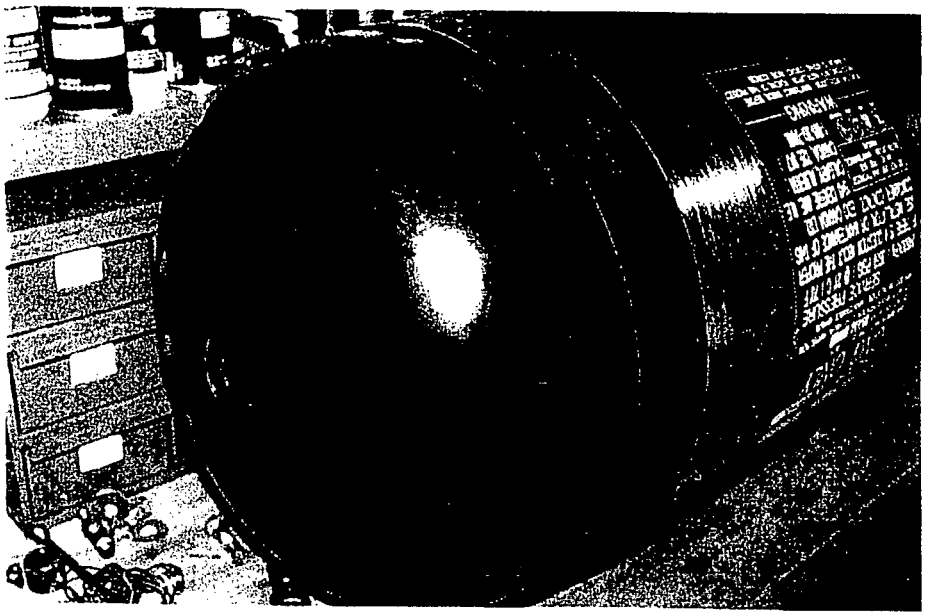

Figure 76. Tank 003 Following Removal of Styrofoam

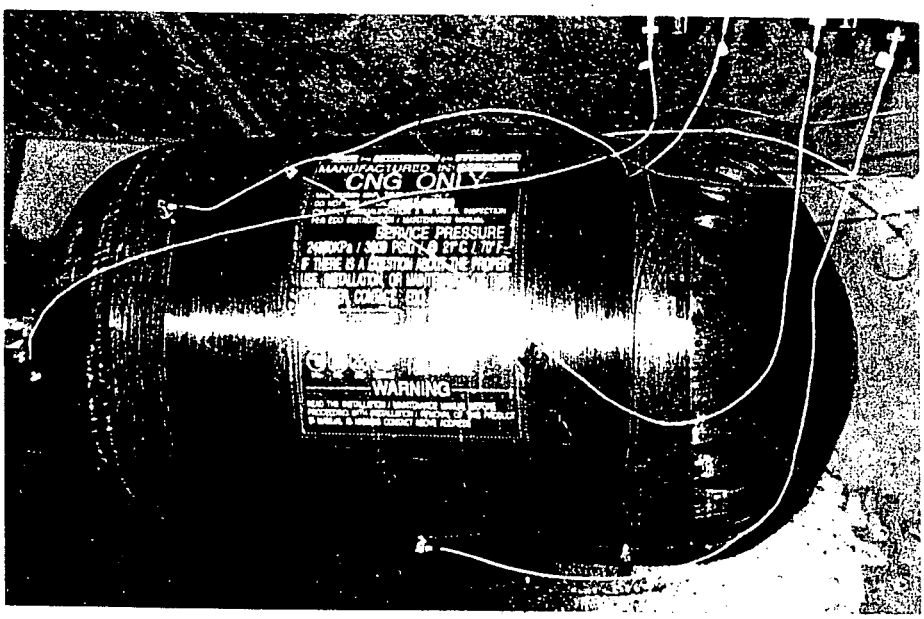

Figure 77. As-Received Tank 003 in the Burst Test Chamber

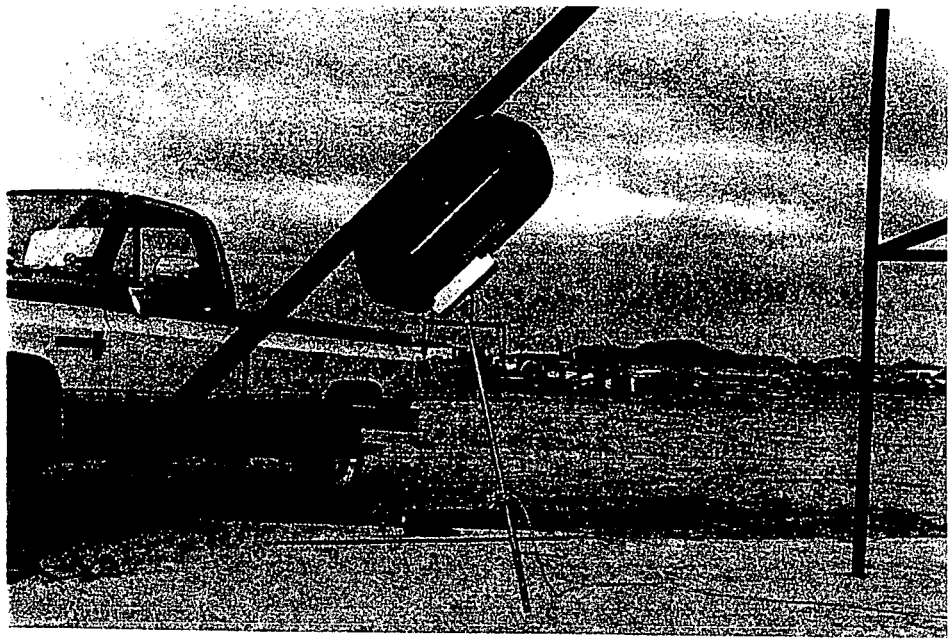

Figure 78. Drop Test Set-up for Tank 003

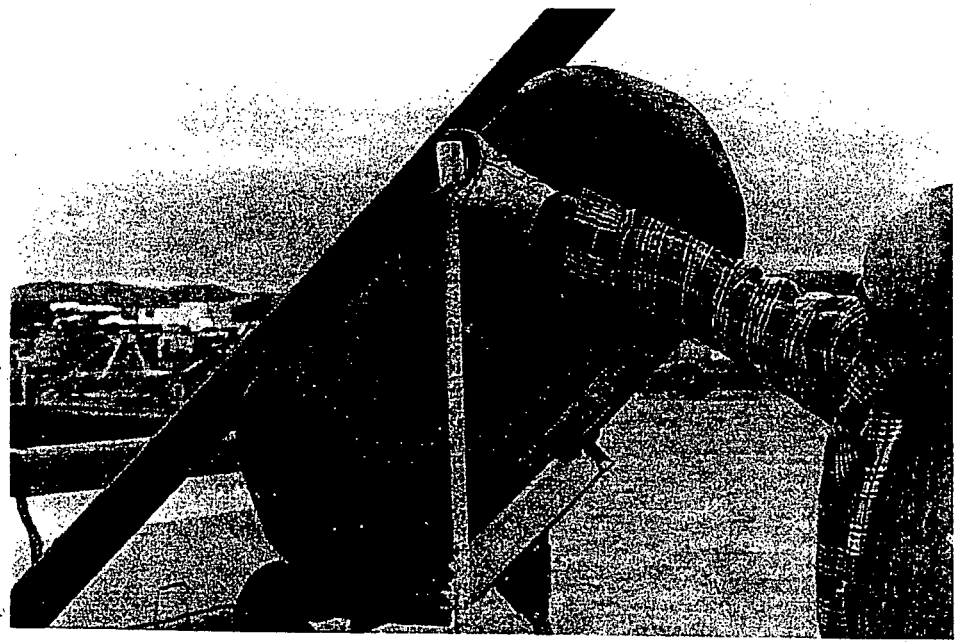

Figure 79. Tank 003 Orientation for Drop Test

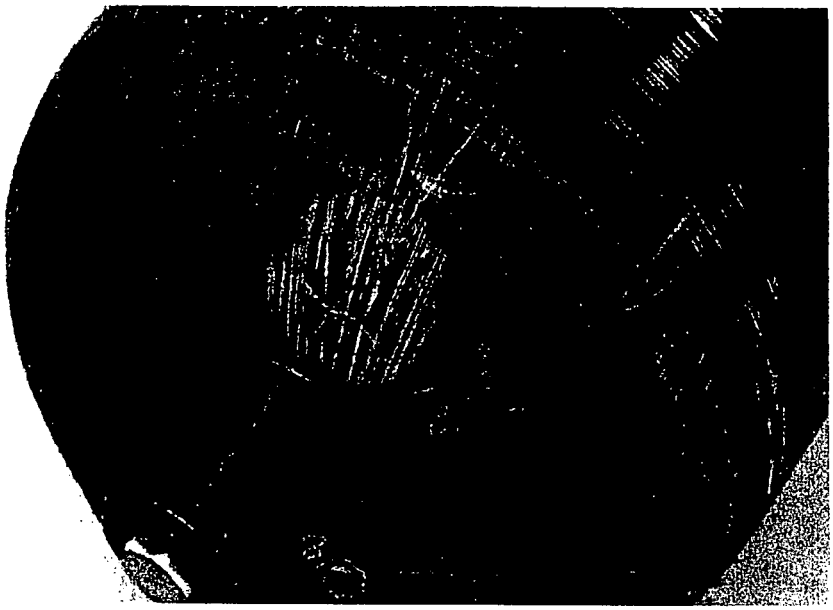

Figure 80. Impact Site on Tank 003

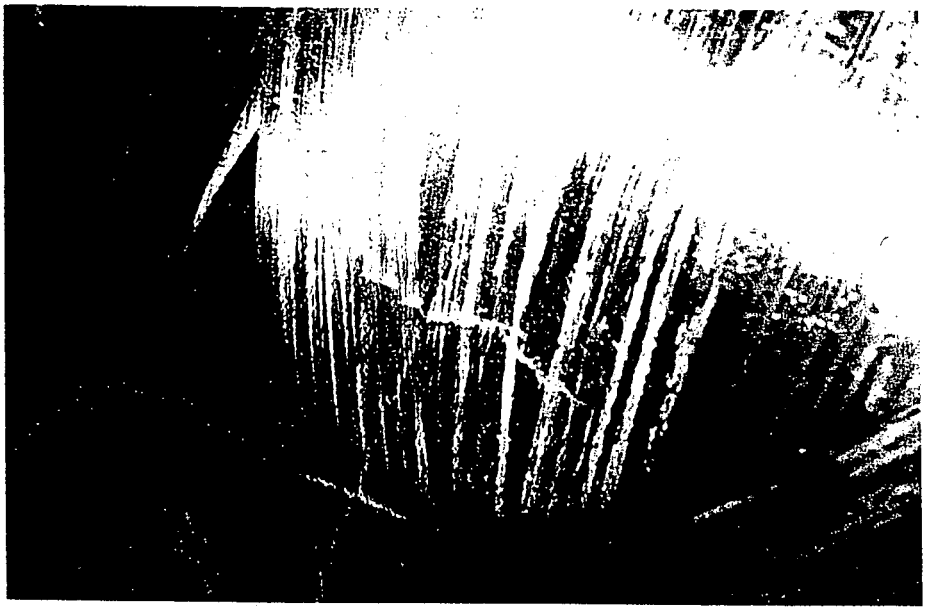

Figure 81. Impact Site on Tank 003, Close-up

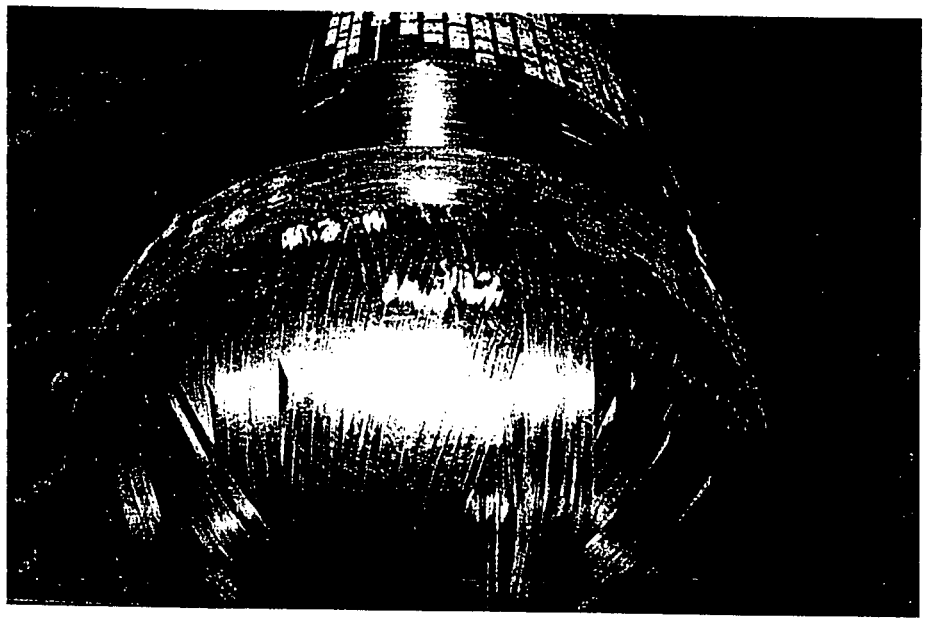

Figure 82. Secondary Damage on Tank 003

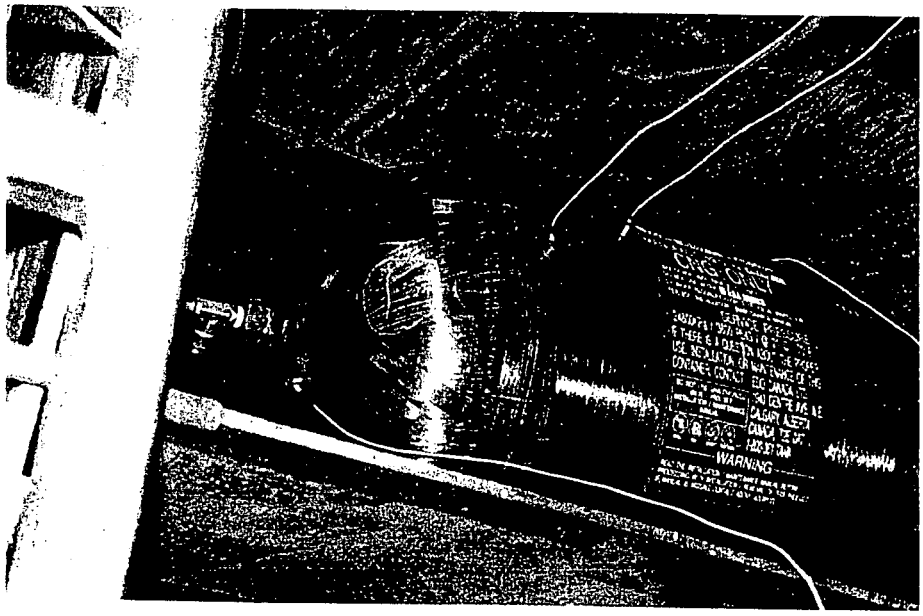

Figure 83. Tank 003 in the Burst Test Chamber, Following the Drop Test

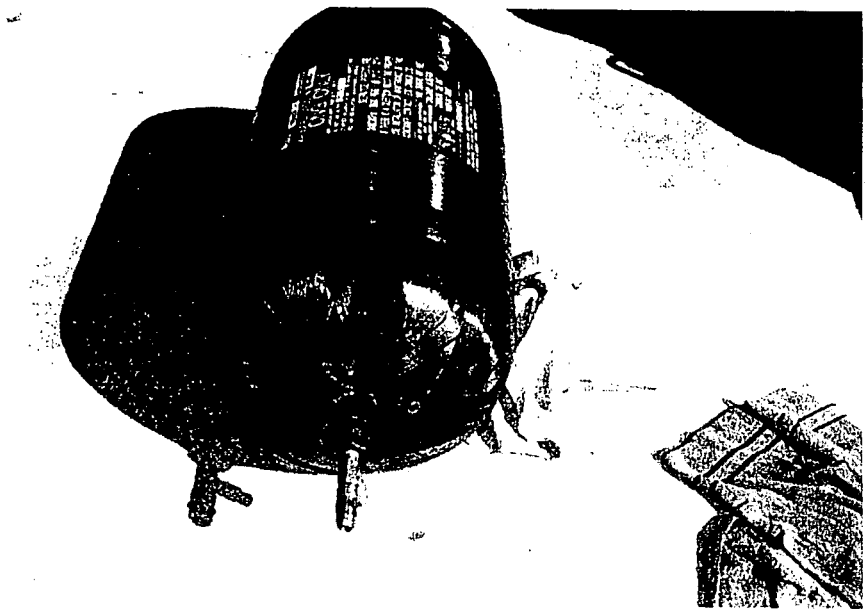

Figure 84. Failed Area on Tank 003

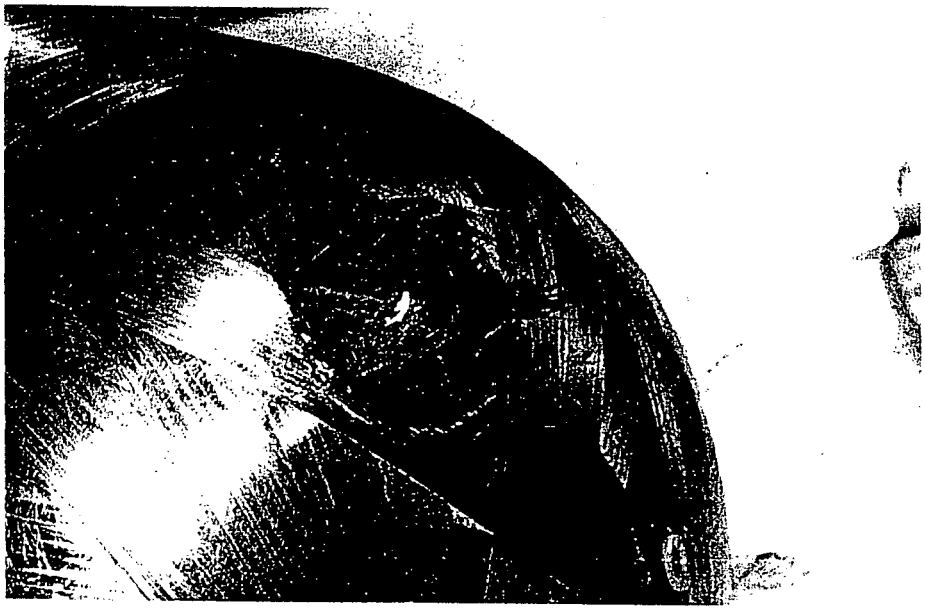

Figure 85. Failed Area on Tank 003, Close-up

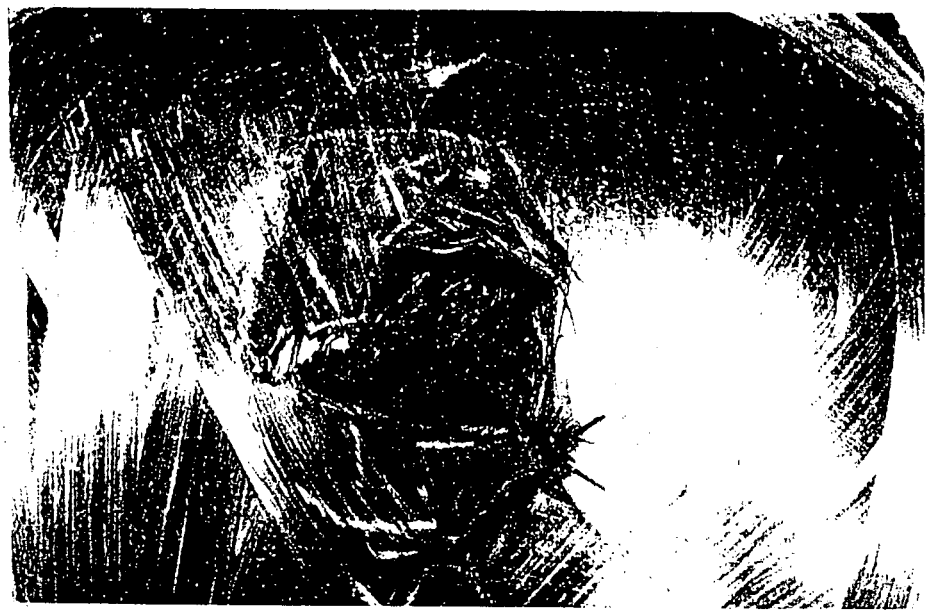

Figure 86. Failed Area on Tank 003, Oblique View

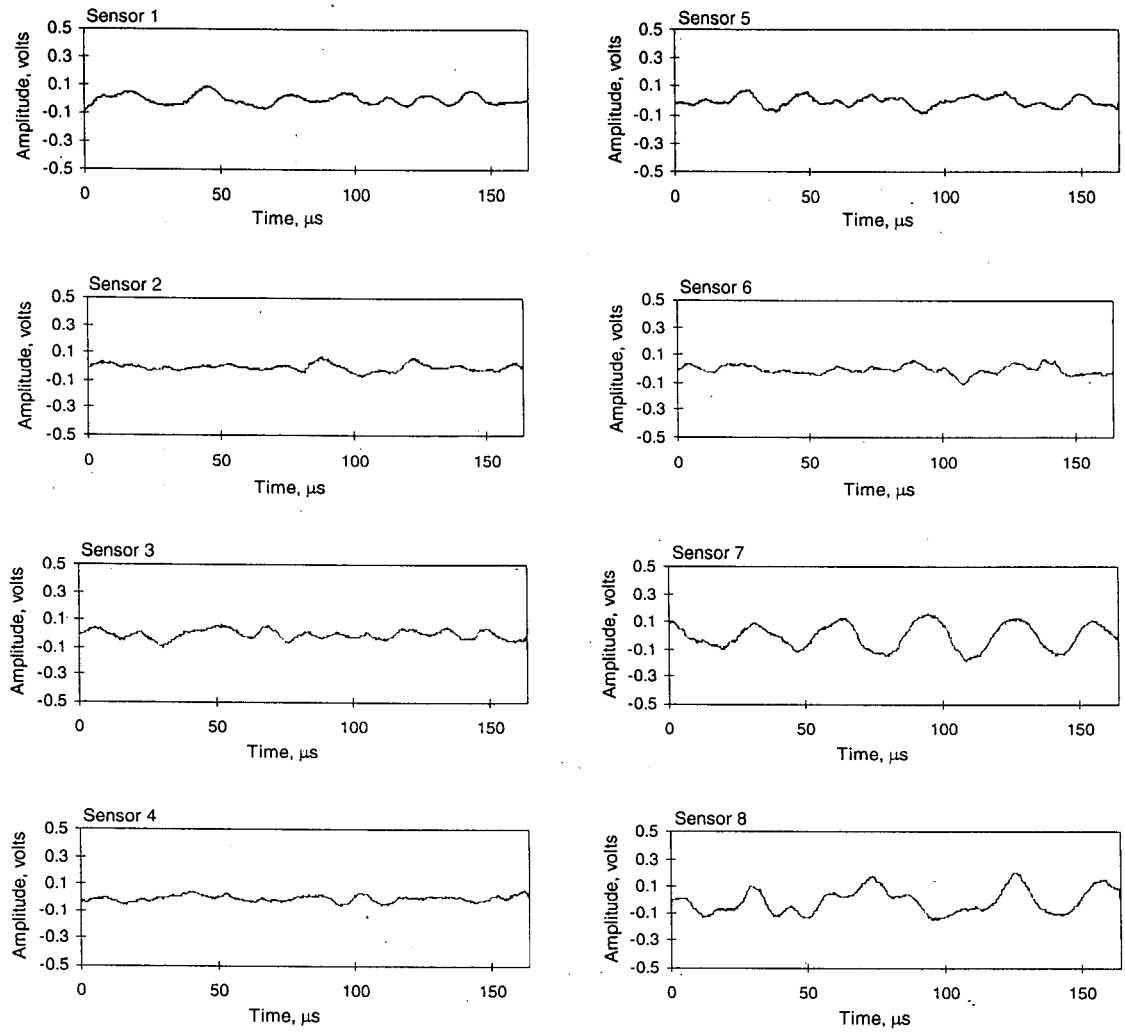

Figure 87a. Waveform from a Typical Noise Event Recorded During the Initial Pressurization of the As-Received Tanks

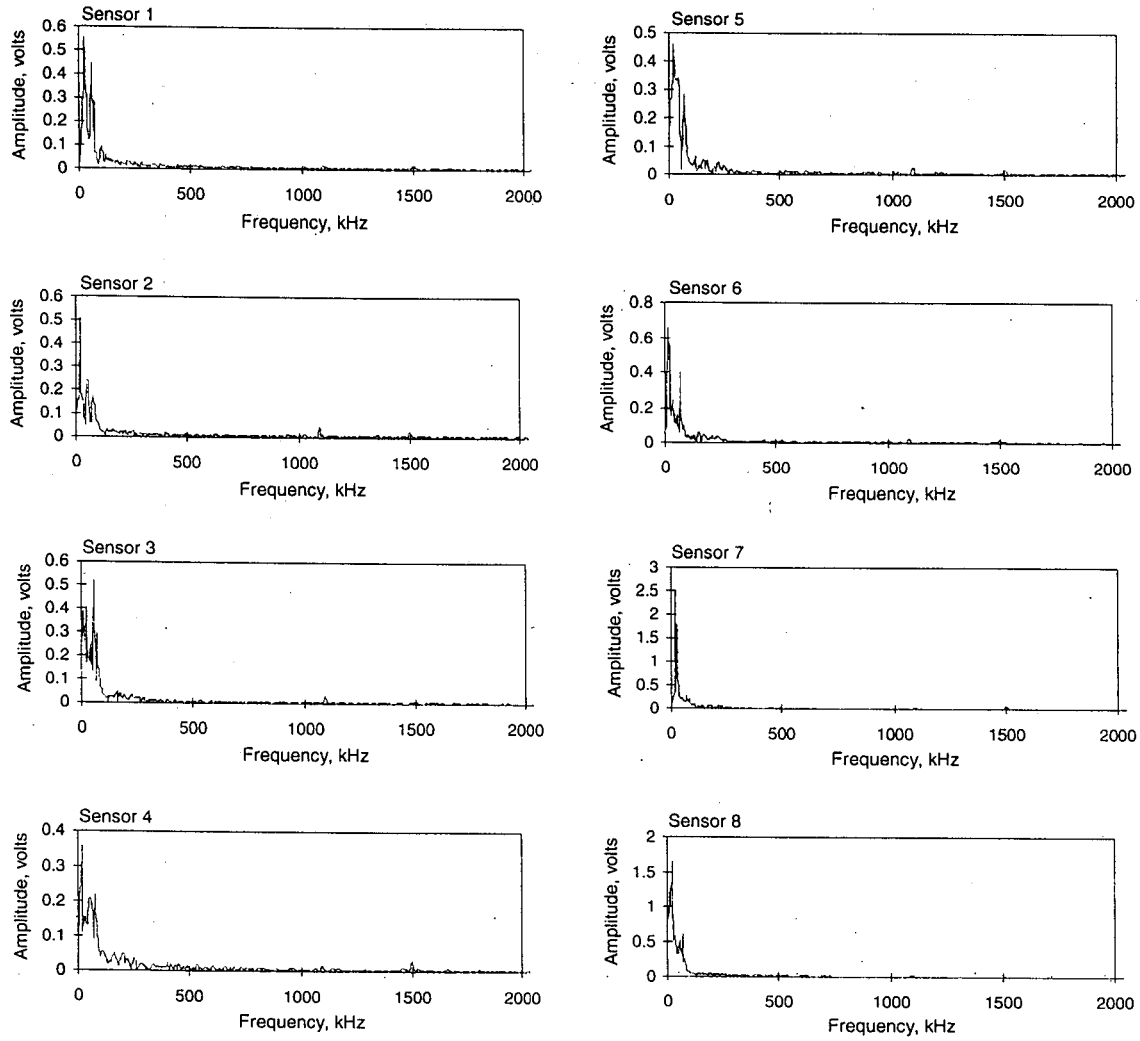

Figure 87b. FFT from a Typical Noise Event Recorded During Pressurization of the As-Received Type 2 Tanks

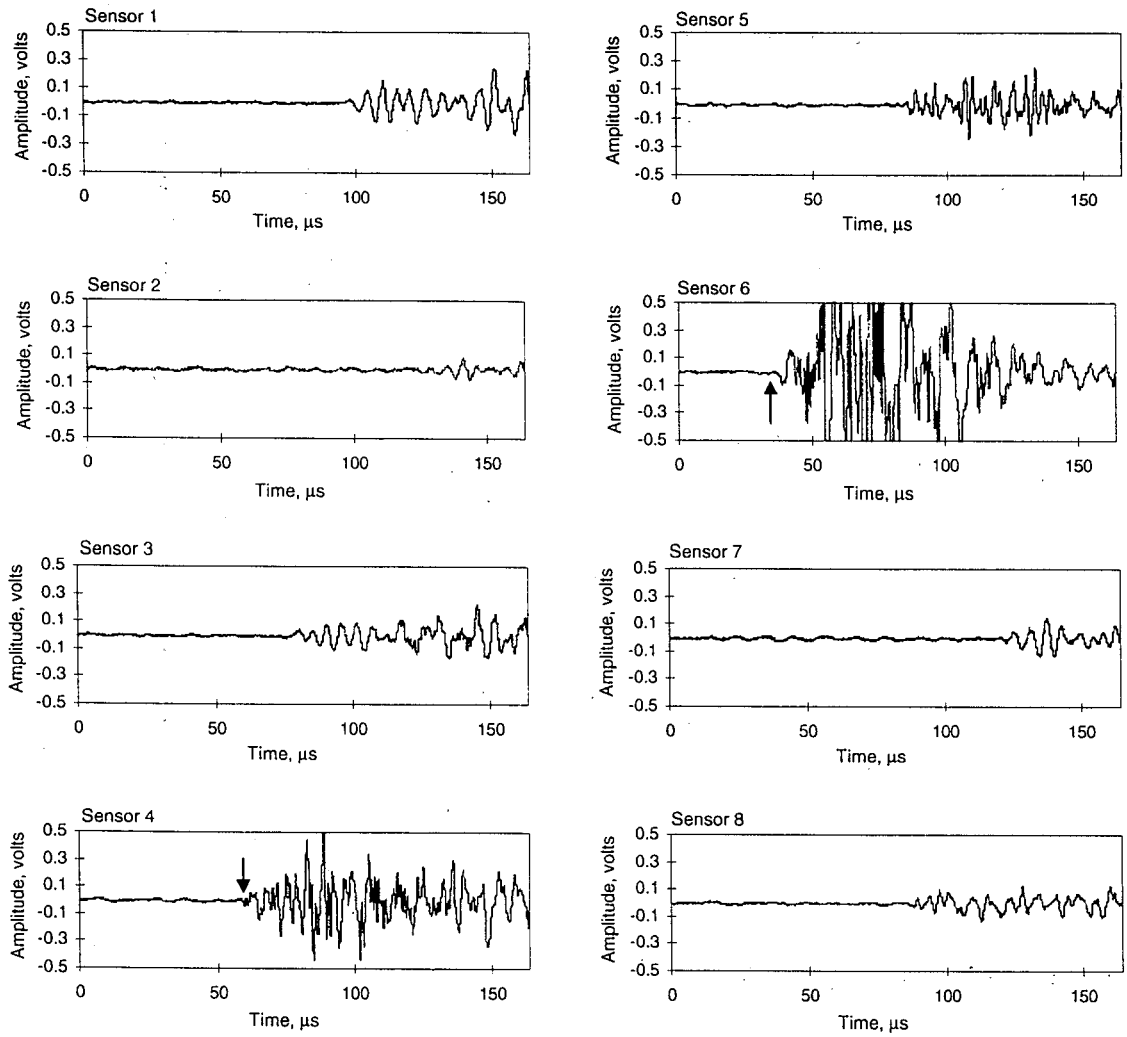

Figure 88a. Waveform from a Typical Structural Event Recorded During Pressurization of the As-Received Type 2 Tanks

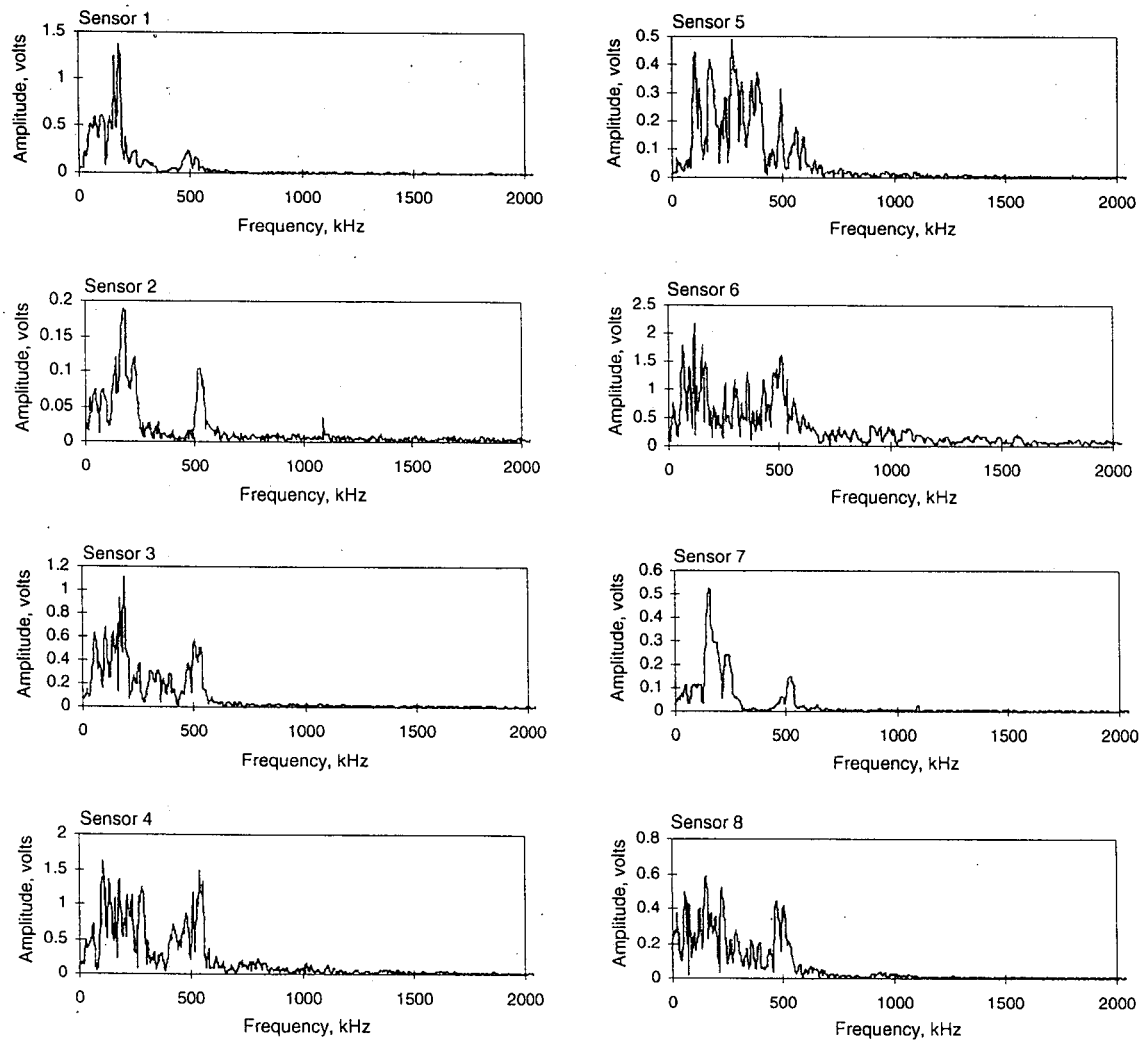

Figure 88b. FFT from a Typical Structural Event Recorded During Pressurization of the As-Received Type 2 Tanks

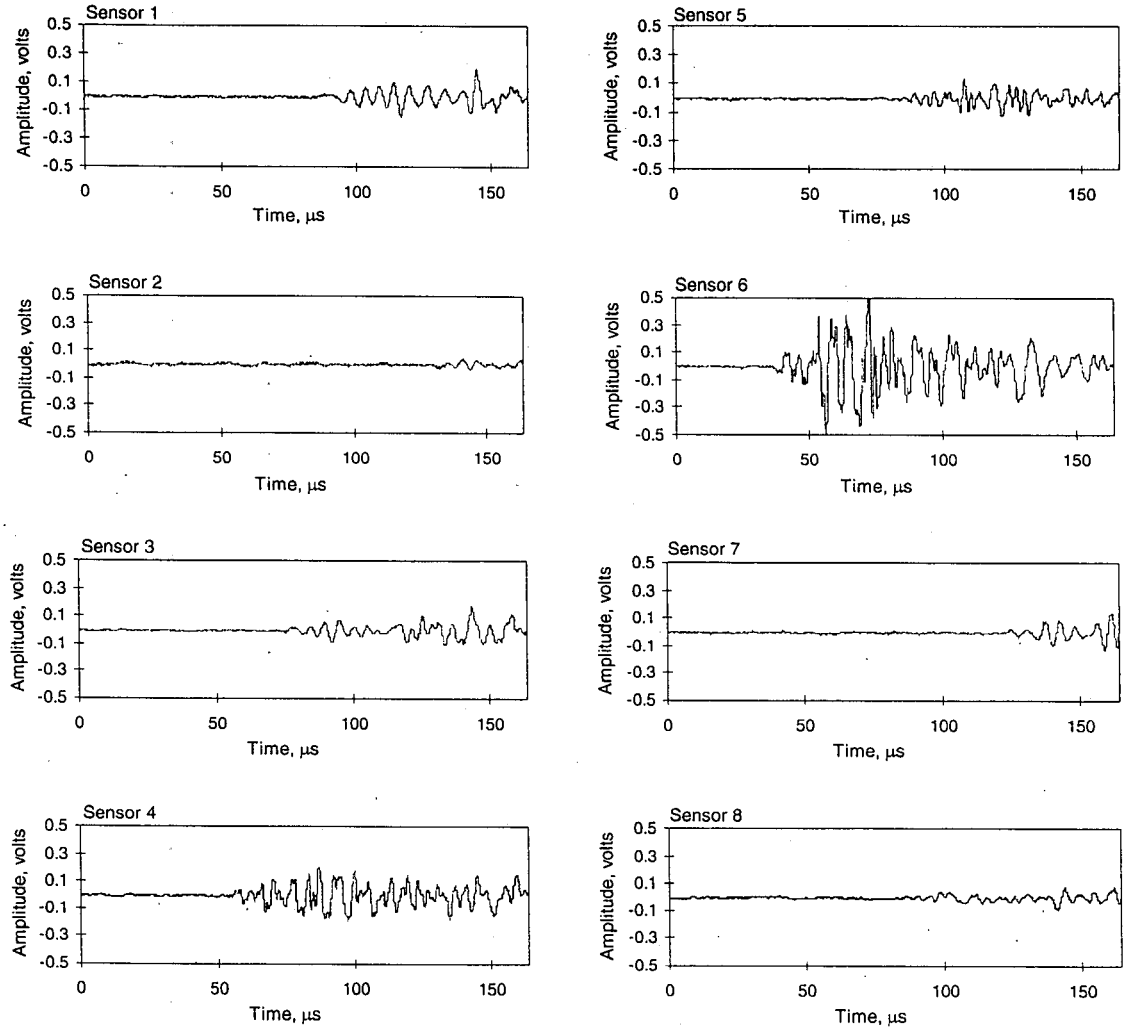

Figure 89a. Waveform from a Typical Event Recorded During Pressurization of the As-Received Type 2 Tanks

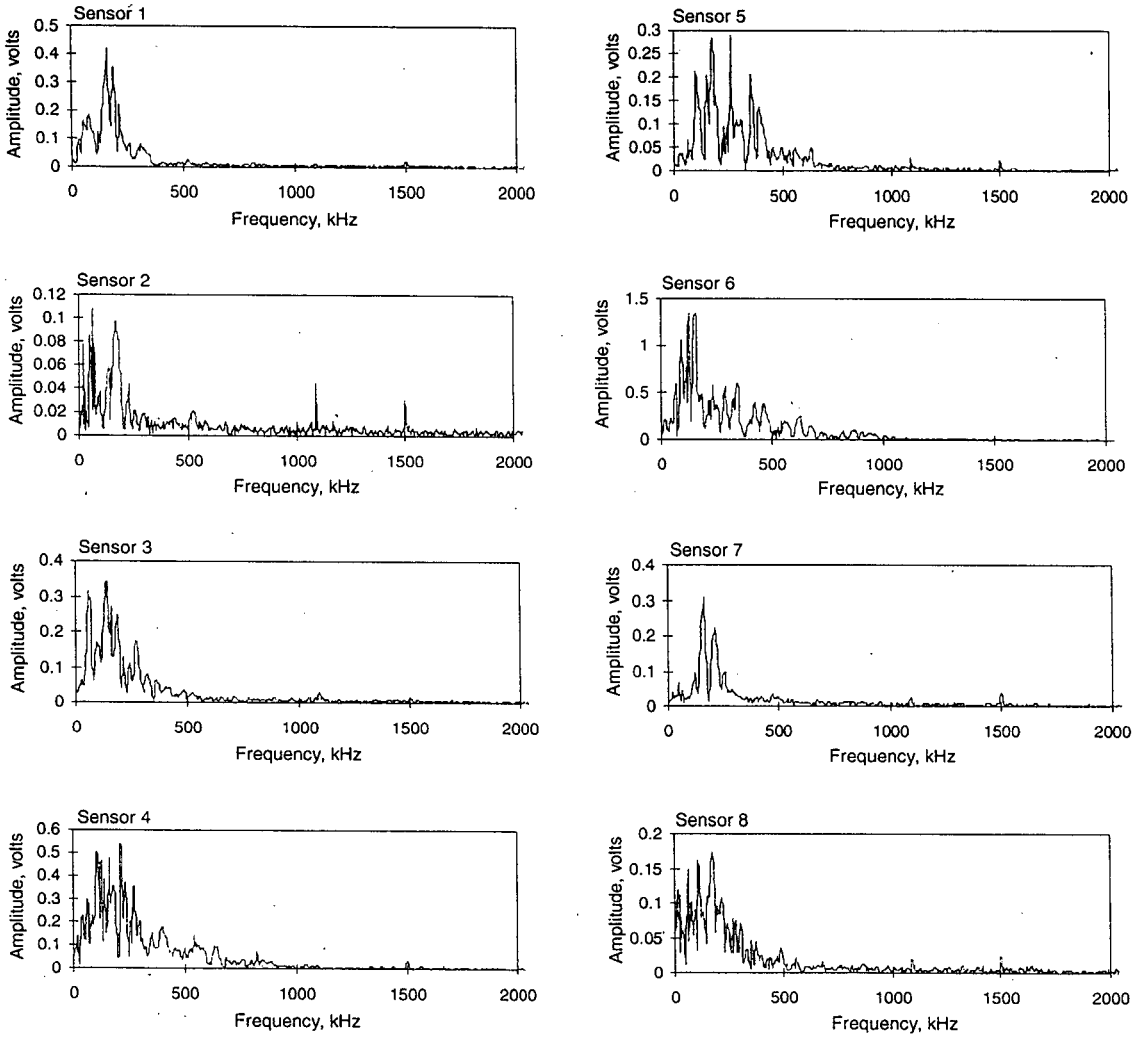

Figure 89b. FFT from a Typical Event Recorded During Pressurization of the As-Received Type 2 Tanks

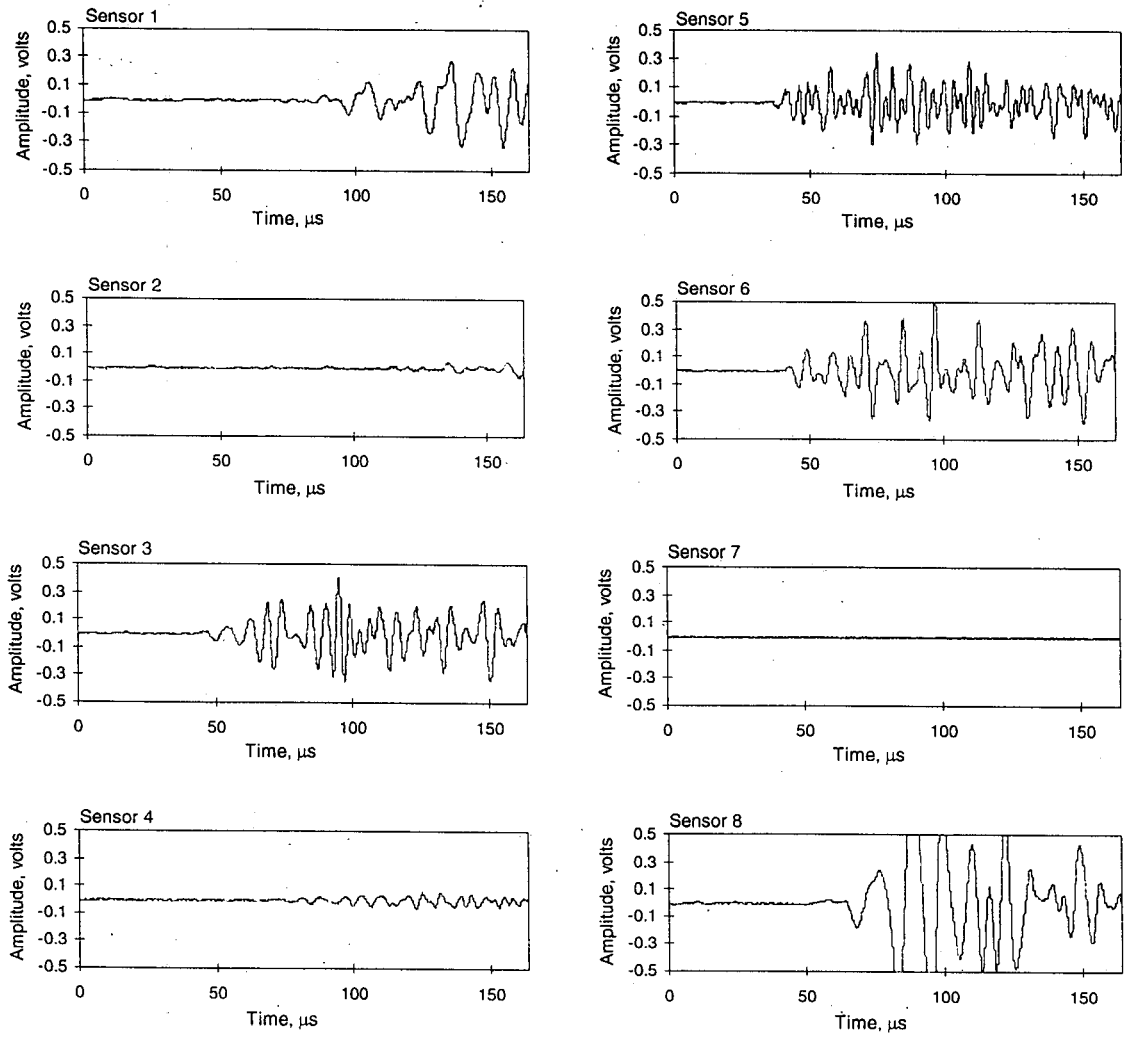

Figure 90a. Waveform from a Typical Event Recorded During Pressurization of the As-Received EDO Type 4 Tank

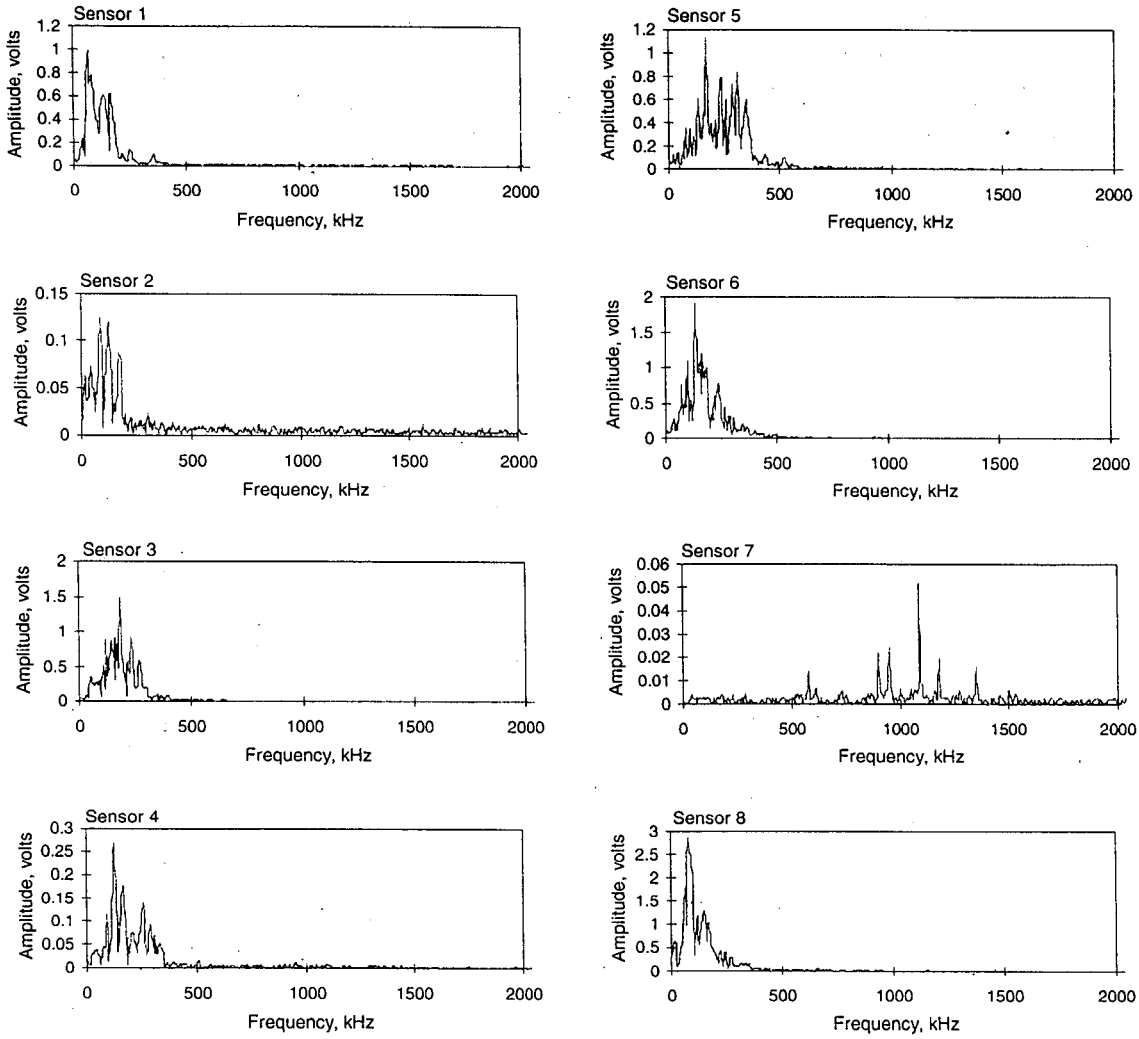

Figure 90b. FFT from a Typical Event Recorded During Pressurization of the As-Received EDO Tank

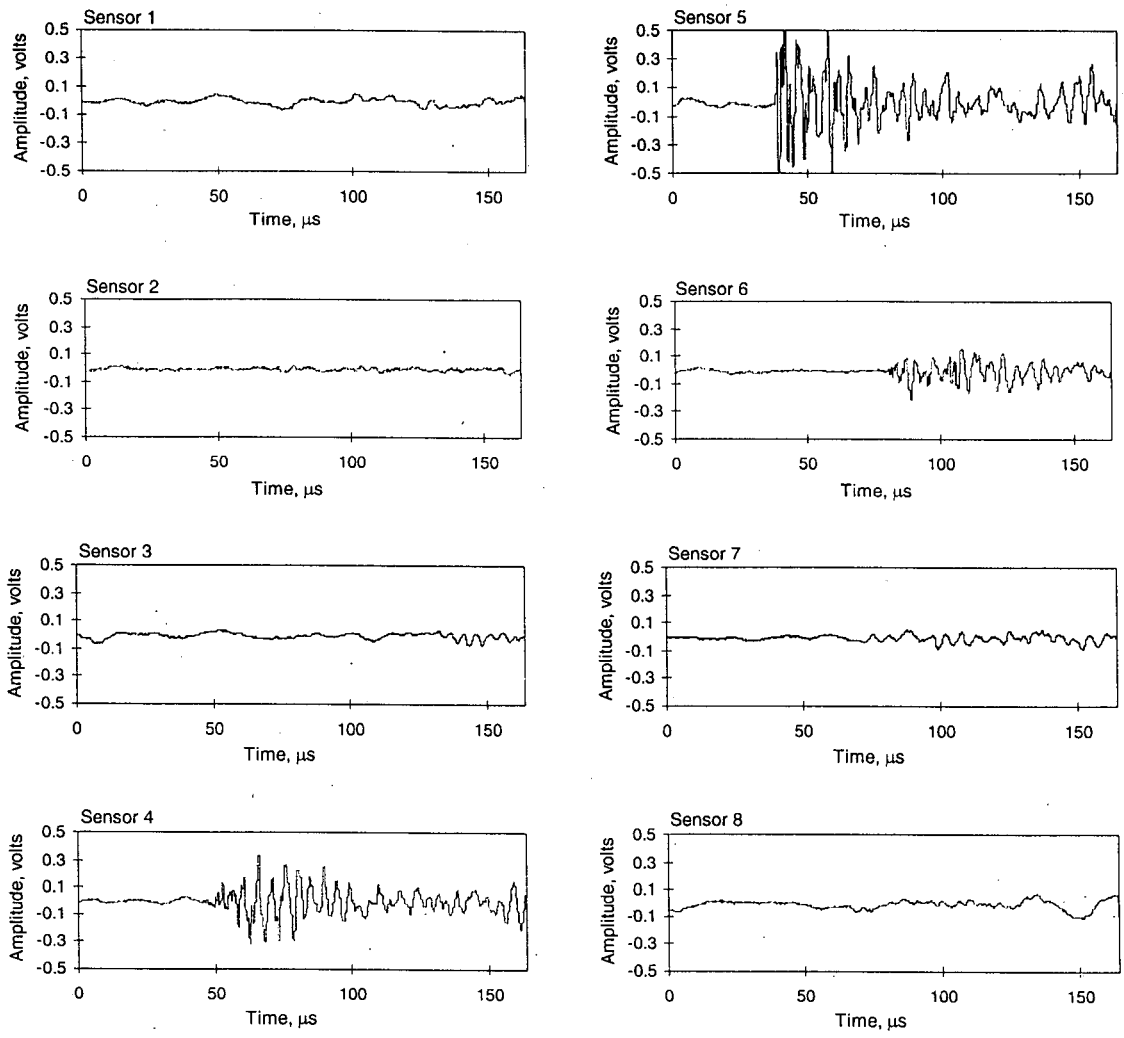

Figure 91a. Waveform from a Typical Event Recorded During Pressurization of a Type 2 Tank with a Saw Cut

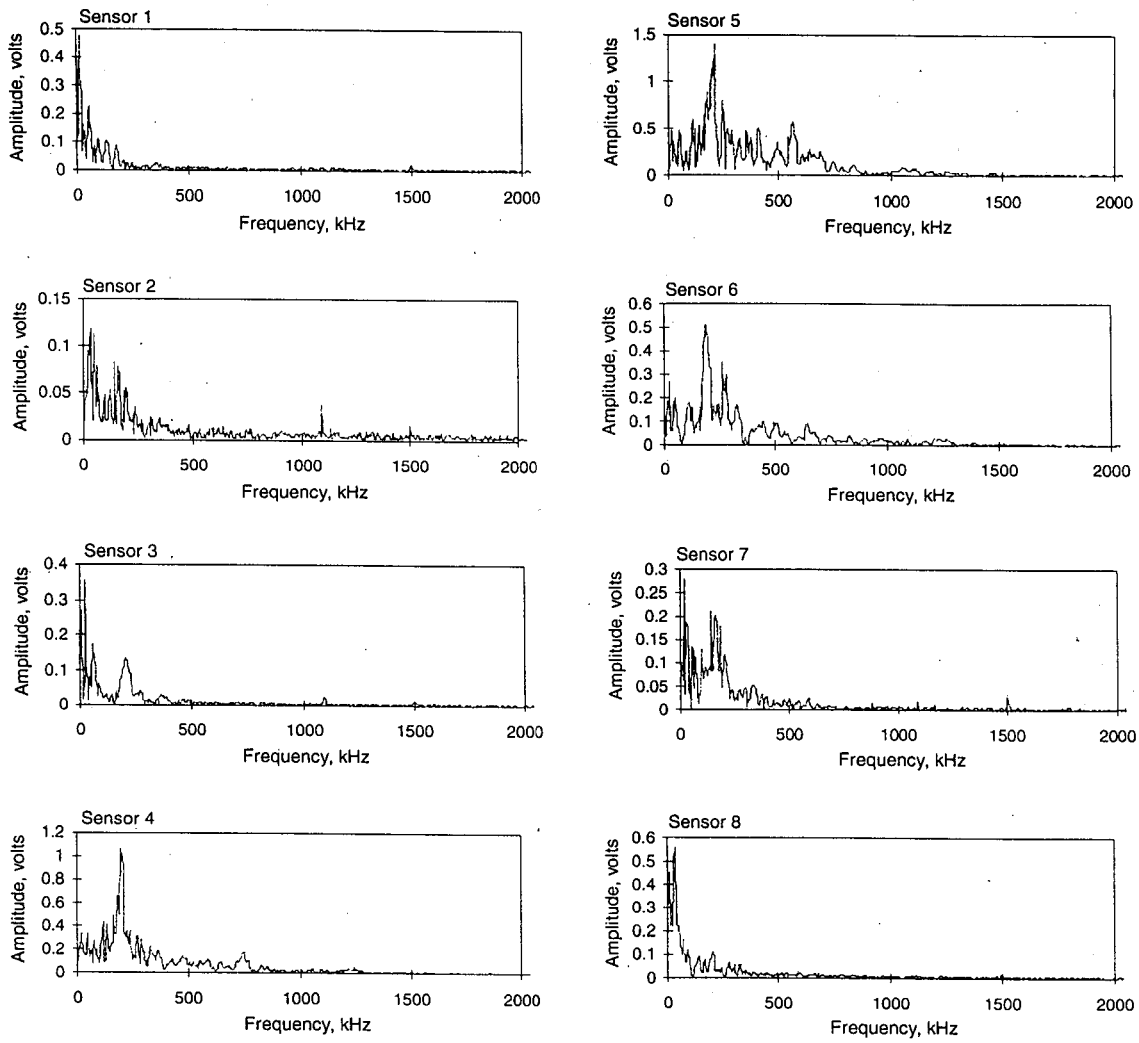

Figure 91b. FFT from a Typical Event Recorded During Pressurization of a Type 2 Tank with a Saw Cut

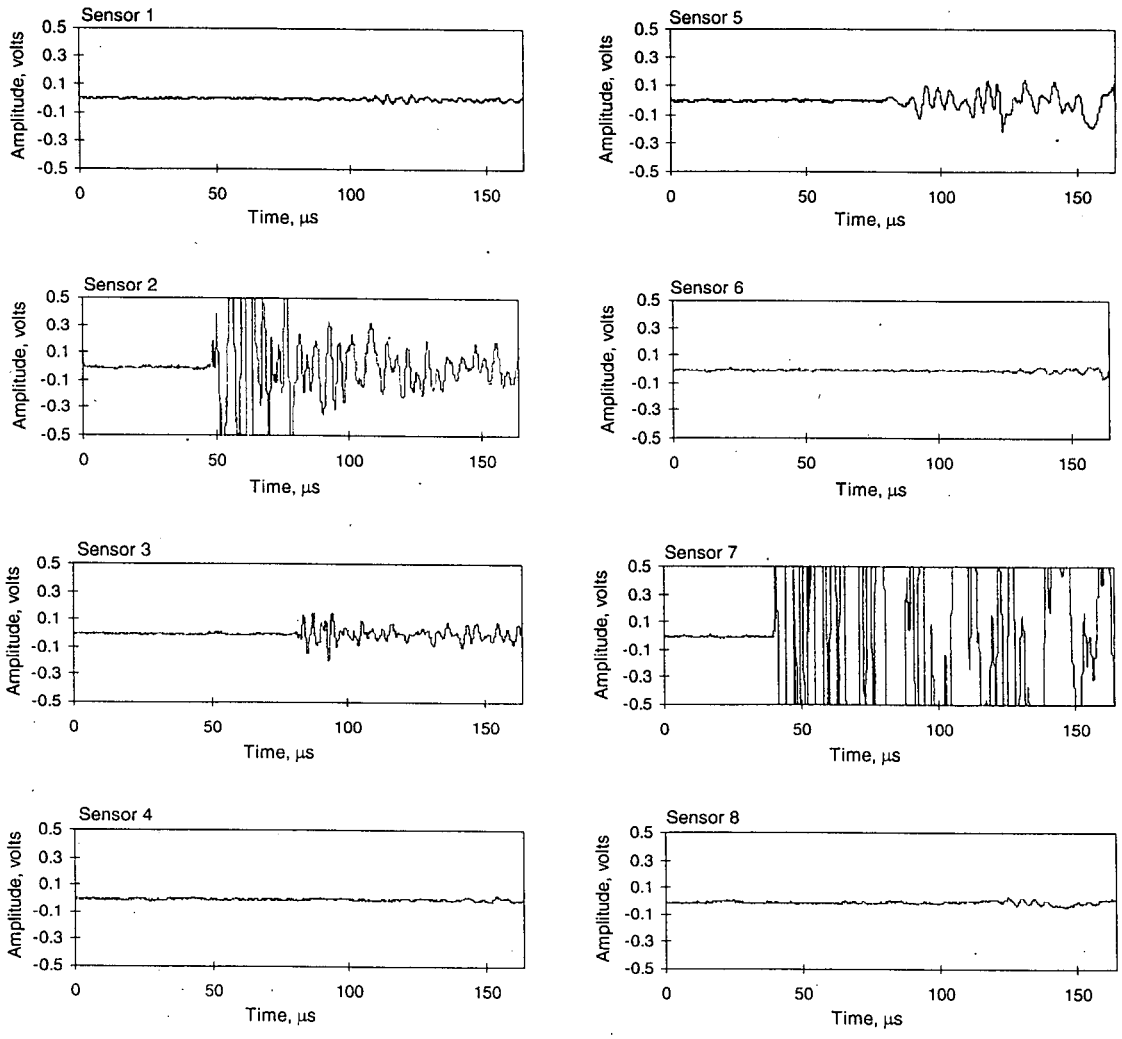

Figure 92a. Waveform from a Typical Event Recorded During Pressurization of a Type 2 Tank with Impact Damage

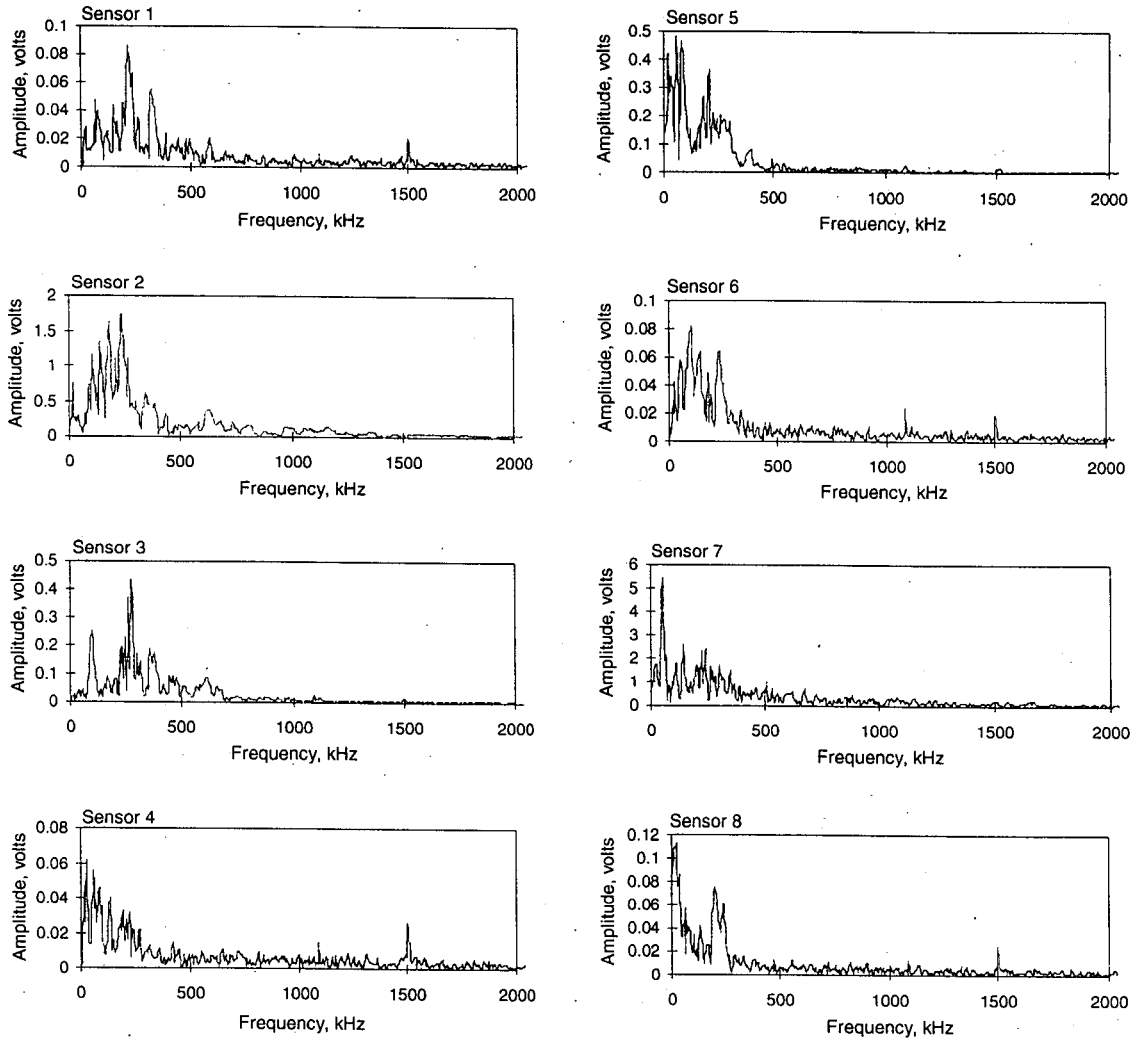

Figure 92b. FFT from a Typical Event Recorded During Pressurization of a Type 2 Tank with Impact Damage

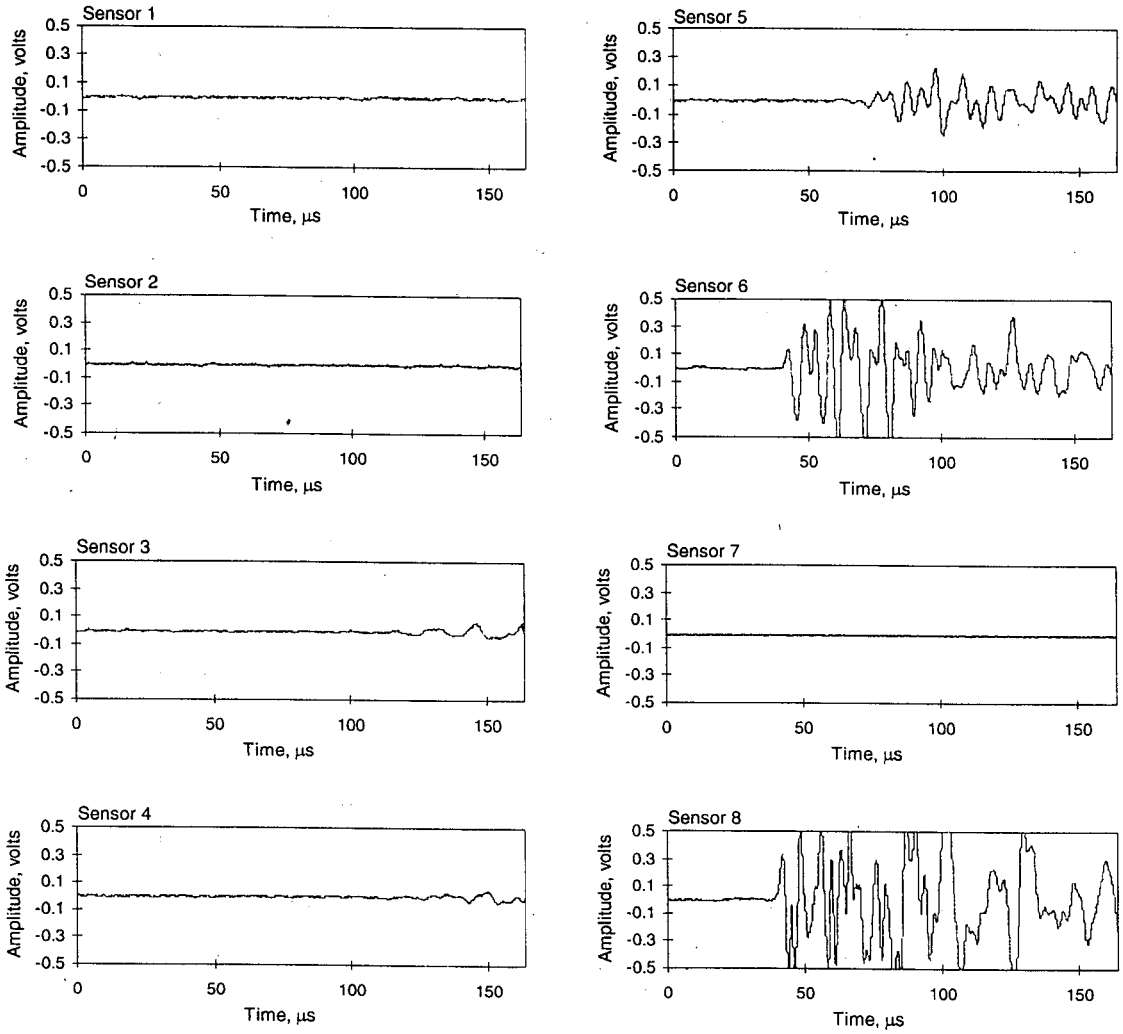

Figure 93a. Waveform from a Typical Event Recorded During Pressurization of the Type 4 Tank with Impact Damage

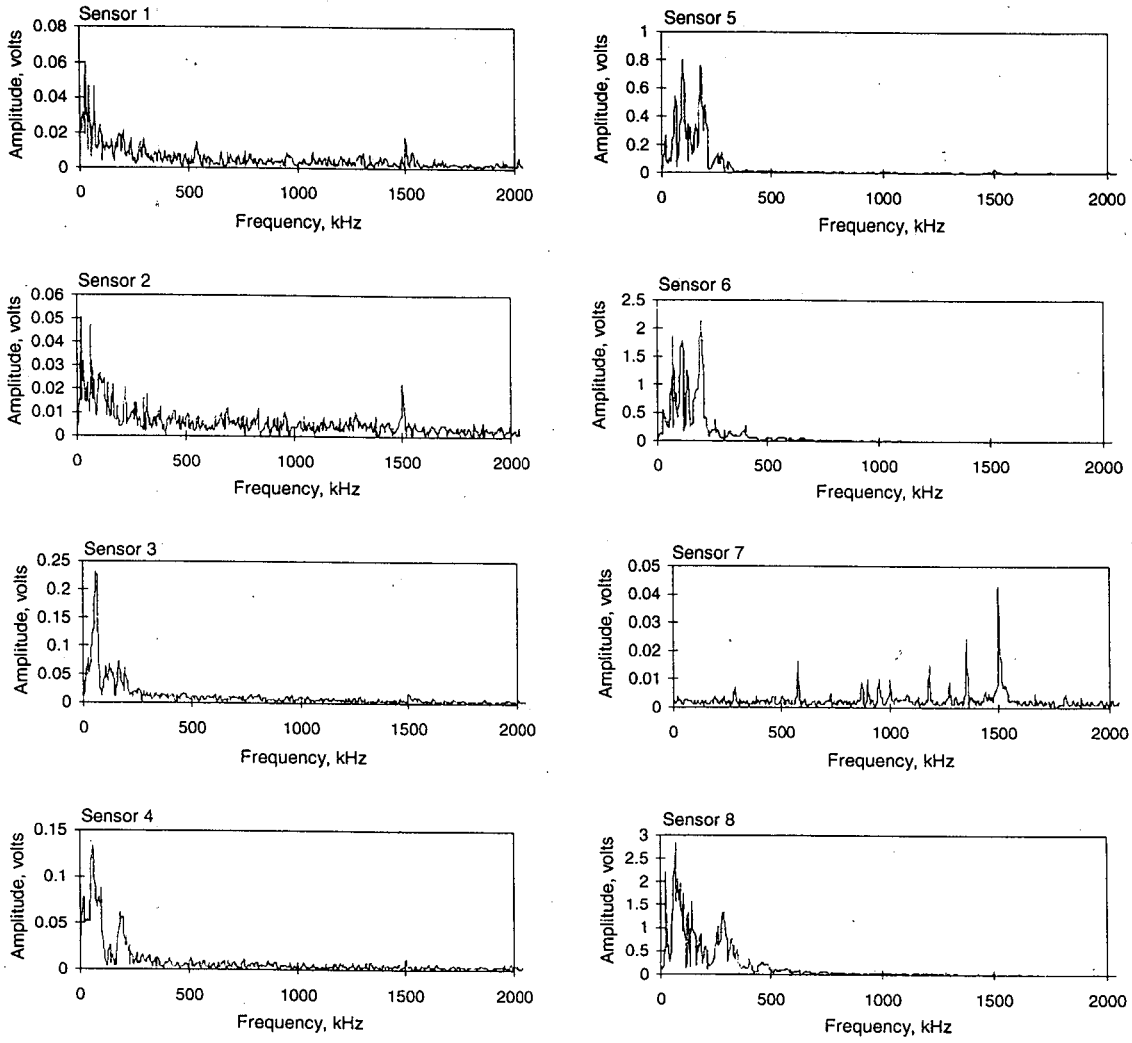

Figure 93b. FFT from a Typical Event Recorded During Pressurization of the Type 4 Tank with Impact Damage

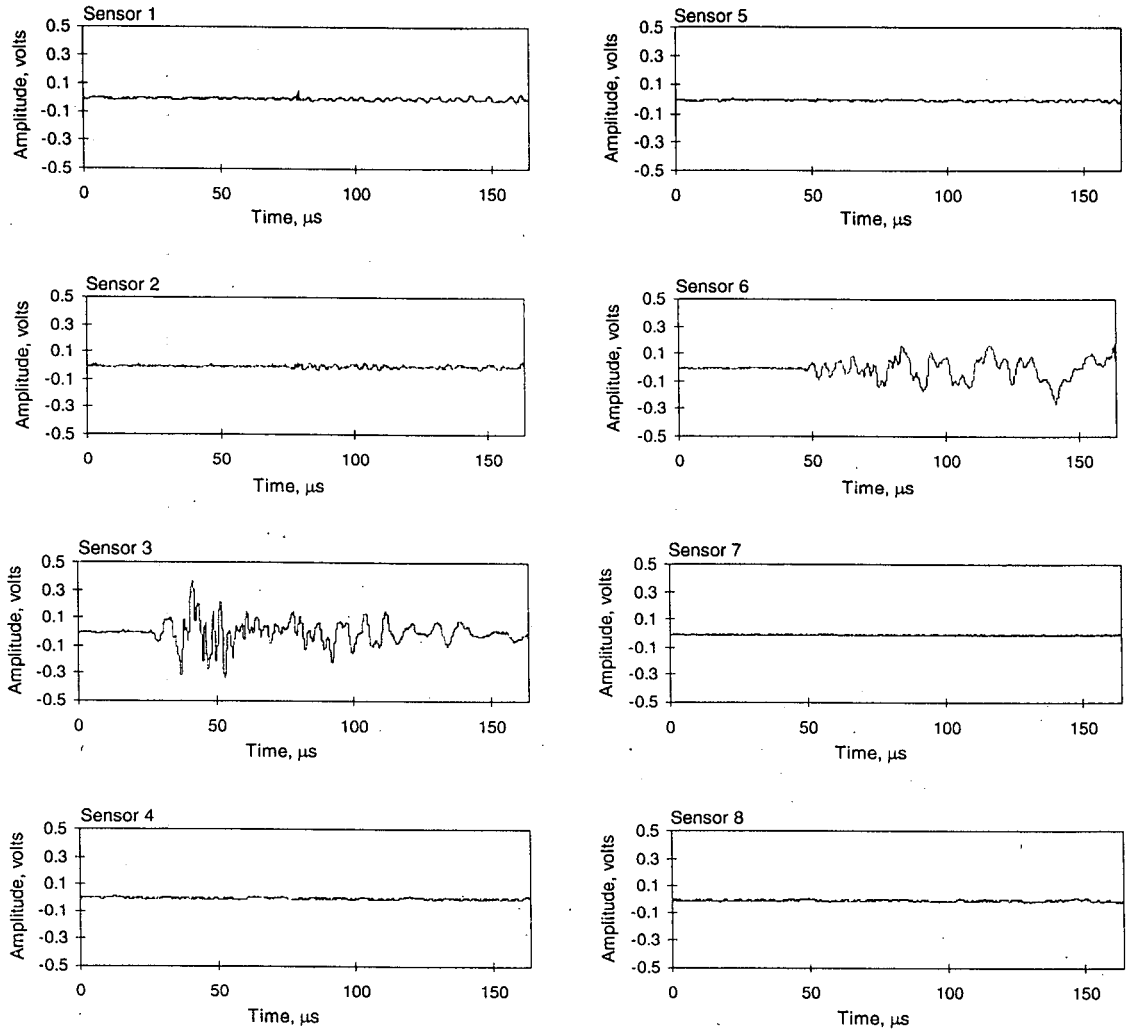

Figure 94. Waveform from a Typical Fretting Event Recorded During Fatigue Cycling of a Type 2 Tank

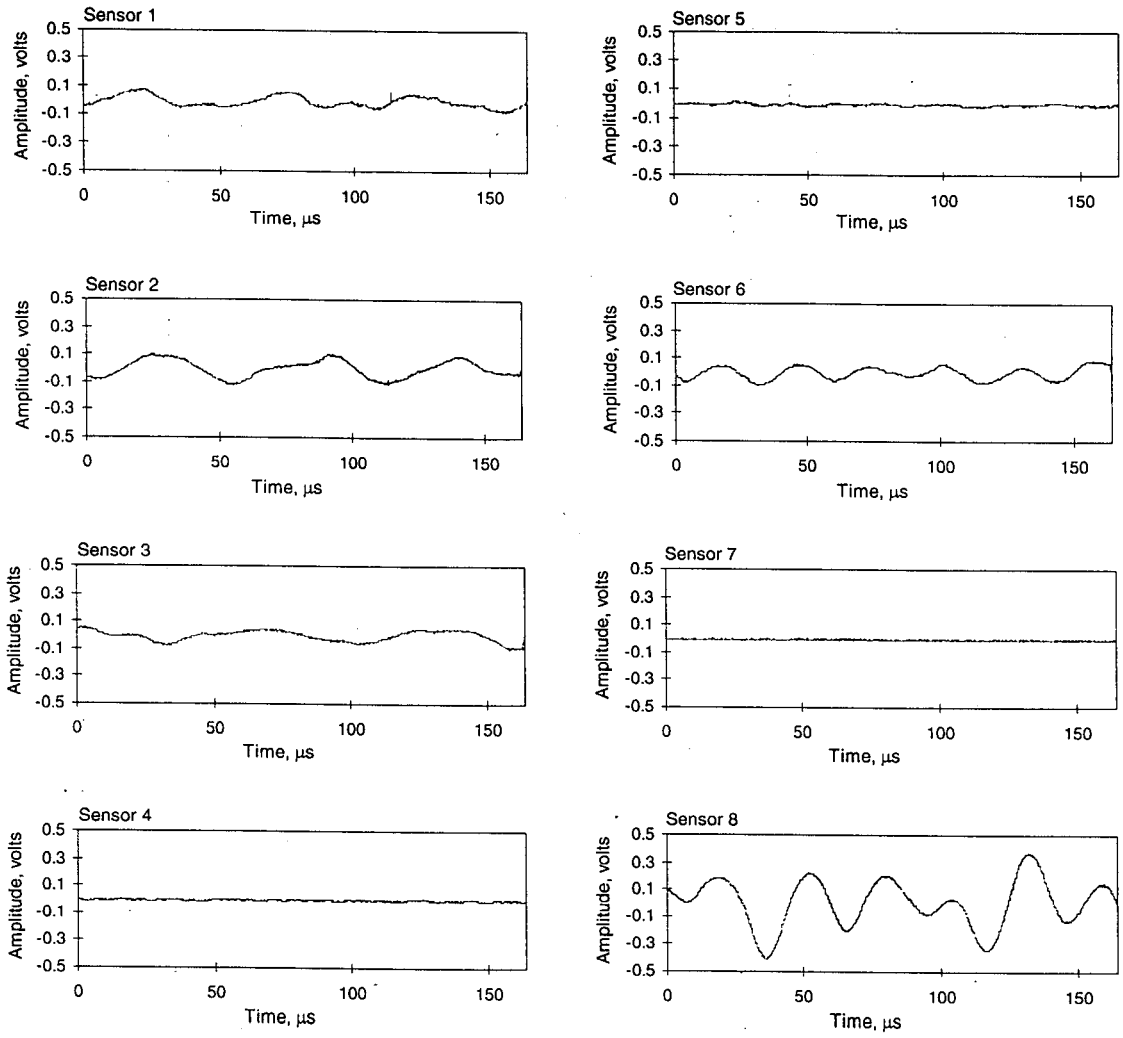

Figure 95. Waveform from a Typical Noise Event Recorded During Type 2 Tank Fatigue Cycling

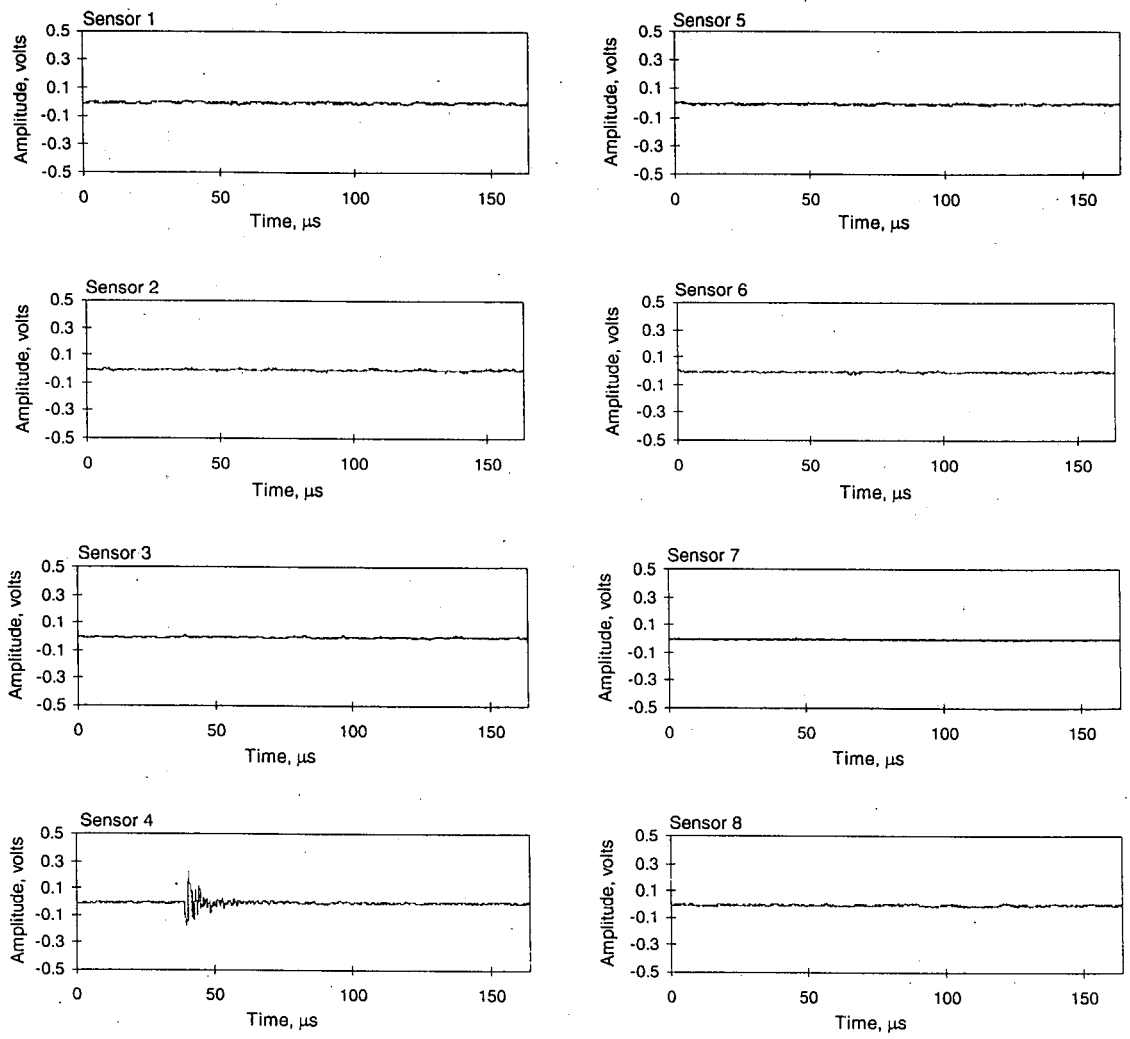

Figure 96. Waveform from a Typical Small Amplitude Event Recorded During Fatigue Cycling of the Type 4 Tank

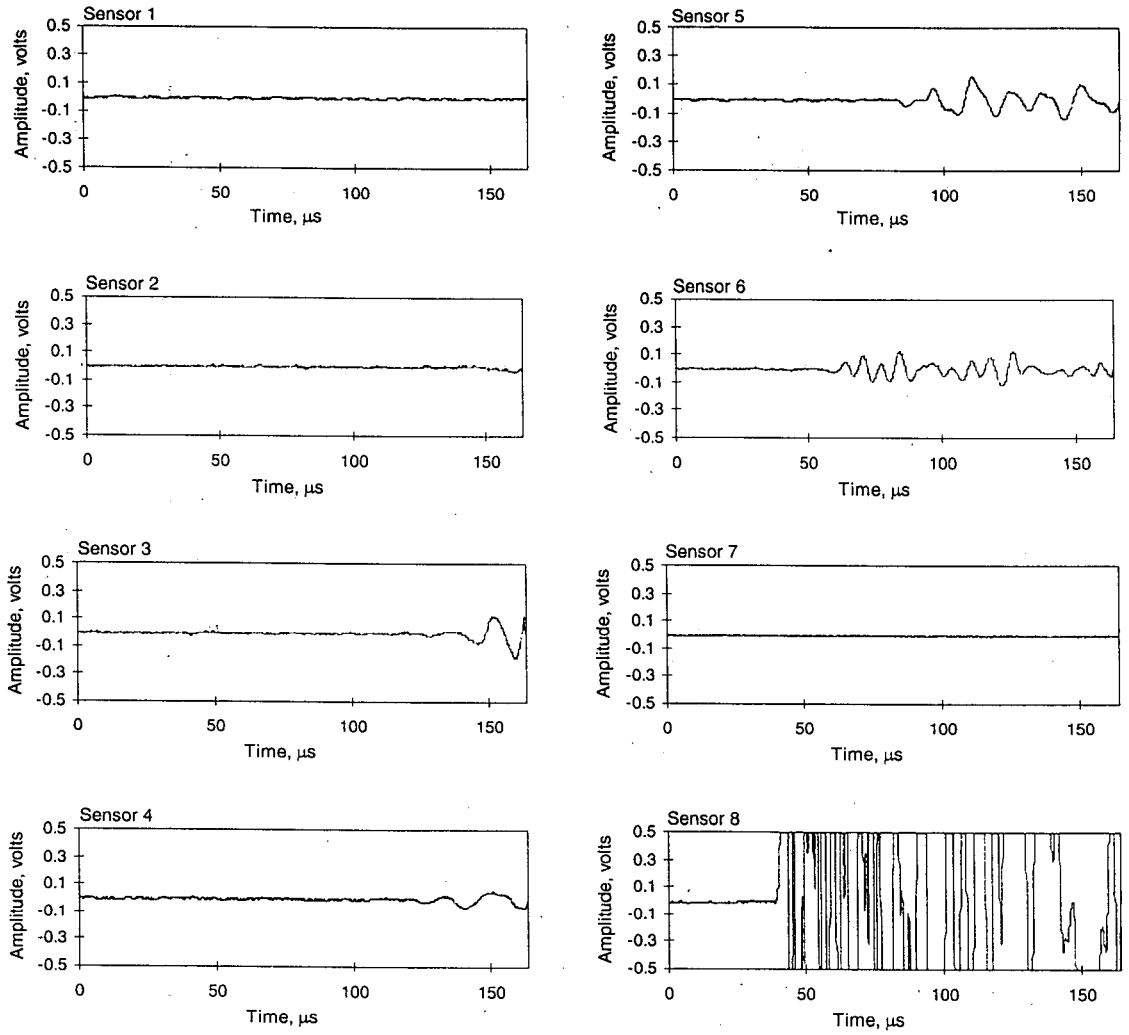

Figure 97. Waveform from a Typical Event from the Impact Area Recorded During Fatigue Cycling of the Type 4 Tank

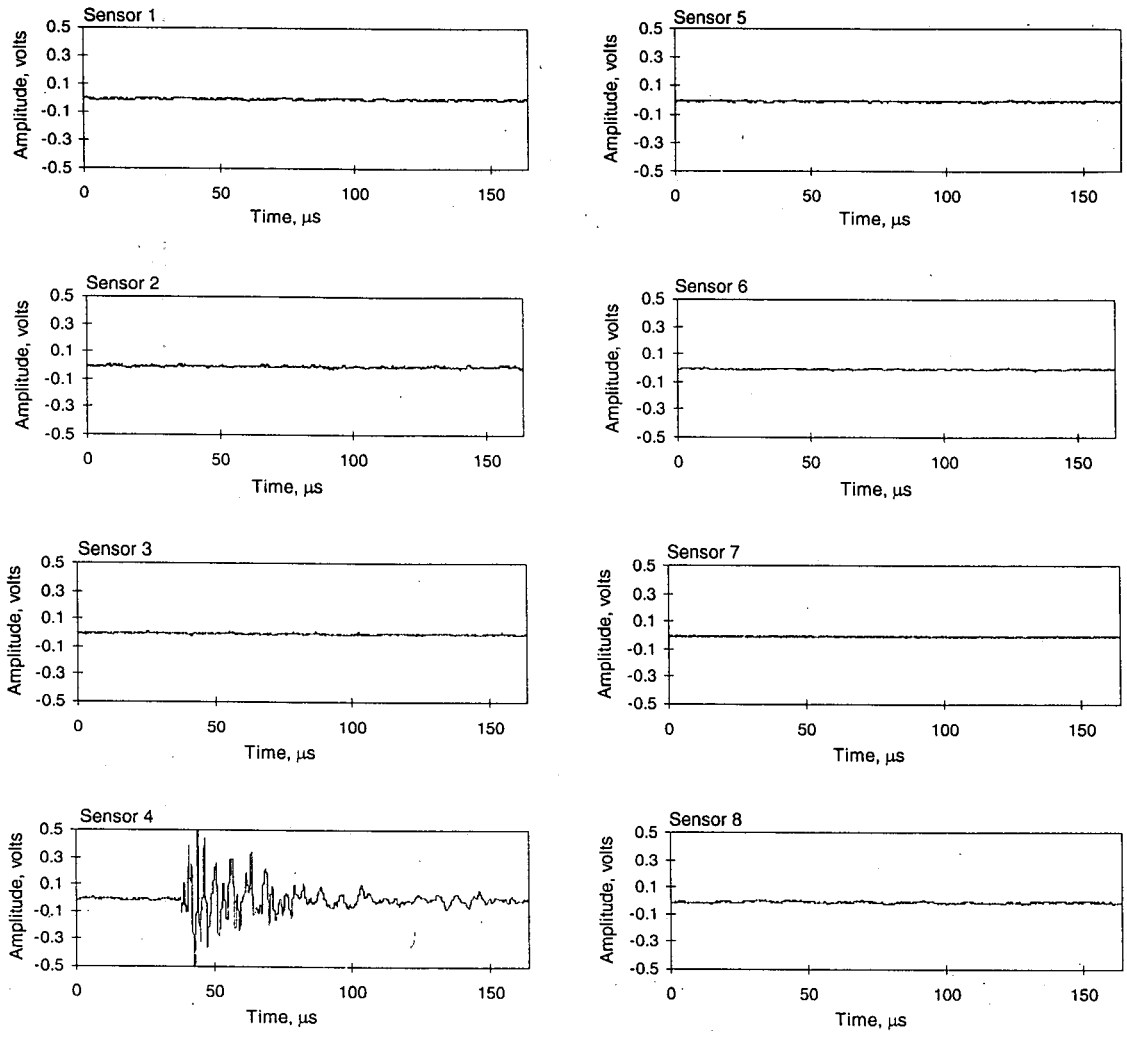

Figure 98a. Waveform from a Typical Small Amplitude, High Frequency Event Just Prior to Failure of the Type 4 Tank

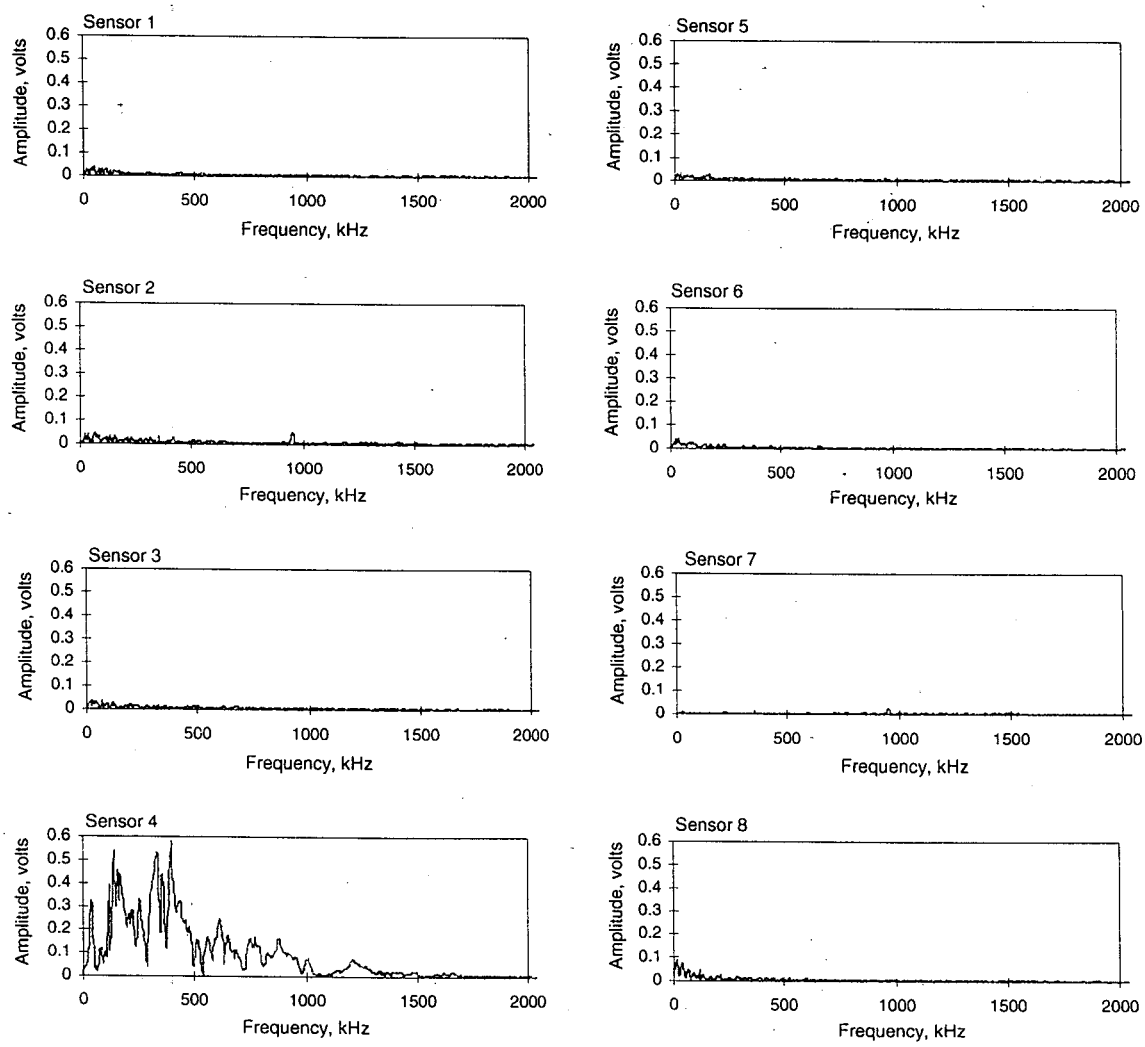

Figure 98b. FFT from a Typical Small Amplitude, High Frequency Event Just Prior to Failure of the Type 4 Tank

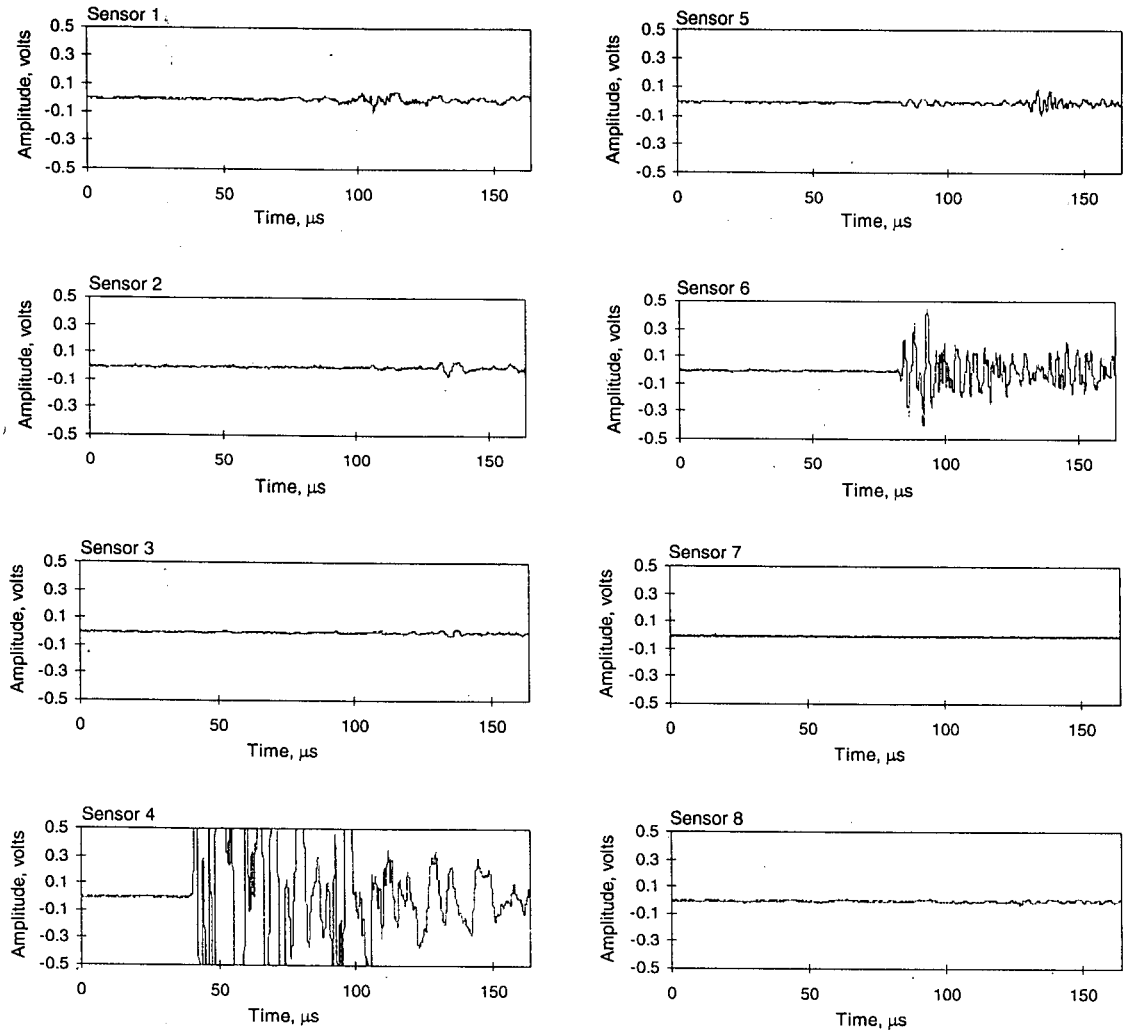

Figure 99. Waveform Recorded During Pressurization Hold After Fatigue Cycling of a Type 2 Tank

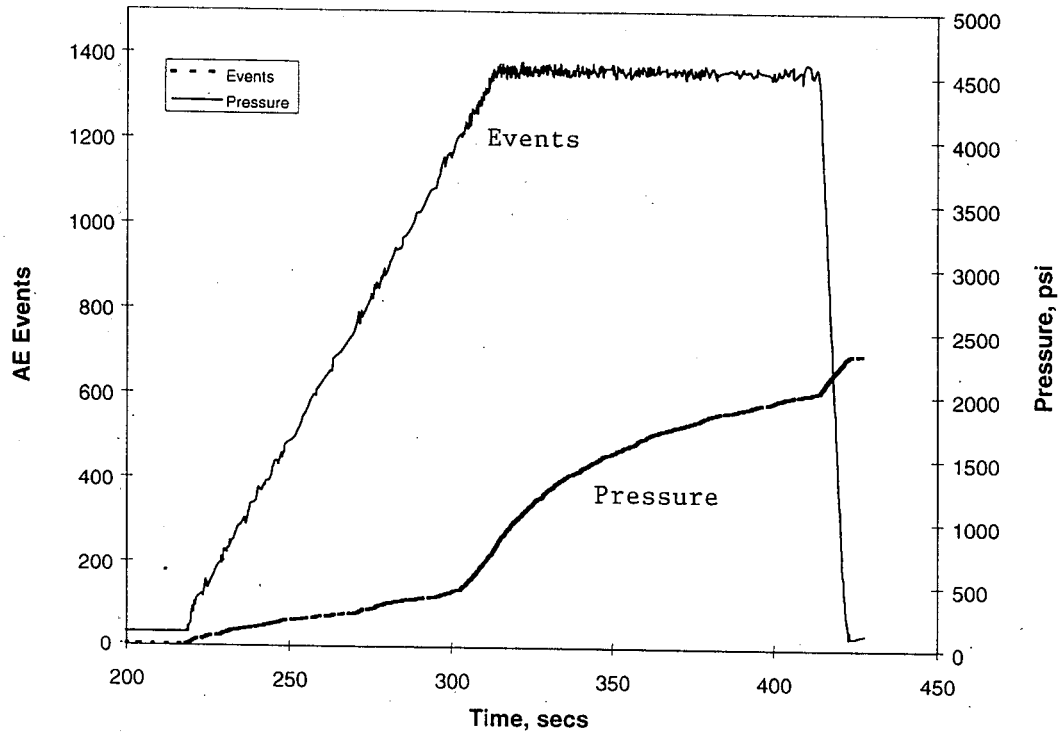

Figure 100. Typical Events versus Time Plot During Pressure Hold After 6,000 Fatigue Cycles of Tank 013

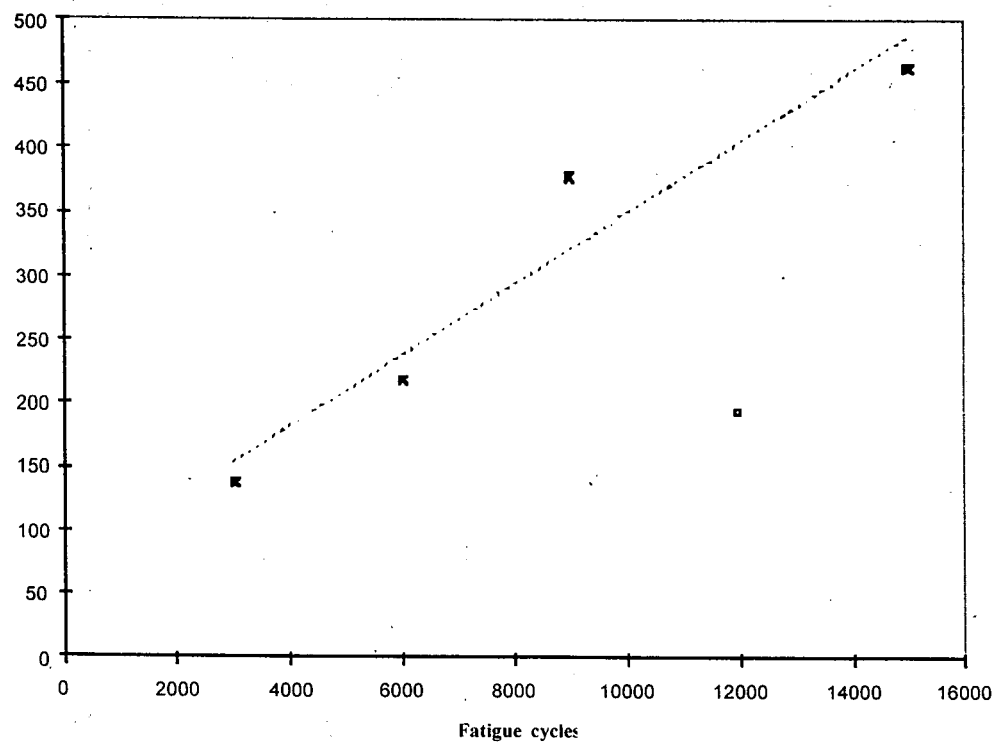

Figure 101. Number of Events During Each Pressure Hold After Fatigue Cycling of Tank 013

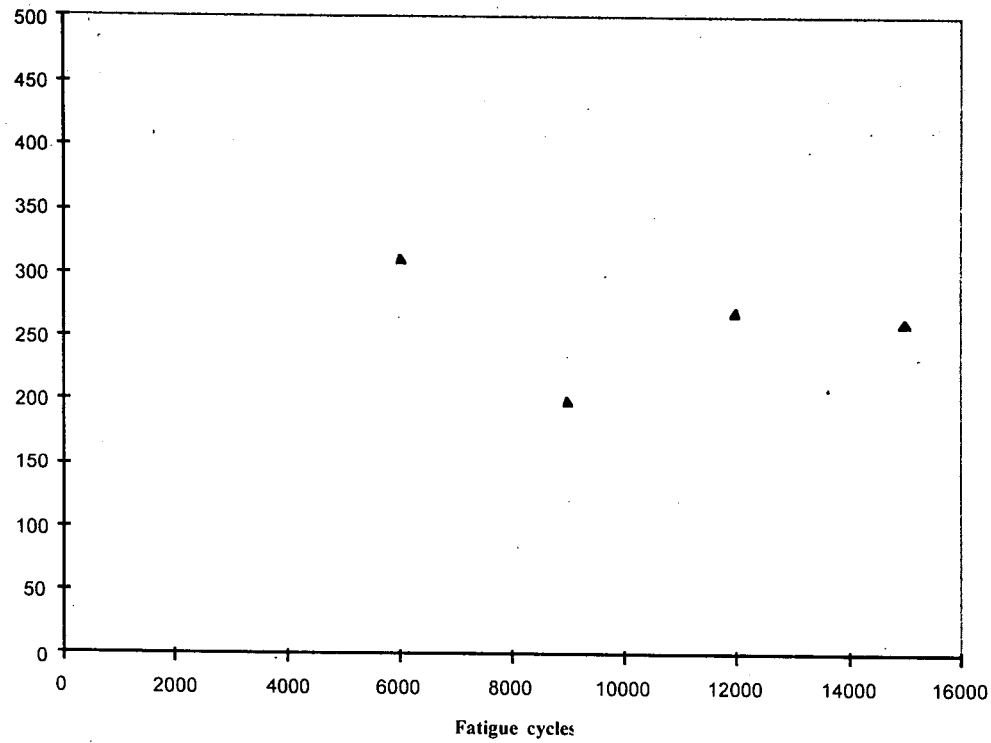

Figure 102. Number of Events During Each Pressure Hold After Fatigue Cycling of Tank 018

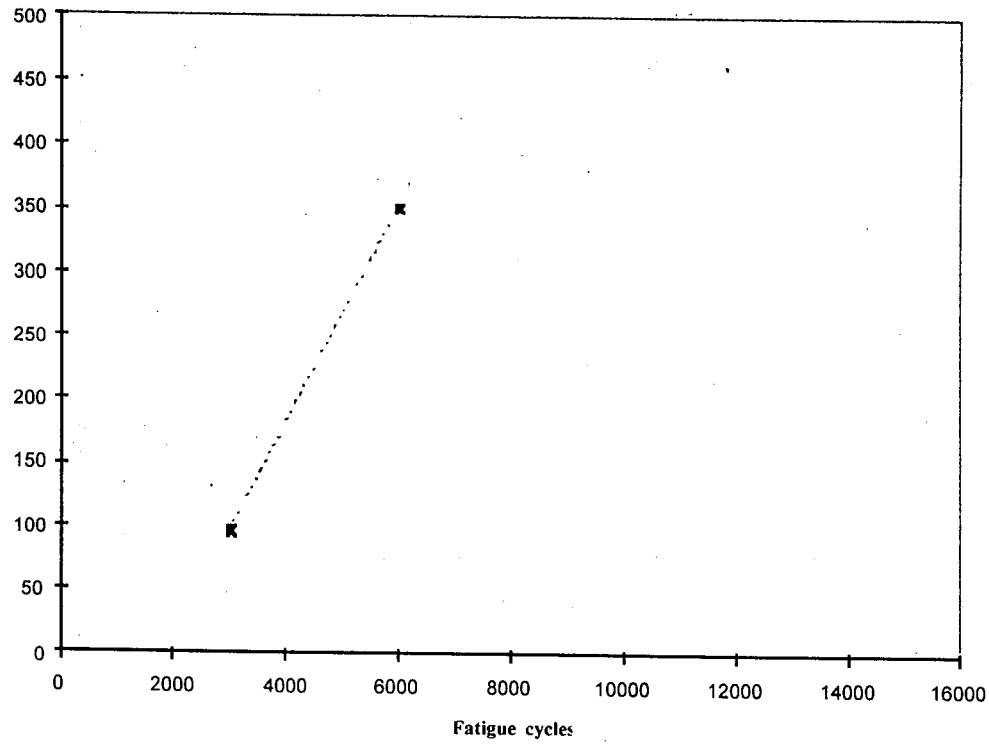

Figure 103. Number of Events During Each Pressure Hold After Fatigue Cycling of Tank 003